ABSTRACT

THE ROLE OF SHORT TERM SYNAPTIC PLASTICITY IN TEMPORAL CODING OF NEURONAL NETWORKS

by
Lakshmi Chandrasekaran

Short term synaptic plasticity is a phenomenon which is commonly found in the central nervous system. It could contribute to functions of signal processing namely, temporal integration and coincidence detection by modulating the input synaptic strength. This dissertation has two parts. First we study the effects of short term synaptic plasticity in enhancing coincidence detecting ability of neurons in the avian auditory brainstem. Coincidence detection means a target neuron has a higher firing rate when it receives simultaneous inputs from different neurons as opposed to inputs with large phase delays. This property is used by birds in sound localization. When there is no plasticity from the inputs, the firing rate of the neuron, depends more on input frequencies and less on phase delays between inputs. This leads to ambiguity in localizing the sound source. We derive a mathematical model of a reduced avian brainstem network and show that inputs with synaptic plasticity, to the coincidence detector neuron, play a vital role in enhancing coincidence detecting ability of the bird. We present comparisons to experiments. In the second part of the thesis, we prove the existence and stability of a n cluster solution in a m-cell network, in the presence of synaptic depression. The model used to represent a single neuron is based on the Hodgkin-Huxley model for the spiking neurons and we use techniques from geometric singular perturbation theory to show that any n-cluster solution must satisfy a set of consistency conditions that can be geometrically derived. The results of both problems are validated using numerical simulations.

THE ROLE OF SHORT TERM SYNAPTIC PLASTICITY IN TEMPORAL CODING OF NEURONAL NETWORKS

by
Lakshmi Chandrasekaran

A Dissertation
Submitted to the Faculty of
New Jersey Institute of Technology and
Rutgers, The State University of New Jersey – Newark
in Partial Fulfillment of the Requirements for the Degree of
Doctor of Philosophy in Mathematical Sciences

Department of Mathematical Sciences
Department of Mathematics and Computer Science, Rutgers-Newark

May 2008

APPROVAL PAGE

THE ROLE OF SHORT TERM SYNAPTIC PLASTICITY IN TEMPORAL CODING OF NEURONAL NETWORKS

Lakshmi Chandrasekaran

4-29-08

Dr. Amitabha Bose, Dissertation Advisor — Date
Professor, Department of Mathematical Sciences, NJIT

4/28/08

Dr. Farzan Nadim, Committee Member — Date
Professor, Department of Mathematical Sciences, NJIT and Department of Biological Sciences, Rutgers-Newark

4/28/08

Dr. Victor Matveev, Committee Member — Date
Assistant Professor of Mathematical Sciences, NJIT

04/28/08

Dr. Horacio G. Rotstein, Committee Member — Date
Assistant Professor of Mathematical Sciences, NJIT

4/28/08

Dr. Jonathan Rubin, Committee Member — Date
Associate Professor of Mathematics, University of Pittsburgh

BIOGRAPHICAL SKETCH

Author: Lakshmi Chandrasekaran

Degree: Doctor of Philosophy

Date: May 2008

Undergraduate and Graduate Education:

- Doctor of Philosophy in Mathematical Sciences,
  New Jersey Institute of Technology, Newark, NJ, 2008
- Master of Science in Applied Mathematics,
  New Jersey Institute of Technology, Newark, NJ, 2008
- Master of Science in Mathematics,
  University of Madras, Tamil Nadu, India, 2003
- Bachelor of Science in Mathematics,
  University of Madras, Tamil Nadu, India, 2001

Major: Mathematical Sciences

Presentations and Publications:

L. Chandrasekaran, V. Matveev and A. Bose "Coding by interspike interval in a globally inhibitory network," Submitted, *Physica D*

L. Chandrasekaran and A. Bose "Analysis of clustered solutions in a globally inhibitory network of spiking cells," SIAM conference on Applied Dynamical Systems, Snowbird, UT, May 27-31, 2007.

L. Chandrasekaran and A. Bose "Analysis of clustered solutions in a globally inhibitory network of spiking cells," Workshop on Mathematical Neuroscience, Center de Recherches Mathematiques, University of Montreal, Canada, September 16-19, 2007.

Success usually comes to those who are too busy to be looking for it.
-Henry David Thoreau (1817-1862)

ACKNOWLEDGMENT

I would like to thank all the people who have been helpful throughout my career in NJIT. First of all, I would really like to thank my advisor, Dr. Amitabha Bose for being very patient, for having more confidence in me than I had in myself and for being a constant source of guidance, encouragement and motivation, throughout this process. Dr. Bose is the best advisor I could have ever had.

I would also like to thank my committee members Dr. Farzan Nadim, Dr. Victor Matveev, Dr. Horacio Rotstein and Dr. Jonathan Rubin for taking the time to read my thesis and for all their valuable comments and suggestions. I would like to thank Dr. Victor Matveev especially, for all his feedback and help with MATLAB simulations for the globally inhibitory network project. Many thanks to Dr. Eliza Michalopoulou for providing me with her laptop to work on and helping me download all the software that I needed during all these years.

I wish to take this opportunity to thank many of the members in the Department of Mathematical Sciences. In particular, special thanks to Dr. Daljit Ahluwalia for his support and dedication to all the graduate students in our department. Thanks to Ms. Susan Sutton for all her timely help and support throughout my graduate life here in NJIT. Thanks to Mrs. Padma Gulati for being so enthusiastic and being excited for me for all my accomplishments. In general, I would like to thank the staff of the Math department for all their help.

I would like to thank all the graduate students in the Department of Mathematical Sciences who have helped me in some way or the other. I would especially like to thank Anisha Banerjee for taking her time and helping me with MATLAB programming, for all her help with LaTeX and for being a good friend through all these years. I would also like to acknowledge Joon Ha with whom I have had many discussions on concepts in dynamical systems and for his time that he spent on having

them. Thanks to Muhammad Hameed for helping me with LaTeX . I would like to thank Christina Ambrosio and Filippo Posta for a good LaTeX style file. It does a great job of laying out my dissertation, so I can spend more time on improving the content. A special thanks to Rudrani Banerjee for taking the time out and teaching me how to use software for statistical calculations during the last stages of completing my thesis. Many thanks to Nick Kintos, Jyoti Champanerkar, Soumi Lahiri, Kamyar Malakuti, Rashi Jain, Matthew Causley, Yogesh Joshi and Tsezar Seman who have been of help to me in some way or the other.

Last but not the least, I would like to thank my parents and sister who have encouraged and supported me always and made it possible for me to finish my dissertation. I would like to thank my sister who has always boosted my confidence, for being proud of me and for telling me that I could accomplish whatever I wanted to. Thanks to my cousin Karthik, uncle Chandran, and aunt Ramani for all their help throughout my stay here in USA. Finally, I would like to thank God for all the blessings in my life, for providing me with all the wonderful opportunities and helping me achieve my dreams.

TABLE OF CONTENTS

Chapter		Page
1	INTRODUCTION	1
	1.1 Role of Short Term Synaptic Depression as a Timing Device	6
	1.2 The Problem of Coincidence Detection	7
	1.3 Mechanisms Involved in Coincidence Detection	10
	1.4 Aim, Model and Results	12
	1.5 Globally Inhibitory Network	14
	1.6 Aim, Model and Results	15
2	COINCIDENCE DETECTION IN THE AVIAN AUDITORY BRAINSTEM	16
	2.1 Model	18
	2.1.1 Role of Depression from NM to NL	22
	2.1.2 Conclusions	44
3	INHIBITION FROM SON TO NM	45
	3.1 Model	48
	3.1.1 Role of Inhibition from SON to NM	51
	3.1.2 Conclusions	60
4	GLOBALLY INHIBITORY NETWORK	62
	4.1 Model	63
	4.1.1 Coupled Equations	66
	4.1.2 Reduction to Slow Manifold	68
	4.2 Results	71
	4.2.1 Existence of a n-cluster Solution	72
	4.2.2 Stability and Basin of Attraction of Solutions	79
	4.2.3 A Complementary Discrete Map Approach	83
	4.2.4 Conclusions	86
5	CONCLUSION	87

TABLE OF CONTENTS
(Continued)

Chapter **Page**

5.1 Summary of Results and Discussion 87

5.2 Future Work 91

6 APPENDIX 94

REFERENCES 96

LIST OF FIGURES

Figure		Page
1.1	Avian auditory brainstem morphology. Figure courtesy: Grothe, 2003 .	9
2.1	Avian auditory network architecture.	18
2.2	Sigmoid showing a_∞ vs i_{eff}.	20
2.3	D and s vs t for large P. D is the solid trace and s is the dotted trace. For large P, D recovers strongly and the maximum steady state value of D is .95 and is close to 1.	21
2.4	D and s vs t for small P. The solid trace is D and dotted trace is s. For small P, recovery of D is weaker compared to large P case and maximum steady state value of D is .85 in this case.	21
2.5	V vs t: a cell spikes when $V = 1$ and after that V is reset to 0.	23
2.6	Schematic of the NM-NL subnetwork; on the right spikes of the individual NM neurons are shown. The lower spike train is offset by $\phi = t_0/P$ from the upper one.	24
2.7	NL firing rate for low frequency NM inputs for high and low synaptic conductance: NL firing rate depends weakly on phase delays for high g_{syn}.	25
2.8	NL firing rate for high frequency NM inputs for high and low synaptic conductance: NL firing rate saturates for phase delays $< 90^o$ for high g_{syn}.	25
2.9	NL firing rate without depression: the firing rate curves are spread apart for different P values. The solid horizontal and vertical lines are discussed in the text. The parameter values are $g_{syn} = .5$, $\tau_k = 5$.	26
2.10	NL firing rate with depression: the firing rate curves are clustered for different P values compared to the non depressing case. The solid horizontal and vertical lines are discussed in the text. The parameter values are $g_{syn} = .5$, $\tau_k = 5$, $r = .75$, $\tau_d = 15$.	27
2.11	Variation in s_{max} with and without depression at $\phi = 60^o$.	30
2.12	Derivative of s_{max} and s^d_{max} with respect to P.	31
2.13	s_{max} vs P vs ϕ without depression.	31
2.14	s_{max} vs P vs ϕ with depression.	32
2.15	Spike times and interspike intervals.	37

LIST OF FIGURES
(Continued)

Figure **Page**

2.16 NL firing rate without depression: firing rate curves are spread apart. MATLAB simulation for the parameter value of $\tau_k = 4$. 38

2.17 NL firing rate with depression: firing rate curves are clustered and are more phase dependent. MATLAB simulation for parameter values of $\tau_k = 4$, $r = .92$ and $\tau_d = 15$. 39

2.18 NL firing rate without depression: firing rate curves are spread apart. XPP simulation for $\tau_k = 4$. 40

2.19 NL firing rate with depression: firing rate curves are clustered. XPP simulation for $\tau_k = 4$, $r = .92$ and $\tau_d = 15$. 41

2.20 NL firing rate without depression: firing rate curves are spread apart. MATLAB simulation for $\tau_k = 4$. 42

2.21 NL firing rate with depression: clustering of firing rate curves. MATLAB simulation for $r = .83$, $\tau_k = 4$ and $\tau_d = 15$. 43

3.1 SON-NM-NL network with inhibition. The input to left NM is stronger than the right side. Thick lines (connections) on the left indicate NM is driven strongly compared to the right NM. 47

3.2 Plot of SON inhibition; there are 3 SON spikes. For every SON spike, s is reset to 1 following which, s decays. 50

3.3 Solving for P; intersection of left hand side and right hand side of equation (3.4). 50

3.4 Period 'P' as a function of applied current with and without inhibition. In the case with inhibition, as current I increases, inhibition delays NM period for currents ranging from (1.2 to 1.3) to lie within $[8, 9.26]$ compared to the no inhibition case where $P \in [7.3, 9]$. 51

3.5 NL firing rate for various applied currents to both NM cells-no SON inhibition. XPP simulation with $g_{son} = 0$. 53

3.6 NL firing rate for various applied currents to both NM cells-with inhibition. XPP simulation for $g_{son} = .08$ and $\tau_s = 20$. 54

3.7 NL firing rate for various applied currents to both NM cells-without SON inhibition. MATLAB simulation with $g_{son} = 0$. 55

3.8 NL firing rate for various applied currents to both NM cells-with SON inhibition. MATLAB simulation with $g_{son} = .08$ and $\tau_s = 20$. 56

LIST OF FIGURES
(Continued)

Figure **Page**

3.9 NL firing rate for different applied currents on one side of NM-without SON inhibition. In all the input biased cases, the firing rate curves are deviated from the case when $I = 1.2$ on both sides. The value of $g_{son} = 0$. 58

3.10 NL firing rate for various applied currents on one side of NM cell-with SON inhibition. There is less deviation of the firing rate curves in the input biased cases when compared to $I = 1.2$ on both sides. The value of $g_{son} = .08$ and $\tau_s = 20$. 59

4.1 An m-cell globally inhibitory network. Each synapse from P to I is excitatory, and each from I to P is inhibitory and displays short-term synaptic depression. 63

4.2 Pyramidal cell v-w phase plane and singular orbit. The double arrows denote a fast transition between silent and active stated. A single arrow denotes the slower transition in each of those states. The horizontal axis is v and the vertical axis is w. 65

4.3 Representative trajectories on the $w - g$ slow manifold. Two cells begin at $t = 0$ and evolve toward the jump curve. When P_1 hits the curve at $t = t^-$, it is reset to $w = w_{rk}$ at $t = t^+$, while P_2 is reset vertically to the position shown. The cells then continue to evolve toward the jump curve. The dotted horizontal lines show that at any moment in time, the cells lie on the same g-level. 70

4.4 Clustered solutions in a 4-cell network. 73

4.5 The curve $\mathcal{C}_w$ on the $w - g$ slow manifold. If the leading cell begins on $\mathcal{C}_w$ at $w = w_0$, $g = g_0$ and hits the jump curve at $t = t_{g_0}$, then the trailing cell starting at $w = w_{rk}$, $g = g_0$ will reach $w = w_0$ at this time. The dotted horizontal lines show that at any moment the two cells lie on the same g-level. 74

4.6 The curves t_{in} and t_{g_0} for two different cases. The concave up grey curve is t_{in}, the concave down curve is t_{g_0} for the case $\tau_w = 5$ and the sigmoidal curve is t_{g_0} for the case $\tau_w = 0.4$. Points of intersection of either of the t_{g_0} curves with the t_{in} curve represent 2-cluster solutions. Note that in the case of small τ_w there are multiple intersections. 76

4.7 Existence of multiple cluster solutions. The concave up t_{in} curve intersects the various t_{g_0} curves corresponding to different sized cluster solutions; equation (4.21) solved for $n = 1, 2, 3$ and 4. As the number of clusters decreases, the inter-spike interval associated with the solution increases. 79

LIST OF FIGURES
(Continued)

Figure **Page**

4.8 Clustering of two initial conditions. At $t = 0$ the two cells start at (w_i, g_0). When the first cell reaches the jump curve at $t = t_f$, we calculate an upper bound for the second cell to reach the jump curve given by the time to vertically travel to the jump curve. If this time is less than the synaptic delay time, then the two cells will merge together into the same cluster. 82

4.9 Convergence to a 2-cluster solution. **A.** The intersection of the two curves represents a 2-cluster solution found by solving (4.14) and (4.21). The filled circles are different iterates of the one-dimensional map of interspike intervals as they converge to the intersection point. **B.** The corresponding time traces of the recovery variable w of the four cells shows how the interspike interval approaches the value 35.5. 85

CHAPTER 1

INTRODUCTION

The brain is a biologically complex entity. There is an astounding variety of neurons and types of communication that takes place between them. A brain has about 10^{11} neurons [25]. An ultimate challenge of biological sciences is to understand the biological basis of mental processes and consciousness by which we learn, remember, act and perceive. A remarkable unity has emerged within biology in the last two decades. The investigation of genes and inferring the amino acid sequences from the proteins that encode them have shown us some unanticipated similarities between the proteins present in the nervous system and those in the rest of the body [30]. This has provided researchers with the ability to outline a general plan for the function of cells. Therefore, the next and even more challenging step in this field is to unify the study of behavior - the science of mind, in particular neural science, which is the science of the brain [30]. This is the step which will lead us to a unified scientific approach towards the study of behavior, based on the belief that all behavior is an output of brain function.

Neuroscience is a field which is dedicated to the study of the nervous system. The main focus in neuroscience is to understand how the neurons transmit signals, how these signals are synthesized, integrated and how this leads to emergence of higher complicated functional activities in the brain. This interest and curiosity in the investigation of neuronal activity by neuroscientists worldwide, stems from a desire to understand the behavior, consciousness and perception of the higher functions in the brain [42], [25].

Much of the current view that we have about neurons, originated in the last century. Ramon y Cajal and Camillo Golgi are two of the pioneers in the study of

neurons from the late 1800s. Golgi developed a way to stain the neurons using silver salts that could reveal their structure under a microscope. Using this staining technique, Ramon y Cayal was able to investigate each individual cell, thus revealing that the nervous tissue is not a continuous web but it is a network of discrete cells. In this way, Cajal developed some of the major concepts and much of the early evidence, for the principle that, it is the individual cell, which is the elementary signaling element of the nervous system [30]. This principle was referred to, as the 'neuron doctrine'. There was more evidence supporting this theory of neuron doctrine through experiments in the 1920s, by embryologist Ross Harrison [30]. Thus Ramon y Cajal provided much of the early evidence required for our basic understanding of the nervous system.

The nervous system consists of two main kinds of cells : the glial cells(glia) and the nerve cells(neurons). Glial cells are much more in number compared to the neurons. They basically surround the neurons. Glia is not known to be directly involved in information processing but play other vital roles such as promoting signalling between the neurons, releasing some chemical substances, like growth factors which help in the nourishment of nerve cells and guiding migrating neurons during brain development [30]

A typical neuron consists of a cell body or the soma, dendrites and an axon. Neurons are living cells and exhibit metabolism like in many other cells. The soma consists of vesicles, nucleus and mitochondria. The dendrites and axon are part of the neuron's unique features. The dendritic processes can be immense and reach out to vast areas of the brain and the length of the axons can be longer than a meter. Neurons receive signals or inputs via dendrites. The dendrites process information that they receive and accumulate them in the soma and send impulses to other neurons via the axon [25]. An axon can convey electrical signals through distances that range from $.1mm$ to $3m$. These electrical signals are referred to as action potentials

which are rapid nerve impulses having an amplitude of roughly $100mV$ and duration of $1ms$ [30].

Action potentials are the basic mechanism by which neurons communicate. The action potential, commonly known as an impulse, is a short electrophysiological event that occurs due to the fact that a neuron's membrane has active properties. The initiation of the action potential takes place at a specialized trigger region at the origin of the axon which is known as the axon hillock, the initial segment of the axon from where they are sent down the axon without any distortion at the rate of $1 - 100m$ per second [30].

These signals are typically stereotyped throughout the nervous system even if they are triggered by a variety of events that occur in the environment. Therefore, signals conveying information about vision are the same as those that convey information about audition [30]. So here we encounter a principle brain function since the information that action potentials convey is not determined by the form of the signal, but it is mainly dependent on the pathway that a signal takes to reach the brain. The brain functions by analyzing and interpreting the patterns of incoming signals which helps in creating our everyday sensation of touch, smell, sound, sight and taste [30].

A single neuron receives multiple signals from other neurons and also signals to many others. The term synapse refers to the junction between an axon of a neuron and a dendritic branch of another neuron. To transmit information between different cells, neurons use two kinds of synapses- chemical and electrical synapses. A chemical synapse consists of pre and post synaptic parts which are separated by a synaptic cleft. When an axon terminal receives an input, it triggers a chain of physiological as well as chemical reactions in the presynaptic neuron. This leads to release of chemical substances called neurotransmitters from vesicles, into the synaptic cleft. These neurotransmitters diffuse across the cleft to reach the postsynaptic cell. They in turn react with the receptors present in the postsynaptic membrane and produce changes

in the membrane potential of the postsynaptic neuron [42].

Although chemical synapses are generally known to be a prevalent form of synaptic transmission, there are certain cells in the retina and also the rest of the nervous system linked by specialized junctions. These are the junctions where synapses are transmitted electrically [42] and are referred to as gap junctions. Electrical synapses occur when pre and postsynaptic membranes are positioned very close to each other and are linked by channels which connect intracellular fluids of both the cells. This close connection leads to the ability of action potentials to spread directly from cell to cell without the usage of chemical transmitters [42].

A synapse could be categorized into two types- either excitatory or inhibitory. It is called excitatory when an increase in its membrane potential causes an increase in the postsynaptic membrane potential which is biologically termed depolarization. When there is depolarizing activity it generally facilitates the generation of an action potential in the postsynaptic membrane. On the other hand, a decrease in postsynaptic membrane potential hyperpolarizes the cell, or decreases the membrane potential of the postsynaptic neuron. This implies that the presynaptic synapse is inhibitory, in other words it tends to suppress the activity of the postsynaptic cell.

The efficacy of a synaptic transmission is not a fixed quantity but it can vary depending on the patterns of ongoing activity. This ability of the synaptic strength to change and become weak or strong as a function of frequency of firing of the neuron is known as short term synaptic plasticity [42]. The two main kinds of plasticity are synaptic facilitation and synaptic depression. If there are short trains of presynaptic action potentials, it could either lead to facilitation of release of transmitter from a presynaptic terminal or depression of release or a combination of both. Short term facilitation is known to persist for several hundreds of milliseconds, whereas depression is known to last for seconds. If a train of stimuli is applied to the presynaptic neuron the amplitude of the resulting postsynaptic potential could either increase or decrease

owing to synaptic facilitation or depression respectively [42]. They are referred to as short term, since their period lasts for as little as a few tens of milliseconds up to tens of minutes [42].

Short term changes that occurs in the amplitude of synaptic potentials have been under extensive study at synapses in the peripheral nervous system like those of the autonomic ganglia or the ones in the vertebrate skeletal muscle [42]. Nonetheless, it has been shown that these changes do occur in the entire central nervous system as well [42].

On the other hand, it has been observed in the central nervous system, that repetitive activity can lead to changes in the synaptic efficacy which can last longer that those seen at the peripheral synapses [42]. They are found to occur in particular locations in the brain. They are intriguing since their occurrence over a long period of time suggests that somehow maybe associated with memory. There are two types of long term plasticity: long term potentiation and long term depression [42].

There has been experimental evidence suggesting that the phenomenon of short term facilitation is related to residual calcium [42]. Due to repetitive stimulation there is continued calcium accumulation in the presynaptic cell which leads to a progressive increase of transmitter release. Therefore, facilitation has been shown to occur due to increase in the probability of transmitter release by the presynaptic terminal.

Short term depression like facilitation is also thought to be presynaptic in origin. Sometimes repetitive activity in the presynaptic cell could also result in depression [42]. Depression occurs when the release of neurotransmitter from the presynaptic cell, with each stimulation is very high. Thus every time the presynaptic neuron fires, a large number of neurotransmitters are released. This results in depletion of vesicles in the presynaptic cell and there are fewer vesicles available for release during the next spike. As a result, there is reduction in the amplitude of the

postsynaptic EPSP, upon repeated stimulation [42]. For our purposes we are basically interested in understanding the effects of the synaptic plasticity and our focus will not be on its mechanisms.

1.1 Role of Short Term Synaptic Depression as a Timing Device

Short-term synaptic plasticity which is commonly found in the central nervous system could contribute to the functions of signal processing, namely coincidence detection and temporal integration. In the case of temporal integrators where the output firing rate mainly depends on an sum of the recent synaptic inputs, it is plasticity that modulates their net input synaptic strength. This modulation could directly lead to the control of function of neural networks and signalling gain [13].

Common instances of temporal discrimination can be found in coincidence detection, input rate filtering, oscillatory networks- the setting of phase offset, cycle period and regulation of spontaneous oscillatory activity [20]. The behavior of an organism depends on these computations. Some of the important applications are in sound localization, sensory input selection and rhythmic motor tasks like the crustacean pyloric rhythm [41] and mammalian intestinal peristalsis [59], [20]. Synaptic depression is known to play a role in enhancing temporal coding. But it is hard to predict the effect that depression has on a neuronal input-output transformation since it is mainly dependent on the kinetics of depression and also the relevant context [1],[6]. Context refers to activity patterns of the individual synaptic inputs and also the intrinsic properties of the postsynaptic membrane [20]. Synaptic depression is so versatile as a timing device, that it successfully helps to explain its omnipresent nature in the nervous system.

In this thesis we are primarily interested in understanding the role of short term synaptic plasticity in temporal coding of neuronal networks. We shall consider two distinct set of problems. One focuses on the coincidence detection in the avian

auditory brainstem. The other centers on the multistability of solutions in a globally inhibitory network.

1.2 The Problem of Coincidence Detection

We first study the phenomenon of coincidence detection. The barn owl uses differences in timing and intensity of a sound which reaches its ears to locate the azimuth and the elevation of the sound source [31]. There are 'space-specific neurons' present in the inferior colliculus (IC) region situated in the auditory midbrain of a bird. These neurons are excited only if sounds emanate from a specific region of space having a particular combination of interaural time difference (ITD) and interaural intensity difference (IID). ITD which is the difference in the time of arrival of sound to both the ears (in submilliseconds) and IID which is the difference in the intensity of sound arriving at the two ears, is commonly used by both birds and mammals as critical cues for sound localization along the azimuthal direction and elevation of the sound source. For both birds and mammals, the processing of ITD presents a huge challenge in processing of temporal information. In vertebrates except for an electric system in some fish, no other neural system even comes close to requiring precise temporal resolution to encode ITDs [22]. The duration of an action potential is almost equivalent to two orders in magnitude greater than the minimal ITDs ($< 10\mu s$) that can be resolved by humans or the barn owls. As a result, the ITD processing structures in both birds and mammals are in need of well suited model systems to study the rules underlying precise temporal processing [22].

There exists four primary nuclei in the avian auditory brainstem for sound processing which includes nucleus magnocellularis (NM) and the nucleus angularis (NA), the two major neurons in the cochlear nucleus forming the auditory pathway to the IC. Figure 1.1 shows the network architecture of the avian brainstem [22].

The NM neurons are the avian analog of the mammalian anteroventral cochlear

nucleus. NM neurons preserve the temporal characteristics of the acoustic inputs and thereby provide necessary information for coincidence detection of interaural time differences. A coincidence detector neuron is one that has higher firing rates when it receives simultaneous or near synchrony inputs. In the avian system nucleus laminaris (NL) cells are coincidence detectors and interpret the phase difference of inputs from the NM neurons on both sides of the brain.

The NM cells have the appropriate physiological and anatomical features which makes them best suited for coding temporal information [61]. First of all NM cells have secure excitatory transmission. There are two or three calcyine terminals, that project onto each NM neuron from the auditory nerve. These terminals generate suprathreshold currents [70]. Second due to the fact that the NM neurons have spherical somata and very few or no dendritic processes there is hardly any attenuation or electronic filtering of excitatory input. The third property of NM neurons is that there is existence of robust low voltage activated K^+ currents which activate rapidly and inactivate slowly. This helps in the fast recovery of NM cells from excitation and prevents the temporal summation of all the multiple inputs [47], [32], [63]. There have been physiological studies to indicate independent processing of phase coding and sound intensity occurring in the auditory brainstem of the barn owl [57]. The NM neurons project bilaterally, sending excitatory inputs to the NL neurons via axons of variable length thus acting as delay lines and are responsible for phase coding [55]. Traditionally, it is believed that ITDs are encoded by an array of coincidence detector neurons that receive excitatory inputs from both the ears via axons of systematically varying lengths which are the 'delay lines', such that a topographic map of the azimuthal auditory space is created [5], [26], [29]. As a consequence neurons which are tuned to the same best frequency display different best ITDs (the ITD at which a neuron has a maximal firing rate) thus almost covering the entire physiological range [22]. This concept of delay lines was proposed by Jeffress, in 1948 [26]. He outlined a

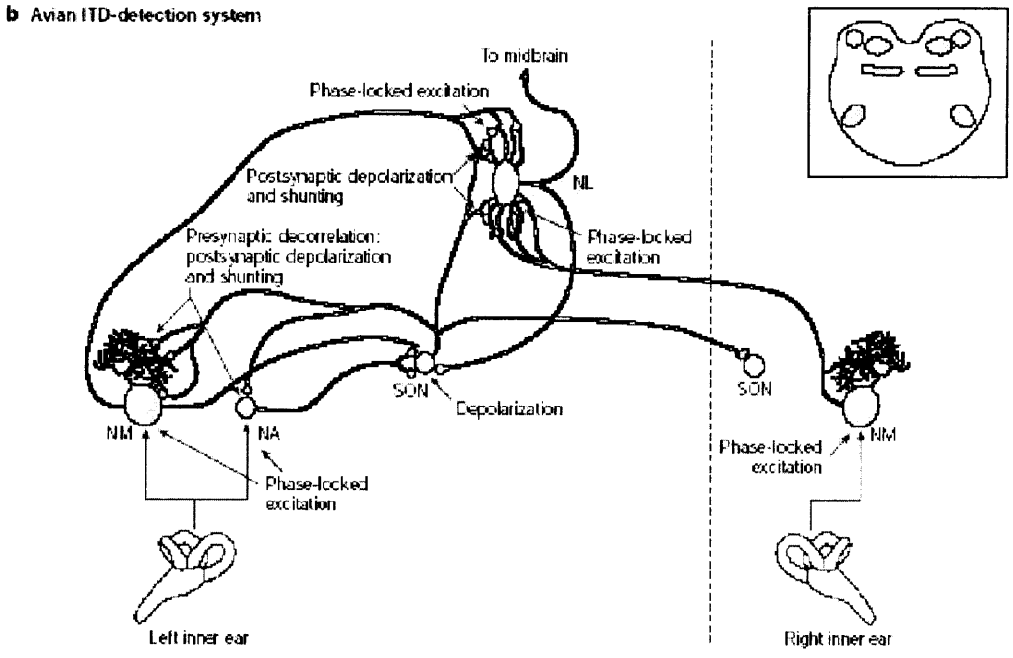

Figure 1.1 Avian auditory brainstem morphology. Figure courtesy: Grothe, 2003

model, that transformed differences that arose in acoustic timing into that of a neural spatial gradient. In other words, this model transformed a time code into a space code.

NA is responsible for encoding sound intensity information to provide cues for sound localization [57]. Both the NA and NM cells receive excitatory input from the auditory nerve (AN) [4], [48], [8], [9], [27], [28]. This form of synaptic connection between the auditory nerve onto the neurons in the cochlear nucleus has a huge impact on the transmission of sound. By using embryonic brain slices of the chick and trains of stimulation injected electrically, Carr and her co-workers have investigated the short term plasticity of these inputs to the NA of the birds where the intensity information is encoded [10]. They found that these glutamatergic excitatory inputs exhibited a mixture of short term plasticity namely synaptic facilitation and depression. They observed that the balance of short term facilitation and depression at the NA synapses helped in maintaining the amplitude of postsynaptic response through-

out the electrical trains at firing rates greater than 100 Hz, which are considered to be high. In the minority of synapses which only exhibited depression, there was saturation of postsynaptic response with increasing intensities which then limited the range of the intensity information conveyed. Therefore, it is evident that short term synaptic plasticity plays a major role in modulating the strength of the synapse by filtering information which is contained in the firing patterns of the neurons.

Carr et al. [10] performed experiments to study the steady-state relationship of input rates of the synapses to the cochlear NA. It was evident from these balanced synapses that they conveyed rate information in a linear fashion thereby transmitting intensity information encoded in the form of a rate code in the NA nerve. There have been studies related to quantitative models of short term plasticity like depression and facilitation which help in identifying potential effects such as adaptation, detecting change, and filtering of signals [1], [65], [12], [15], [64].

Zhang and Trussell [70] did voltage clamp experiments in the avian nucleus magnocellularis and observed that the chick auditory nerve synapses onto the nucleus magnocellularis (NM) of the cochlear nucleus and expresses strong short-term depression. The NM cells send bilateral bouton-like excitatory synapses onto the nucleus laminaris (NL), a group of specialized cells for coincidence detection of interaural delays in birds. In fact, NL neurons are the first to calculate the ITD for locating sound source in birds [11]. This feature of coincidence detection is an important property in many neural functions such as direction of visual movement [46], computing of ITD [26], pattern recognition [23] and echo suppression [54] in small mammals. The NL neurons are homologous to the medial superior olive (MSO) in mammals.

1.3 Mechanisms Involved in Coincidence Detection

There are two mechanisms which have been suggested to maintain the sensitivity of ITD in NL neurons despite sound level variations.The first mechanism is that the

synapse from NM to NL exhibits synaptic depression which suggests that depression plays a role in characterizing the timing circuits [33], [13]. It is shown in [7] that in a NL cell that received synaptic depression, there is increased consistency in response to ITD over a threefold range of input discharge rate. When there is no depression ITD sensitivity decreased with increased rate of input. Cook et al. [13] performed experiments on the chick brainstem. They observed that synaptic depression from NM to NL could play a role in preserving coincidence detection in NL neurons. In order to test this hypothesis of depression being a gain control mechanism, they went on to model the NM-NL network to perform simulations. They had an extensive model for the NL cell. Their NL cell had a $20\mu m$ diameter soma and had nine dorsal and ventral dendrites. Each of these dendrites received a uniform distribution of NM synapses around their midpoint. Their results show that in the absence of depression when the NM firing frequency and synaptic conductance is low then the NL neuron does not fire at all for any phase delay between NM inputs. If the NM firing frequency is high, and synaptic conductance is high, then the NL firing rate saturates and remains high and does not change at all for phase differences $< 90^o$. This showed that in order to provide appropriate coincidence detection at high and low NM firing frequencies, the conductance needs to be varied. But [13] showed that depression from NM to NL provides a mechanism to automatically adjust the synaptic conductance inversely to the NM firing frequency. This is because high frequency NM inputs recover weakly from depression and low frequency inputs exhibit stronger recovery from depression. Therefore, this leads to better coincidence detection among the NL neurons since they depend less on input frequencies and it is the degree of input synchrony (phase difference) variable that is encoded by the NL neuron [13].

The second mechanism for maintaining ITD sensitivity of NL neurons is the presence of SON inhibition to NM synapses which can enhance coincidence detection of the NL neurons. The superior olivary nucleus (SON) which is located in the ventro-

lateral part of the avian brainstem receives excitatory inputs from NA and NL and it sends inhibitory synapses back onto NA, NL and also NM [49]. It has been observed that the morphological and physiological property of the SON neurons make them suitable for temporal integration. It is found in [49] that the direct stimulation of the SON evokes a long lasting inhibition among the NL neurons. Therefore, there is blockade of intrinsic spike generation among the NL neurons. These findings indicate the existence of GABAergic inhibitory feedback to the NL neurons. A mechanism by which SON evoked inhibition affects ITD is discussed in [49].

It has been shown through experiments [35], that in the absence of SON inhibition to NM, high sound levels could strongly drive each NM. As the result, a high firing rate from either side might lead to "false alarms" in NL neurons. That is, if there is coincident firing of many NM fibers from any one side, that alone can evoke spiking among NL neurons thus creating ambiguity among NL neurons in being able to discriminate binaural coincidences from strong monaural excitation. The presence of SON can potentially prevent strong unilateral excitation since the SON inhibition is proportional to the activity of NM. Therefore, the experiments in [35] suggest that if there is increased activity of NM neurons on one side, that will lead to stronger recruitment of SON inhibition which could eventually reduce NM activity [44].

1.4 Aim, Model and Results

Our primary goal is to fully comprehend how synaptic plasticity, in NM excitatory inputs to the NL neurons and the SON inhibitory inputs to the NM neurons contributes toward improving ITD sensitivity among NL neurons. We explore this phenomenon of coincidence detection by first constructing a qualitative firing rate model. This model is straightforward to work with because it focuses only on the average firing rate of the neurons and not their individual membrane properties. In particular, we investigate how the firing rate of a model NL cell can be made to be more dependent

on ITD than on input frequencies. We find that in the absence of depression, when there is high synaptic conductance for high frequency NM inputs, the NL firing rate is very high and saturates for phase differences $< 90^o$. Also in the low conductance, low frequency NM input case, the NL firing rate depends weakly on phase delays of inputs. These results are consistent with the findings of the Cook et. al [13] paper. When we include synaptic depression from NM to NL we find that depression plays a role of gain control mechanism. Since the high frequency inputs exhibit weak recovery and low frequency NM inputs recover strongly from depression, now the NL firing rate is more dependent on phase delays than input frequencies as shown in [13]. We obtain estimates on some main parameters that affect the firing rate curves, namely the depression time constant, synaptic conductance and the parameter which determines the extent of the depression variable.

We then model the NM-NL network using integrate and fire neurons. We obtain similar observations to the firing rate model. In the presence of depression from NM to NL, the NL firing rate curves behave more as a function of phase and are less input frequency dependent, compared to the no depression case. We use XPP to perform simulations and validate it with a semi-analytical solution of the integrate fire equation using MATLAB. There is qualitative agreement between our XPP and MATLAB results. We make parameter estimations for the integrate and fire neurons similar to the firing rate model to find that there is an interplay between the depression time constant and the parameter that controls the extent of depression.

We extend this model of integrate and fire neurons to incorporate inhibition from SON to NM. We investigate whether SON affects the period of the NM neurons or if it promotes phase locking among the NM neurons during high intensity inputs to NM neurons. Either or both of these implications of the SON feedforward synapse to the NM neurons would play a major role in determining the firing rate of the NL neuron, thereby affecting coincidence detection. We are also interested in investigat-

ing the monaural excitation problem. The way we incorporate monaural excitation in our model is by increasing the applied currents on one side of the model. As a result, increased applied current leads to higher frequency firing of those NM neurons.

Our results show that when the NM neurons, on one side of the brain receives high frequency inputs compared to the other side, there is ambiguity among the NL neurons in discriminating between strong monaural excitation versus binaural coincidence detection. We then include SON inhibitory input to the NM neurons. We know from literature, that the activity of SON on a particular side of the brain is proportional to the amount of NM excitation on that side [61]. Therefore, whenever the NM cell on one side is driven more compared to the other, SON inhibition is more on that side. We find that SON tends to equalize the firing rate of NMs on both sides over a range of applied currents which depend on the parameters of the system.

1.5 Globally Inhibitory Network

The second part of the thesis concerns multistability of solutions in a globally inhibitory network of spiking cell. Considerable attention has been given to the idea that neurons convey information in their patterns of activity to downstream targets. There are two general ways in which this information is transmitted. One way is through the firing rate of individual or groups of neurons. In this scenario, downstream neurons interpret the changes in firing rate to discern the behavior of the upstream network. The second way that neurons may transmit information is through their spike times [3]. For example, two neurons may fire at the same rate, but a downstream target neuron may determine the degree of synchrony of the cells based on the difference of their spike times. Coincidence detection is a classic example of this phenomena whereby a downstream target neuron will only fire if it receives inputs from different neurons within a very small window of time.

1.6 Aim, Model and Results

In this section, we will consider a globally inhibitory network that is loosely based on the CA1 hippocampal structure. The network consists of m uncoupled pyramidal cells that all synapse onto a common interneuron. The interneuron sends inhibition that exhibits short-term synaptic depression (STSD) to each of the pyramidal cells.

The main result of this chapter is to show how short term synaptic depression allows the globally inhibitory network to exhibit multiple stable solutions, all for the same set of parameters. In particular, we show that in a network of m pyramidal cells, there can exist stable cluster solutions of size $n \leq m$ for any n. A n-cluster solution is one in which the network breaks up into n out-of-phase groups. Within each group the cells are fully synchronized, but the clusters are separated by a well defined interspike (intercluster) interval. Cluster solutions are distinguished by the fact that different clustered solutions have different interspike intervals and these different intervals are fully determined by the extent of synaptic depression associated with that cluster. We will show that the interspike interval decreases with the number of clusters. Short term synaptic depression allows there to be m different interspike intervals thus implying that the network can transmit m different codes. This work extends to the work of [68] and also Rubin and Terman [51] who show that a globally inhibitory network without depression displays bistability between a synchronous and a single clustered solution.

CHAPTER 2

COINCIDENCE DETECTION IN THE AVIAN AUDITORY BRAINSTEM

In this section we first describe the model used to study the role played by synaptic depression in enhancing coincidence detection in the NL neurons. A fundamental way by which animals and birds perceive their presence in the environment is through localizing a sound source. This provides them with a mechanism of locating where their mate or their prey is or the direction from where they could be threatened by a predator. From early literature, we know that the difference of time of arrival of sound to both ears (ITD) is a major cue for sound localization [11]. There have been physiological observations in both owls and mammals which have confirmed the phase locking of action potentials to input stimulus in the brainstem. This property of phase locking generates the sensitivity of interaural-delay [38]. Therefore, it is evident that the timing of inputs plays a critical role in binaural sound information processing. Over the past few years it has been identified by researchers that depressing synapses influence temporal discrimination to a great extent [20]. One of their major roles is in auditory coincidence detection [13], [33].

The relevant auditory neurons having synaptic connections from the auditory brainstem through the inferior colliculus (IC) neurons in the auditory midbrain can be seen from 2.1. As shown in the figure, the auditory nerve (AN) sends feedforward excitatory synapses onto the cochlear neurons nucleus magnocellularis (NM) and nucleus angularis (NA) [22]. AN does not send direct synapses onto the NL neurons but the NM cells send a depressing synapse onto the NL neurons. The IC receives excitatory inputs from both the NA and NL neurons. We are first interested in modeling the behavior of NL neurons in response to the excitatory input from NM.

The second factor which is believed to be instrumental in enhancing coincidence detection among the NL neurons is the inhibitory feedback from SON located in the auditory brainstem to NL. As indicated in the figure, SON receives excitatory inputs from the NA and NL cells. SON sends feedback inhibitory synapses onto NM, NA and also the NL cells.

Cook et al., [13] explored the effects of synaptic plasticity in the NM to NL synapse. They studied the NL firing rate in the presence of synaptic depression using a multi compartment model. Their model NL cell had a $20-\mu m$ diameter soma that has nine ventral and dorsal dendrites. Each of the dendrites had a uniform distribution of the NM synaptic inputs around their midpoint. They connected a myelinated axon to the soma through an initial segment so that unambiguous counting of propagated action potentials could be done. Through simulations they observed that firing rate saturation in response to high intensity inputs in the case of high synaptic conductance resulted in the steep decline of output rate as a function of phase delay. They showed that this problem can be avoided by using smaller synaptic conductance. However in this case at low intensity inputs, the firing rate of NL cells is almost zero for increasing phase delays. This indicated that a different post synaptic potential amplitude is required to generate coincidence detection among NL neurons. They found that this problem could be resolved by including synaptic depression and also that the intrinsic properties of the NL neuron contributed towards enhancing coincidence detection. Their findings suggest that the inclusion of depression provides a balance between high sustained input rate and low steady state post synaptic potential amplitude. The result is that, in the presence of depression, the output (firing rate of NL cell) is more a function of input synchrony and less dependent on input rate or alternatively input frequency. We are interested in determining how much of their results can be explained simply as a result of synaptic depression. In other words we shall disregard much of the intrinsic properties of the NL neuron.

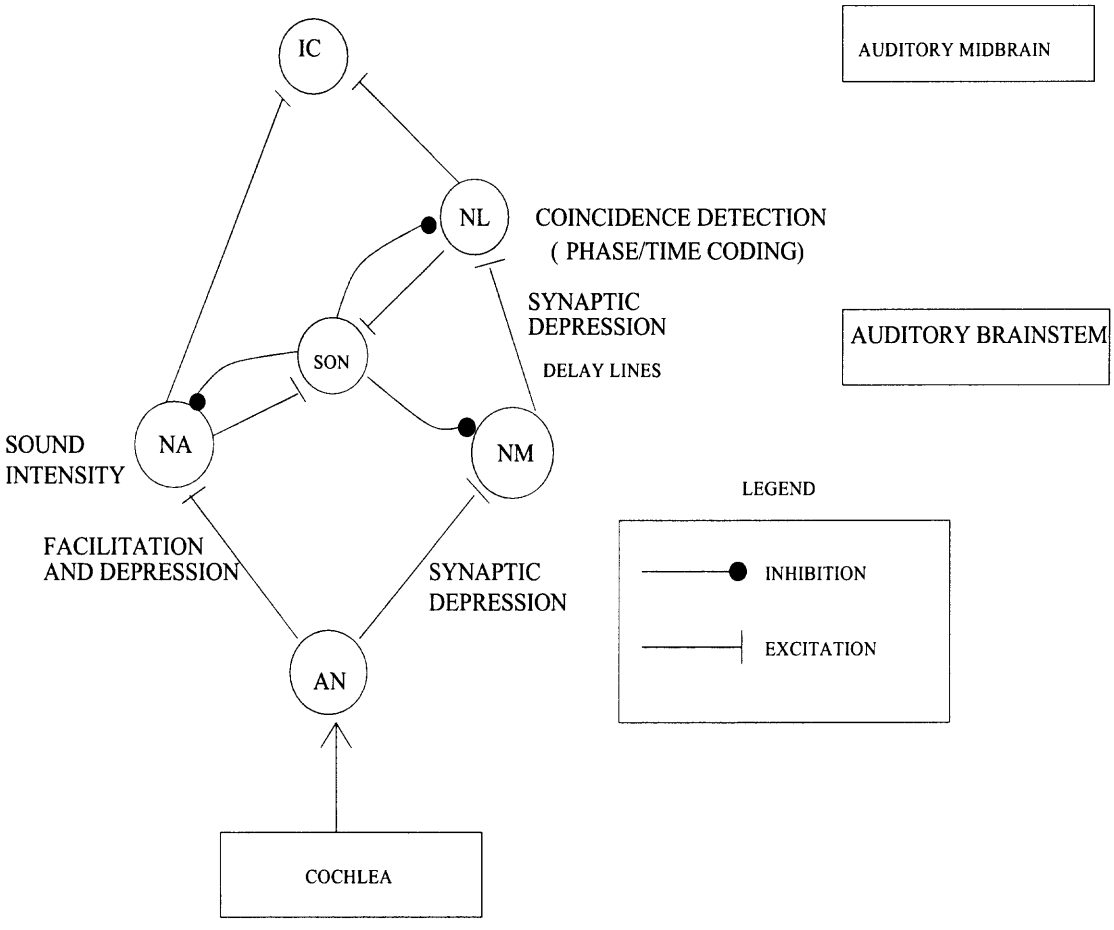

Figure 2.1 Avian auditory network architecture.

2.1 Model

To begin with, we use a firing rate model similar to [56], to describe the activity of a single NL neuron receiving depressing excitatory inputs from the two NM neurons. NM_1 represents inputs from the left side of the brain and NM_2 represents inputs from the right side. The general equation which governs the activity of an NL neuron is given by,

$$\frac{da}{dt} = \frac{(a_\infty(I_{eff}) - a)}{\tau_a} \tag{2.1}$$

Here a is the activation variable pertaining to the NL cell. The NM cell's

input to NL, a_∞ is a sigmoid shown in Figure 2.2 and expressed as

$$a_\infty(I_{eff}) = 1/(1 + exp^{-(I_{eff}-\alpha)/k_a}) \tag{2.2}$$

The parameter α is the half-activation value of a. The parameter I_{eff} determines the input to the NL neuron from the NM cells described by $I_{eff} = g_{syn} * s$ where g_{syn} is a parameter for synaptic conductance. τ_a is the time constant with which the network activity reaches the value $a_\infty(I_{eff})$. We model the NL cell in such a way that it receives inputs from two NM cells defined by s_1 and s_2 where $s = s_1 + s_2$. s_1 is the variable measuring the strength of synaptic input to the NL cell from NM_1, and s_2 measures the strength of the input from NM_2. We assume that the input from NM_2 arrives with a delay of t_0 where $t_0 \in [0, P/2]$, P is the period of NM activity. The value of the sigmoid's steepness is given by k_a. As k_a becomes smaller, the sigmoid gets steeper. The negative (positive) sign in front of the exponent determines if the sigmoid is increasing or decreasing thus indicating excitatory or inhibitory input. First we consider the input to NL to be non-depressing and we do not explicitly model the activity of the NM cell but instead we just model its synapse onto the NL cell. Whenever an NM cell spikes the associated s_i variable is reset to equal one. Between spikes s_i is described by

$$\frac{ds_i}{dt} = \frac{-s_i}{\tau_k} \tag{2.3}$$

for $i = 1, 2$, where τ_k denotes the time constant of decay of either synapses.

When the synapses are depressing, a variable D measures the level of synaptic depression [1] and is independent of s. When an NM cell spikes s is set equal to D and D is reset to rD. Here r is a positive parameter which is less than 1 and denotes the decrement of the D variable due to depression when the synapse is active. This can be summarized by noting that when there is a spike by a NM neuron, say at time

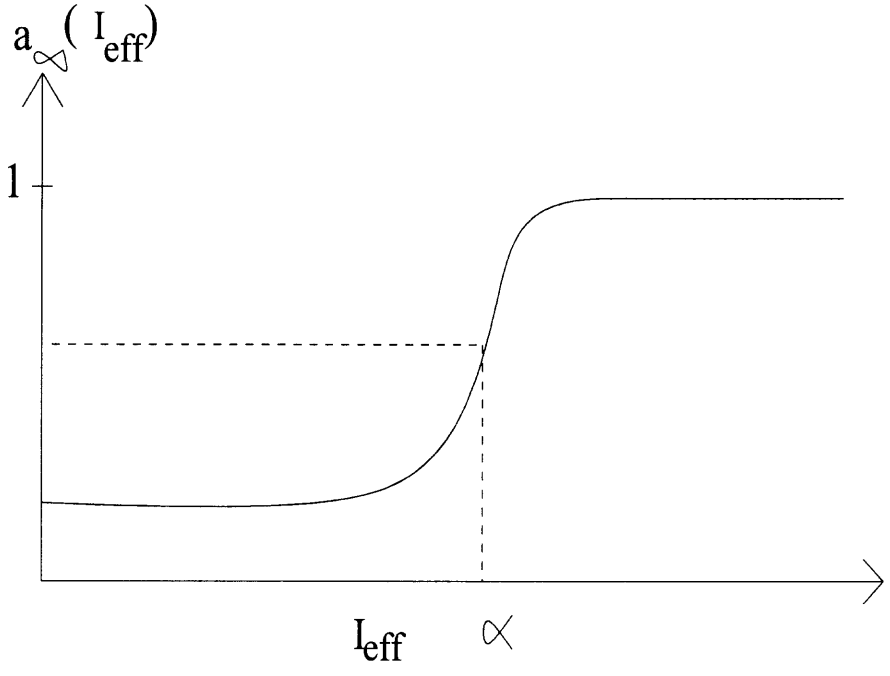

Figure 2.2 Sigmoid showing a_∞ vs i_{eff}.

t, the variables D_i and s_i obey

$$\begin{aligned} D_i(t^+) &= r_i D_i(t^-) \\ s_i(t^+) &= D_i(t^-) \end{aligned} \tag{2.4}$$

When the cell is silent, the synapse recovers from depression, and its effect on the post synaptic cell decays.

$$\begin{aligned} \frac{dD_i}{dt} &= \frac{1 - D_i}{\tau_d} \\ \frac{ds_i}{dt} &= \frac{-s_i}{\tau_k} \end{aligned} \tag{2.5}$$

Figures 2.3 and 2.4 are illustrations of the dynamics of the depression and the synaptic input variables as a function of period P.

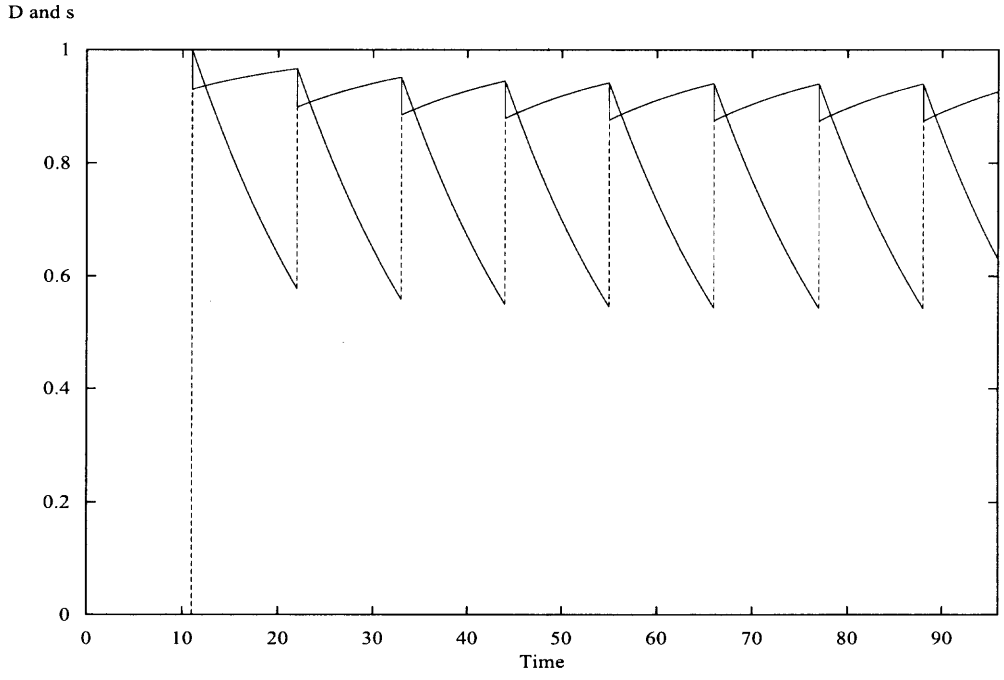

Figure 2.3 D and s vs t for large P. D is the solid trace and s is the dotted trace. For large P, D recovers strongly and the maximum steady state value of D is .95 and is close to 1.

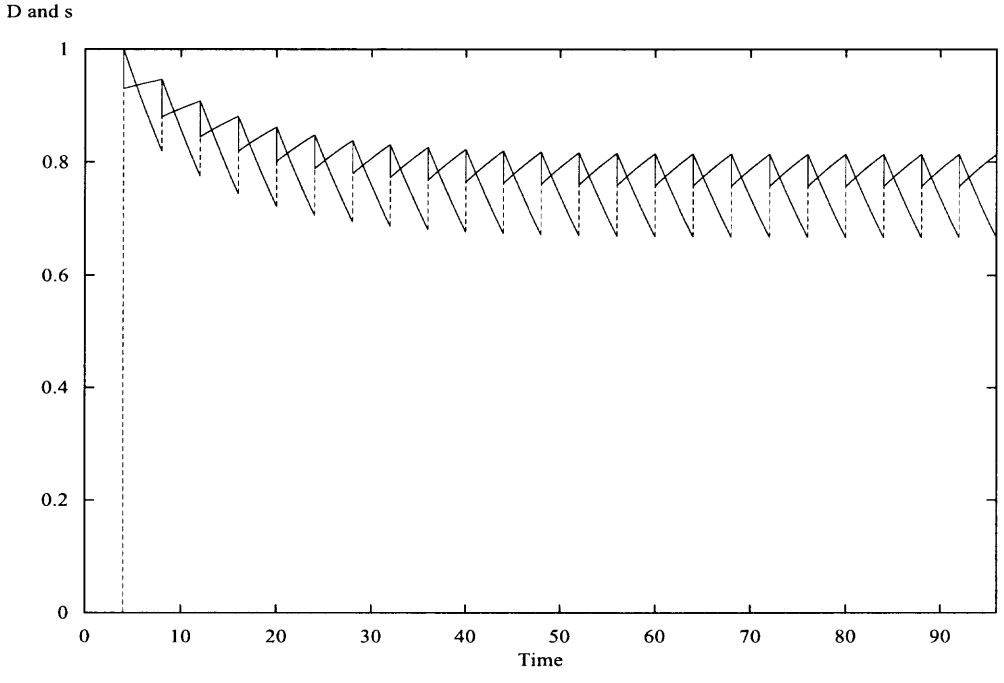

Figure 2.4 D and s vs t for small P. The solid trace is D and dotted trace is s. For small P, recovery of D is weaker compared to large P case and maximum steady state value of D is .85 in this case.

When the firing frequency of NM is low (high P), then its synapse is strong. But if NM fires at a high frequency then its synapse will be weak. Therefore, it can be seen from Figures 2.3 and 2.4 that at a low NM firing frequency the D variable reaches its steady state with a maximum at a value closer to 1 than when when NM firing frequency is high. In Figure 2.3 maximum of the steady state value of D is .92 and in Figure 2.4 the value is closer to .82. These figures are obtained by simulating equations (2.4) and (2.5) and using XPP [17].

When we move away from firing rate models we will use an integrate and fire model to describe activity of the neurons. The general equation describing a model neuron is:

$$\frac{dv}{dt} = I - v, \quad I > 1$$

If $v(t^-) = 1$ there is a spike and after that, v is reset to 0, i.e $v(t^+) = 0$. I denotes the applied current that the cell receives. The general equation of v, which is the voltage of a cell receiving synaptic input is the following:

$$\frac{dv}{dt} = I - v - \bar{g}_{syn} s(v - E_{syn}) \tag{2.6}$$

where E_{syn} is the reversal potential of the synaptic current, s denotes the synaptic strength and $\bar{g}_{syn}$ is the maximum synaptic conductance. Figure 2.5 shows a typical voltage trace of a cell using an integrate and fire model.

2.1.1 Role of Depression from NM to NL

Using the model described in the previous section where one NL cell receives excitatory inputs from NM cells of the left and right ear, we now study how the firing rate of the NL cell depends on the phase delay of the inputs from the NM cells. As we can see in Figure 2.6, there are NM neurons from the left and right ear sending depressing excitatory synapses onto the NL neuron. The input period of both NM

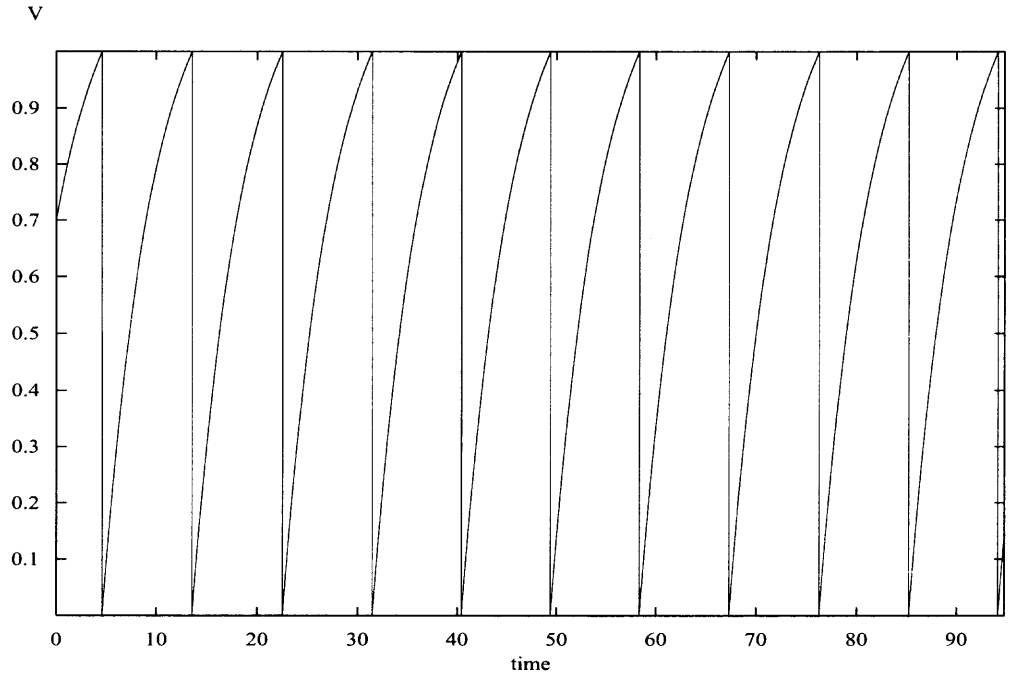

Figure 2.5 V vs t: a cell spikes when $V = 1$ and after that V is reset to 0.

cells is given by P. If NM_1, spikes at $t = 0, P, 2P....$ then we assume there is a time delay of t_0 for the input NM_2, i.e. it fires at $t = t_0, P + t_0, 2P + t_0.....$ The phase difference of the inputs is given by $\phi = \frac{t_0}{P}$.

We first study the activity of the NL cell using the firing rate model. We calculate the firing rate value as follows. Our time constant value τ_a is chosen small so that the NL activation variable a can be approximated by $a_\infty(I_{eff})$ at steady state. We compute the firing rate at every sample phase location, by simply calculating the maximum amplitude of a when it reaches steady state. This equals $a_\infty(I_{eff})$ when I_{eff} is evaluated at a maximum of these synaptic inputs.

Figure 2.7 shows the firing rate of the NL cell in response to low frequency input with $P = 20$ in the presence of high and low synaptic conductance. Figure 2.8 illustrates the NL firing rate as a function of high frequency NM inputs in the presence of high and low synaptic conductance. As is evident from Figure 2.7 when the synaptic conductance is low at $g_{syn} = .2$, the firing rate of the NL cell only de-

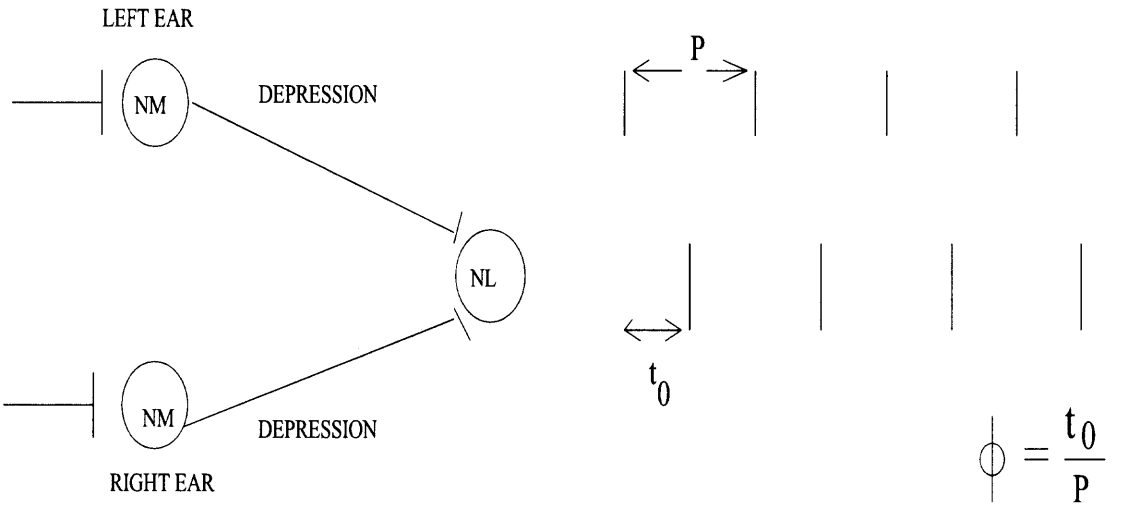

Figure 2.6 Schematic of the NM-NL subnetwork; on the right spikes of the individual NM neurons are shown. The lower spike train is offset by $\phi = t_0/P$ from the upper one.

pends weakly on phase delays. But we can see from Figure 2.8 that for high synaptic conductance at $g_{syn} = .5$, for high frequency NM input the firing rate curve saturates for phase delays less than 90^o. These findings are consistent with the results shown in Cook et. al, [13].

We want to study how these firing rate curves change as both a function of frequency and phase. Thus we will study the problems for various values of P. Figure 2.9 illustrates the firing rate of a NL cell as a function of phase delay without synaptic depression with $g_{syn} = .5$.

Figure 2.10 shows the NL cells's firing rate as a function of phase delay in the presence of depression with $g_{syn} = .5$. In the figures, the parameter P indicates different NM periods used in our simulation. It is evident from the figures that in the case of no depression, as the input frequency decreases, the NL firing rate curves spread out. Alternatively with depression, with decreasing frequency, the firing rate curves begin to overlap and only gradually deviate from each other as phase delay increases. Thus the inclusion of depression in our model makes the firing rate of the NL neurons more frequency independent and instead more dependent on phase delay

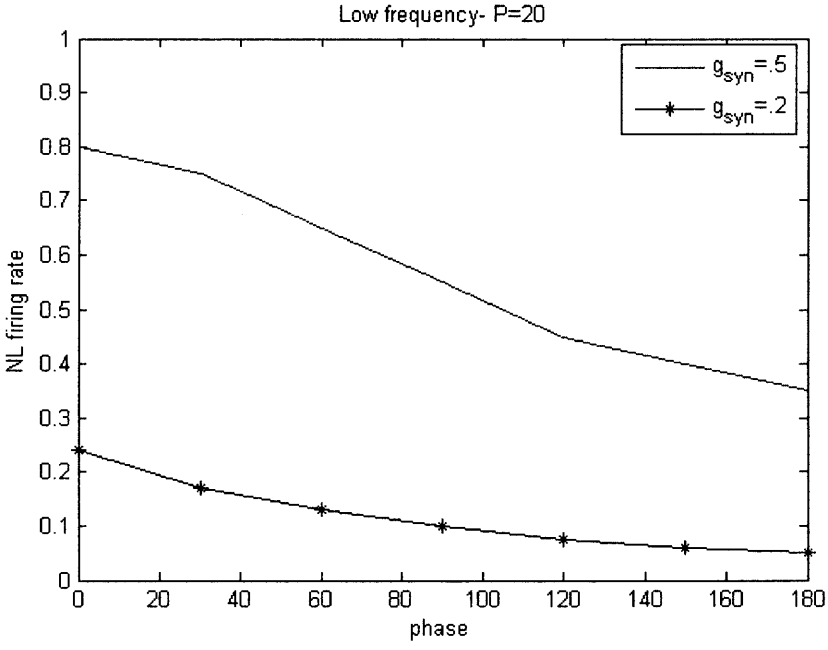

Figure 2.7 NL firing rate for low frequency NM inputs for high and low synaptic conductance: NL firing rate depends weakly on phase delays for high g_{syn}.

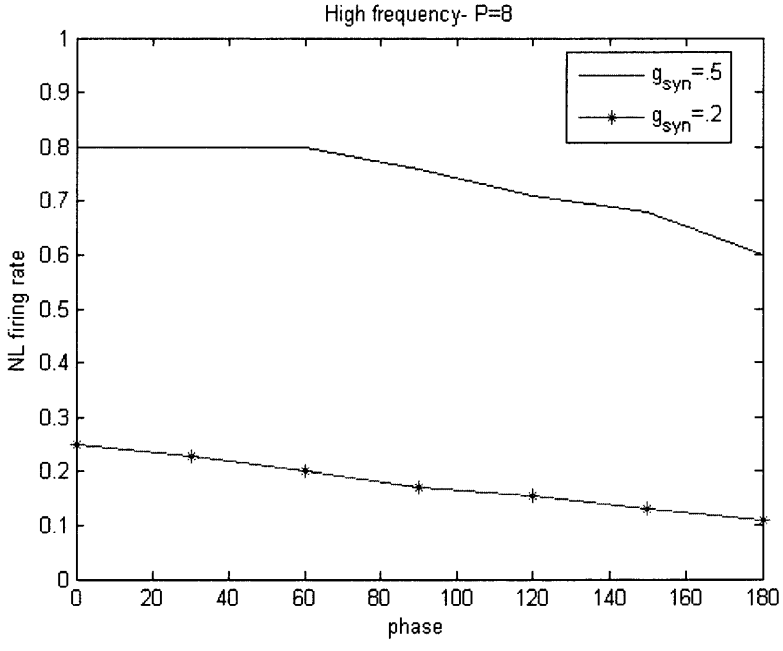

Figure 2.8 NL firing rate for high frequency NM inputs for high and low synaptic conductance: NL firing rate saturates for phase delays $< 90^o$ for high g_{syn}.

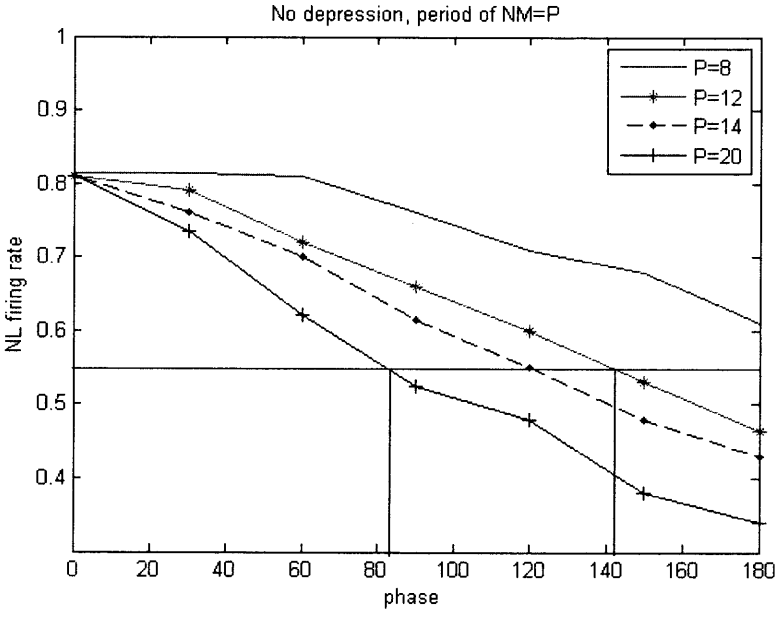

Figure 2.9 NL firing rate without depression: the firing rate curves are spread apart for different P values. The solid horizontal and vertical lines are discussed in the text. The parameter values are $g_{syn} = .5$, $\tau_k = 5$.

as in [13]. The reason for the clustering of firing rate curves in case of depression is that when we include synaptic depression, if there is high input frequency then the recovery of the NM neuron's synapse from depression is weaker. This decreases the firing rate of the NL neuron. When the NL neuron receives low input frequency there is stronger recovery of the NM neuron's synapse from depression which increases the firing rate of the NL neuron. This provides a balance of the postsynaptic response which is measured by the firing rate of the NL cell. As a result of depression, there is a decrease in the NL firing rate in spite of the high frequency inputs and we find an increase in NL firing rate during low frequency inputs.

The bird interprets these results in the following way. Whenever the NL neuron in the auditory brainstem receives sound inputs there is a corresponding firing rate associated with it. The bird transforms the rate value to a phase location in space as indicated in the Figures 2.9 and 2.10. In Figure 2.9 we have drawn a horizontal line

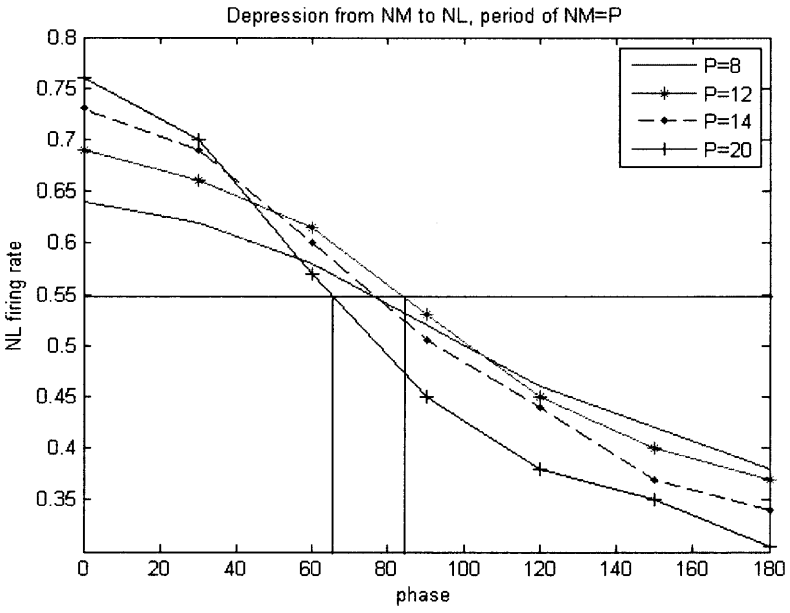

Figure 2.10 NL firing rate with depression: the firing rate curves are clustered for different P values compared to the non depressing case. The solid horizontal and vertical lines are discussed in the text. The parameter values are $g_{syn} = .5$, $\tau_k = 5$, $r = .75$, $\tau_d = 15$.

across the firing rate curves that corresponds to a certain firing rate value, namely .55. The bird interprets this value and tries to match it to a location in space which can be inferred from the x axis of phase delays in our figure. It is evident from Figure 2.9 that the value .55 corresponds to multiple locations in the phase space as indicated by two vertical lines. In this case, the range of possible phases is 82^o to 141^o. This causes ambiguity for the bird in being able to localize the sound source.

We repeat this exercise in Figure 2.10 and we can see that the firing rate value of .55 corresponds to a narrower range of phase location. Here the range of possible phase values is 63^o to 83^o. Therefore, in the case of Figure 2.10, which is obtained by including synaptic depression from NM to NL, the bird is able to locate the sound source more accurately compared to Figure 2.9. This shows how depression enhances the coincidence detecting ability of the NL cell.

To understand better how depression acts as a gain control mechanism, we

analytically quantify how the firing rate depends on phase difference, period and the parameters of depression and recovery in the following way.

In the case of no depression if NM_1(left NM cell) spikes at $t = 0$ and has decayed till $t = t_0$ and NM_2 spikes at $t = t_0$ then inputs to the NL cell are given by

$$\begin{aligned} s_2(t_0) &= 1 \\ s_1(t_0) &= e^{-t_0/\tau_k} \end{aligned}$$

where t_0 is the time lag in the inputs, and falls in the interval $[0, P/2]$. Therefore, the maximum of inputs is described by the equation

$$s_{max}(t_0) = 1 + e^{-t_0/\tau_k} \tag{2.7}$$

where s_{max} behaves as a function of P through

$$t_0 = \frac{\phi P}{360^o} \tag{2.8}$$

ϕ denotes phase delay of inputs and ranges from 0^o to 180^o. We calculate the slope of s_{max} as a function of P as given in the following equation:

$$\frac{ds_{max}}{dP} = \frac{-\phi}{360^o \tau_k} e^{-\phi P/360^o \tau_k} \tag{2.9}$$

It should be noted from equation (2.9) that $\frac{ds_{max}}{dP}$ is negative, implying that $s_{max}(t_0)$ is decreasing as a function of P. This is true in the non depressing case. This is also evident from Figure 2.11 and helps to explain the reason for the dependence of s_{max} on input periods P. In the absence of depression, a smaller s_{max} implies a lower firing rate for the NL cell.

In the case of depression, s_{max} will depend on D. We first calculate the steady state value of depression, D. We consider equations (2.4) and (2.5) that describes the dynamics of D. When the NM neuron spikes D is reset to rD where $0 < r < 1$.

To be very specific, $D(t^+)$ is equal to $rD(t^-)$ where $D(t^-)$ is determined by equation (2.5) since at t^- the NM neuron is silent and so D recovers and approaches 1 with a time constant of τ_d. Therefore, we solve for D from equation (2.5) and obtain the maximum value of D. This is the maximum steady state value of D and we name it D^*. Solving equation (2.5) with initial condition $D(0) = D_0$, we find

$$D^* = 1 - (1 - D_0)e^{-t/\tau_d} \tag{2.10}$$

At steady state we impose that $D_0 = rD^*$. We substitute for D_0 in equation (2.10) to obtain the following.

$$D^* = \frac{1 - e^{-P/\tau_d}}{1 - re^{-P/\tau_d}} \tag{2.11}$$

In this case of depression, from NM to NL, when NM_2 spikes at t_0 the synaptic input at t_0 is given by:

$$s_2(t_0) = D^* \tag{2.12}$$

If NM_1 spikes at $t = 0$ and decays until t_0, then its input at t_0 is described by:

$$s_1(t_0) = D^* e^{-t_0/\tau_k}$$

The maximum of the two synaptic inputs is then given by the following equation.

$$s^d_{max}(t_0) = D^*(1 + e^{-t_0/\tau_k}) \tag{2.13}$$

where t_0 follows equation 2.8. Figure 2.11 shows the variation of s_{max} and s^d_{max} with respect to P (over a certain range), for a fixed phase ϕ. As we can see from Figure 2.11 that for a fixed phase, s^d_{max} with depression varies less with respect to period P than the s_{max} without depression. Since firing rate a is a function of s_{max} (through

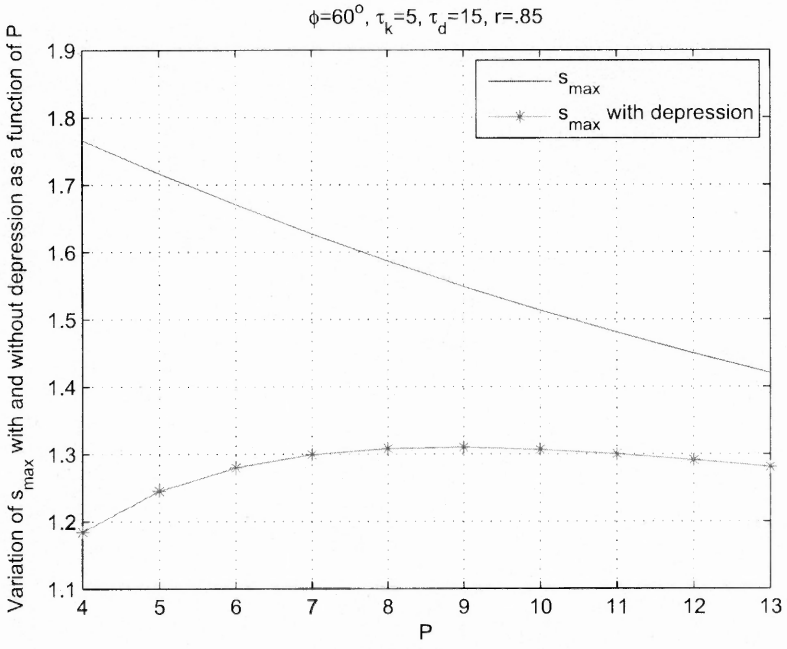

Figure 2.11 Variation in s_{max} with and without depression at $\phi = 60^o$.

equation (2.1)) it can be seen that the firing rate in this case with depression varies less as P increases. To explain why, we calculate the derivative of s^d_{max} in equation (2.13), as a function of P and obtain the following expression.

$$\begin{aligned} \frac{ds^d_{max}}{dP} &= \frac{dD^*}{dP}(1 + e^{-t0/\tau_k}) - \frac{\phi}{\tau_k} e^{-\phi P/\tau_k} D^* \\ &= \frac{(1-r)e^{-P/\tau_d}}{(1 - re^{-P/\tau_d})^2}(1 + e^{-t0/\tau_k}) - \frac{\phi}{\tau_k} e^{-\phi P/\tau_k} D^* \end{aligned} \tag{2.14}$$

It is clear from equation (2.9) that without depression s_{max} is decreasing. But with depression from equation (2.14) it can be seen that $\frac{ds^d_{max}}{dP}$ can have a zero. In general, this derivative can be made small over a range of P values as shown in Figure 2.12. We plot equations 2.9 and 2.14 in MATLAB to study their variation with respect to P, for a fixed phase ϕ. It is evident from Figure 2.12 that the curve $\frac{ds^d_{max}}{dP}$ in general; is closer to 0 compared to the curve of $\frac{ds_{max}}{dP}$.

Figures 2.13 and 2.14 are three-dimensional representation of s_{max} vs P vs ϕ for the cases of no depression and with depression respectively. We can infer from the

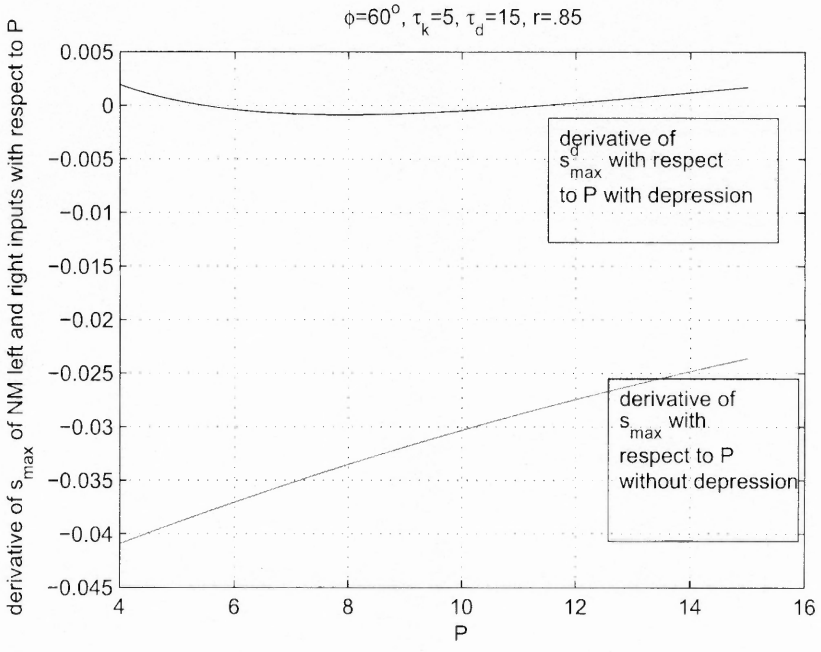

Figure 2.12 Derivative of s_{max} and s^d_{max} with respect to P.

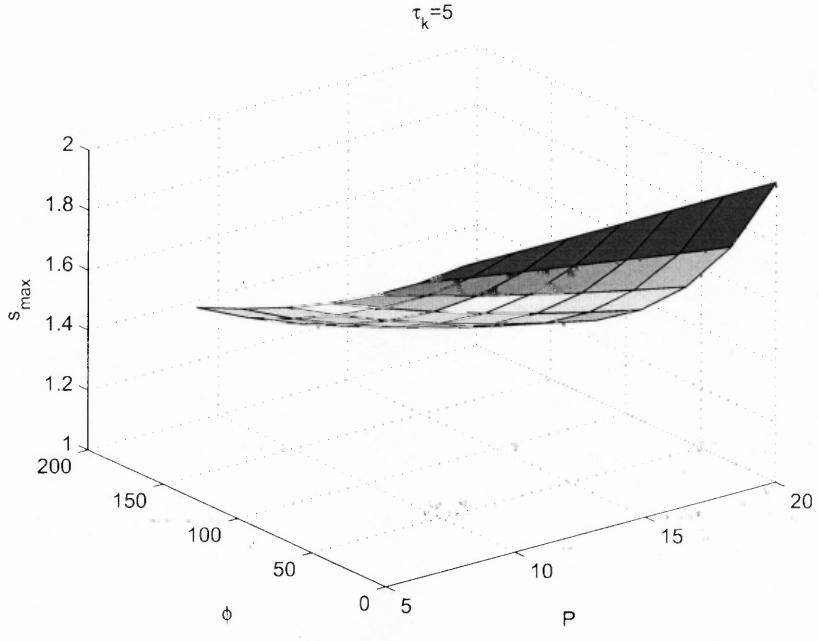

Figure 2.13 s_{max} vs P vs ϕ without depression.

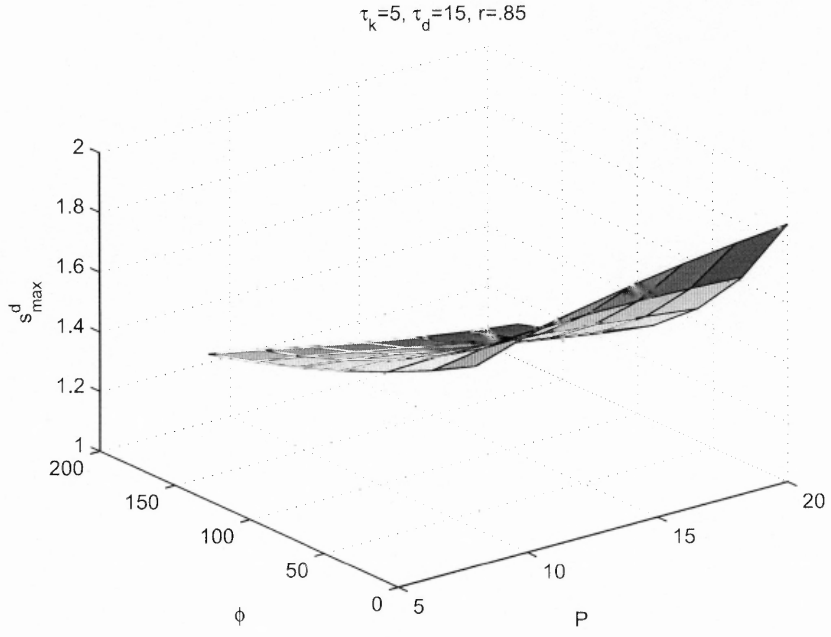

Figure 2.14 s_{max} vs P vs ϕ with depression.

Figures 2.13 that when there is no depression the s_{max} curve appears spread out both with respect to ϕ and P and the derivative of s_{max} seems to be always negative with respect to P and ϕ. In contrast, from Figure 2.14 we can observe that at least for certain range of ϕ values approximately from 90^o to 150^o and also a range of P values from 10 to 15 the s^d_{max} curve appears to be flat, compared to the non depressing case. Also we can see that there is a variation in the slope of s^d_{max} with respect to P. This shows that over a range of P values depression plays a role in making the NL firing rate curves respond more to phase delays than input frequencies.

The value of s^d_{max} and its derivatives clearly depends on a number of parameters. To get an understanding of how they may affect these quantities, consider a fixed phase delay of $\phi = 60^o$. The main parameters of interest for this model are τ_d, τ_k and r. To begin with, we discuss the role of r. It is evident from equation (2.11), that if $r = 1$ then there is no depression since the value, $D^* = 1$. For fixed values of τ_d and τ_k, if r is close to 1 then since the low frequency inputs recover strongly from

depression, there is no effect of depression. But the high frequency inputs experience the effect of depression since their recovery from depression is weaker. For instance, in our firing rate model when τ_d and τ_k are fixed and if we let $r = .85$ then the range of periods for which the s^d_{max} curve is almost independent of P lies between $[4, 12]$. But if we let $r = .7$, then the depression affects lower frequency inputs because the high frequency inputs are in a highly depressed state as r decreases. In this case, the range of periods for which s^d_{max} remains nearly constant is $P \in [8, 30]$.

Next, we fix r and τ_k and vary τ_d. In the extreme cases, if $\tau_d \to \infty$, then from equation (2.11), $D^* \to 0$ which implies that the NM synapses are in the depressed state for a very long time and therefore, have no chance of recovery. On the other hand if $\tau_d \to 0$, equation (2.11) gives us that $D^* \to 1$ which indicates there is no depression. However it should be noted that there exists an interplay between the parameters r and τ_d. If r is very close to 1 then a larger value of τ_d is required for the lower frequency NM inputs to experience the effect of depression. Similarly if the value of r is smaller, in order for the depression to take effect on the high frequency NM inputs, a smaller value of τ_d is required. Therefore, smaller values of τ_d affect only high frequency inputs since the depression variable recovers quickly and larger values of τ_d affect low frequency inputs since the depression variable takes more time to recover. For example if $\tau_d = 15$ for fixed values of $r = .85$ and $\tau_k = 5$ the s^d_{max} curve remains nearly constant for values of P in the range of $[4, 12]$. If τ_d is increased to 30 for the same fixed values of r and τ_k, we observe that the range of P for which the s^d_{max} curve is almost constant as a function of P has shifted and lies between $[10, 22]$.

Finally, we fix r and τ_d and look at the effect that the parameter τ_k has on the clustering of the NL firing rate curves. In extreme conditions, if $\tau_k \to \infty$ then the value of s_{max} equals two and it is proportional to D^* and if $\tau_k \to 0$ then s^d_{max} is equal to D^*. As it is evident in both the cases, the s^d_{max} curve cannot be independent

of P since s^d_{max} is proportional to the depression variable alone. In other words small values of τ_k for large P values are not preferred since the synapse in this case decays too quickly and P remains in the silent state for a long time. Similarly if the P values are small and in comparison, if τ_k value is too large then the synapse does not decay at all and remains always close to 2. Therefore, intermediate values of τ_k are required such that s^d_{max} remains constant over a range of values of P.

From this discussion it is evident that the simple firing rate model gives us a good insight about the role played by these parameters in promoting the clustering of NL firing rate curves by making them frequency independent and more phase dependent. We can perform similar study of the role of these parameters for any other phase value as well as shown in our three dimensional figures.

Although by observation it is evident that, Figure 2.10 exhibits more clustering and is mostly frequency independent compared to Figure 2.9, we wish to quantify the firing rate curves in both these cases. To do that, we used straightforward statistical techniques. In both the figures, samples were taken at every 30^o of phase values ranging from 0^o through 180^o. We took the averages of all the four firing rate values at every sample value which is given in the following expression.

$$\begin{aligned} \overline{a(i)} &= \sum \frac{(a_\infty(I_{eff}))}{n} \\ &= \sum_{i=1}^{n} \frac{1}{(1+e^{-(g_{syn}D^*(1+e^{-\phi P_i/\tau_k})-\alpha)/k_a})n} \end{aligned} \tag{2.15}$$

In our case, $n = 4$ since we have four firing rate curves, for each of the seven sample ϕ values, in Figures 9 and 10. In our calculations $D^* = 1$ when there is no depression and D^* equals the value of the expression in equation (2.11) when there is depression. Thus we obtain an averaged firing rate curve with averaged value, $\overline{a(i)}$ for each of the value of phase difference, ϕ.

We next compute the standard deviation of these values from those corresponding

values on the averaged curve at every sample phase value, given by equation (2.16)

$$\sigma(j) = \sqrt{\frac{1}{n}\sum_{i=1}^{n}(\frac{1}{(1+e^{-(g_{syn}D^*(1+e^{-\phi P_i/\tau_k})-\alpha)/k_a})} - \overline{a(i)})^2} \tag{2.16}$$

where $j = 1, ..7$. Each count of j corresponds to every sample phase value, ϕ. Therefore, this calculation provides us with 7 standard deviation values at each value of ϕ. Following this, we find the coefficient of variation, $C.V.$ given by

$$C.V. = \frac{S}{\bar{X}}100 \tag{2.17}$$

where S and $\bar{X}$ are the pooled standard deviation and pooled mean of the data from our population. The pooled mean $\bar{X}$ and variance S^2 are calculated in the following way.

$$\begin{aligned} \bar{X} &= \frac{1}{7}\sum_{j=1}^{7}\bar{a}(j) \\ S^2 &= \frac{1}{7}(\sum_{j=1}^{7}\sigma(j)^2 + \sum_{j=1}^{7}(\bar{a}(j) - \bar{X})^2) \end{aligned} \tag{2.18}$$

Standard deviation, S is the square root of variance S^2. It turns out that $C.V. = 6.88$ for Figure 2.10 with depression and $C.V. = 13.5$ for Figure 2.9 in the no depression case. Since $6.88 \leq 13.5$, we can see that the firing rate curves in the case of depression are more clustered than when there is no depression. It should be noted that we can also explore the dependence of $C.V.$ on the parameters of interest.

We now study the network in Figure 2.6 with a spiking model namely the integrate and fire model. The equation describing the dynamics of the NL neuron is

$$\frac{dv}{dt} = I - v - g[s_1 + s_2][v - E_{syn}] \tag{2.19}$$

When $v(t^-) = 1$, the neuron spikes and we reset $v(t^+) = 0$. Again we would like to calculate the firing rate of the NL cell. This requires us to solve for the unknown

spike times for a given period of NM input P. The way we compute the firing rate of NL is the following. We fix an upper bound for the interspike interval called $\overline{isi}$ and determine all NL spikes denoted by m whose interspike intervals, isi, are less than $\overline{isi}$. We calculate the interburst frequency where the spikes are considered to be in a burst only if $isi < \overline{isi}$. Therefore, the firing rate is then defined as

$$f.r. = \frac{m}{\sum isi} \tag{2.20}$$

such that $isi < \overline{isi}$.

We denote the sum of synaptic inputs by $s(t) = s_1(t) + s_2(t)$ where $s_1(t)$ and $s_2(t)$ behave in the following way in the case of no depression:
For $t < t_0$

$$\begin{aligned} s_1(t) &= e^{-t/\tau_k} \\ s_2(t) &= e^{-(P-t_0)/\tau_k} e^{-t/\tau_k} \end{aligned}$$

and if $t > t_0$

$$\begin{aligned} s_1(t) &= e^{-t/\tau_k} \\ s_2(t) &= e^{-(t-t_0)/\tau_k} \end{aligned}$$

where $t_0 \in [0, P/2]$. The term, $e^{-(P-t_0)/\tau_k}$ in the expression of $s_2(t)$ when $t < t_0$ denotes the transient of the input from the previous cycle. In other words, our expression for both s_1 and s_2 are considered when the synapse has reached steady state. We choose s_2 to equal $e^{-(t-t_0)/\tau_k}$ when $t > t_0$ to indicate that at $t = t_0$, $s_2 = 1$. We solve for the first spike time, denoted t_1. Using the integrating factor method [50], imposing that a spike occurs when $v(t_1) = 1$ with $v(0) = 0$ we first obtain,

$$ve^{\int_0^{t_1}(1+g(s_1(t)+s_2(t)))dt} = \int_0^{t_1} (I + g(s_1(t) + s_2(t))E_{syn}) e^{\int_0^{t_1}(1+g(s_1(t)+s_2(t)))dt} dt \tag{2.21}$$

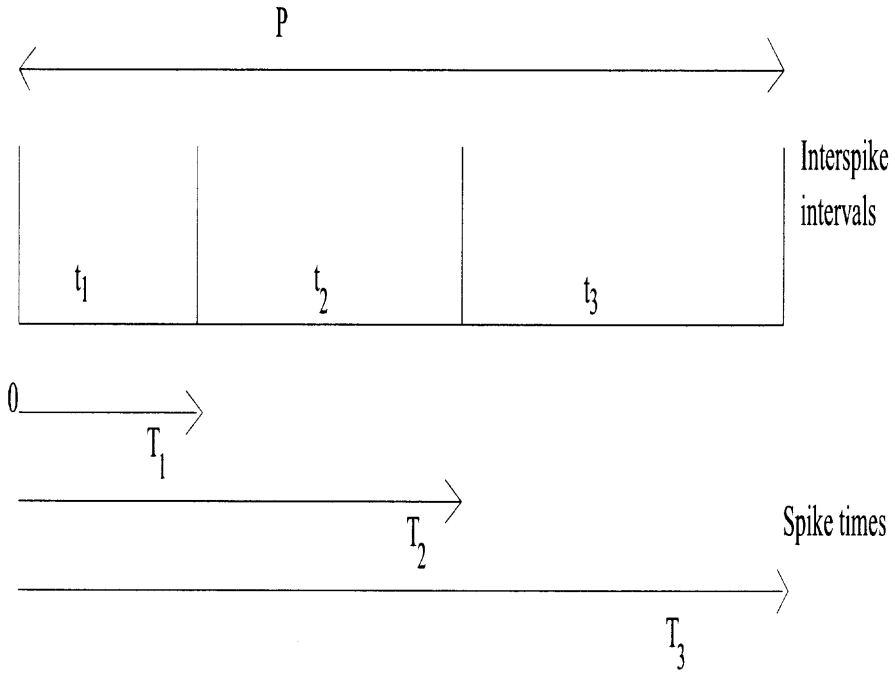

Figure 2.15 Spike times and interspike intervals.

Rearranging terms, we obtain the following expression:

$$(1-I)(e^{t_1-g\tau_k e^{-t_1/\tau_k}})+Ie^{-g\tau_k}=gE\int_0^{t_1}e^{-t/\tau_k}e^{t-g\tau_k e^{-t/\tau_k}}dt \tag{2.22}$$

where $E = E_{syn} - I$. The LHS and RHS of (2.22) each define curves that can be plotted as a function of t_1. At their intersection we obtain the value t_1 corresponding to the first NL spike time. Then we update for t_1 in equation (2.22) in the following way. We take into consideration the amount of time for which the synaptic input has decayed, we let $s(0) = e^{-t_1/\tau_k}$. We then solve for the next spike time t_2 by setting $v(0) = 0$ and $v(t_2) = 1$. After solving for t_2, we can solve for t_3 by setting $v(0) = 0$, $v(t_3) = 1$, $s(0) = e^{-(t_1+t_2)/\tau_k}$ and so on. The times t_1, t_2 and t_3 etc. are all interspike intervals. In other words the next spike time is $T_2 = t_1 + t_2$ implying that the second $isi = t_2$. We compute the n^{th} interspike interval t_n until $t_1 + t_2 + ... + t_{n+1} > P$ or until $t_j > \overline{isi}$ for some j as shown in Figure 2.15. We then compute the firing

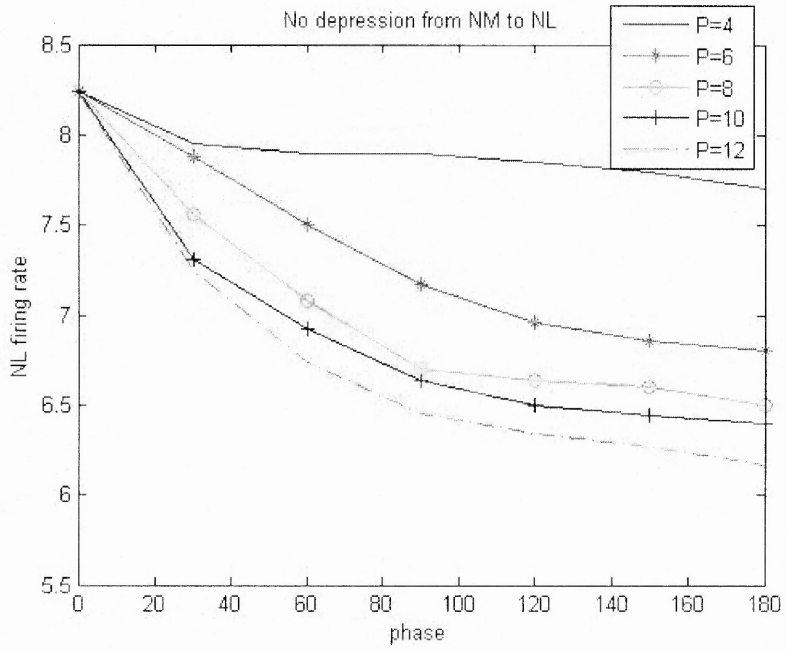

Figure 2.16 NL firing rate without depression: firing rate curves are spread apart. MATLAB simulation for the parameter value of $\tau_k = 4$.

rate using (2.20). We used this procedure to numerically solve for the spike times using MATLAB. Figure 2.16 shows the phase vs NL firing rate relationship without depression. In this figure we can see that the firing rate curves plotted for various NM periodic input P values are spread apart. Especially for high frequency NM inputs(low P) values like $P = 4$, it is evident from the figure that the NL firing rate is weakly dependent on the phase delays.

In the case of depression from NM to NL, the synapses $s_1(t)$ and $s_2(t)$ obey the following equations: For $t < t_0$

$$\begin{aligned} s_1(t) &= D^* e^{-t/\tau_k} \\ s_2(t) &= D^* e^{-(P-t_0)/\tau_k} e^{-t/\tau_k} \end{aligned}$$

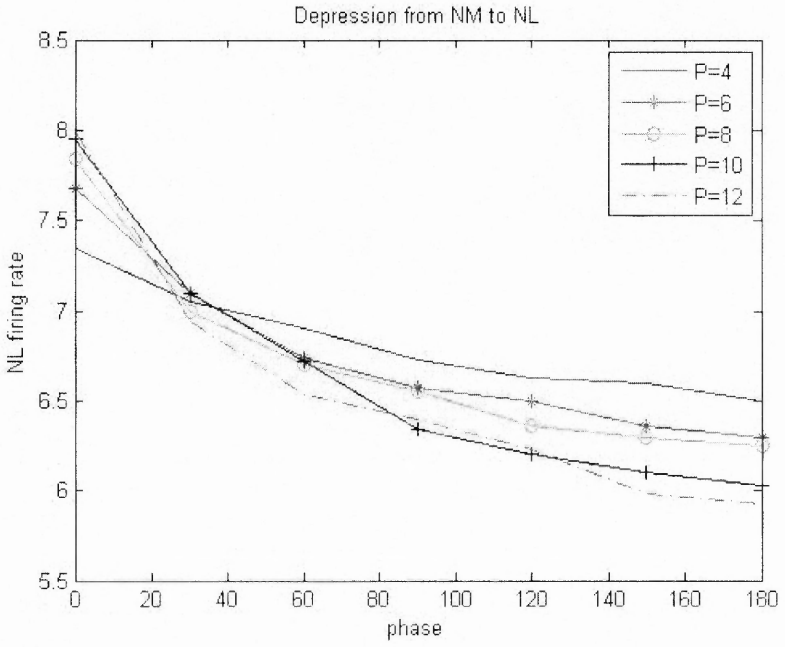

Figure 2.17 NL firing rate with depression: firing rate curves are clustered and are more phase dependent. MATLAB simulation for parameter values of $\tau_k = 4$, $r = .92$ and $\tau_d = 15$.

and if $t > t_0$

$$s_1(t) = D^* e^{-t/\tau_k}$$

$$s_2(t) = D^* e^{-(t-t_0)/\tau_k}$$

where D^* denotes the maximum (steady state) value of depression as described in equation (2.11). Figure 2.17 illustrates the NL firing rate curve when there is depression from NM to NL. From these two Figures 2.16 and 2.17 it is evident that the firing rate curves in the case of depression are clustered and therefore, behave more as a function of phase and less dependent on the input frequencies. We performed similar statistical analysis using equations (2.15)-(2.17), on these curves to show that depression enhances coincidence detection by making NL firing rate curves behave as a function of phase and less dependent on input frequencies. The coefficient of variation $C.V. = 8.82$ in the non-depressing case while in the case with depression

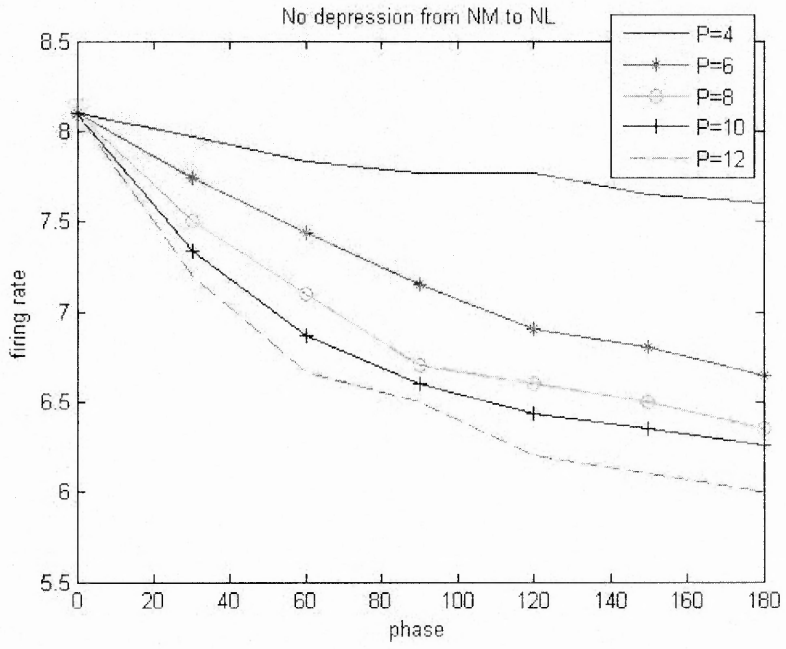

Figure 2.18 NL firing rate without depression: firing rate curves are spread apart. XPP simulation for $\tau_k = 4$.

$C.V. = 5.45$. Clearly since $5.45 < 8.82$, the firing rate curves are more clustered in the case when there is depression from NM to NL than the no depression case.

We have also performed simulations with the no depression and depression cases from NM to NL using XPP with the same set of parameters that we used in MATLAB. Figures 2.18 and 2.19 are from our simulations for both the cases. The coefficient of variation in Figure 2.18 and 2.19 are 8.84 and 5.49, respectively. Again we can conclude that in the case of depression, firing rate curves display more clustering than the non-depressing case.

The coefficient of variation analysis indicates that our simulation results from XPP qualitatively agree with the MATLAB results. Similar to our firing rate model, parameter estimations for r, τ_d, τ_k can be made for this model also, which affect the firing rate curves of the NL in the same way.

As mentioned earlier, when $r = 1$ equation (2.11) shows $D^* = 1$ which implies there is no depression. For fixed values of $\tau_d = 15$ and $\tau_k = 4$, when $r = .92$ we obtain

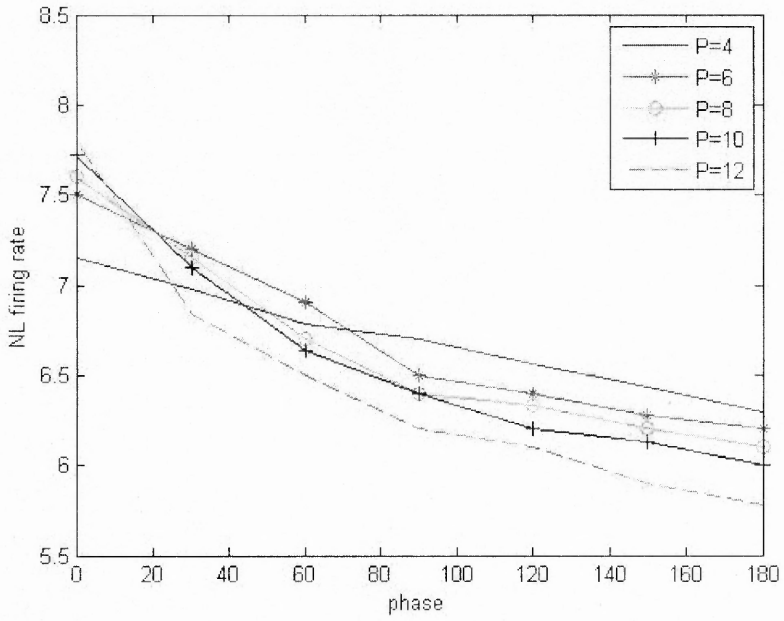

Figure 2.19 NL firing rate with depression: firing rate curves are clustered. XPP simulation for $\tau_k = 4$, $r = .92$ and $\tau_d = 15$.

Figure 2.19 where there is clustering of firing rate curves for $P \in [4, 12]$. If we decrease r to equal .83 for the same fixed values of τ_d and τ_k, the firing rate curves cluster for $P \in [10, 20]$. This is because, when r is closer to one, since the low frequency NM inputs recover strongly from depression, they do not feel the effect of depression. But in this case, since the high frequency NM inputs exhibit weak recovery from depression, they experience the effect of depression which leads to suppression of the net synaptic strength over an input period P. Since the period of NL spike is effectively a function of this synaptic strength $s(t)$, from (2.22) this leads to reduction in the number of NL spikes over a summation of interspike intervals which is less than P, see (2.1). In other words, the firing rate of NL is reduced for all the high frequency periods in a certain range. This leads to clustering of NL firing rate curves for high frequency NM inputs when $r = .92$, for fixed τ_d and τ_k.

On the other hand, when $r = .83$ the high frequency NM inputs are highly depressed and unable to recover from depression. But since the low frequency NM

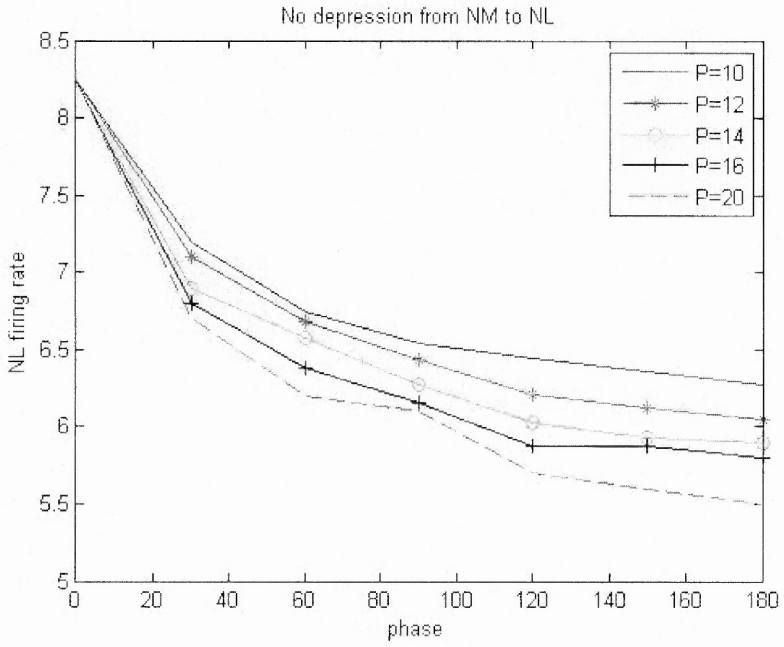

Figure 2.20 NL firing rate without depression: firing rate curves are spread apart. MATLAB simulation for $\tau_k = 4$.

inputs recover strongly from depression, their effective synaptic strength increases when compared to the non depressing case. Again from equation (2.22), since the NL firing rate is a function of the net synaptic strength $s(t)$, there is an increase in the NL firing rate over low frequency NM input periods in a certain range. Therefore, we find clustering of NL firing rate curves for higher NM period(low frequency) values, in this case. This is illustrated in Figures 2.20 and 2.21

Next, we explore the effects of varying τ_d and fixing the other parameters in our simulations. As per our earlier discussion using the firing rate model, in the extreme case when $\tau_d \to \infty$ from equation (2.11) we obtain $D^* \to 0$. This means there is too much depression and the NM inputs are always depressed and have no chance to recover. Also when, $\tau_d \to 0$, equation (2.11) gives us $D^* \to 1$ which implies existence of no depression. If we fix $r = .93$, $\tau_k = 4$ and let $\tau_d = 15$, then as described earlier, we obtain clustering of NL firing rate curves for $P \in [4, 12]$. Now if we let $\tau_d = 30$ there is clustering of firing rate curves for $P \in [14, 22]$. Here the interplay

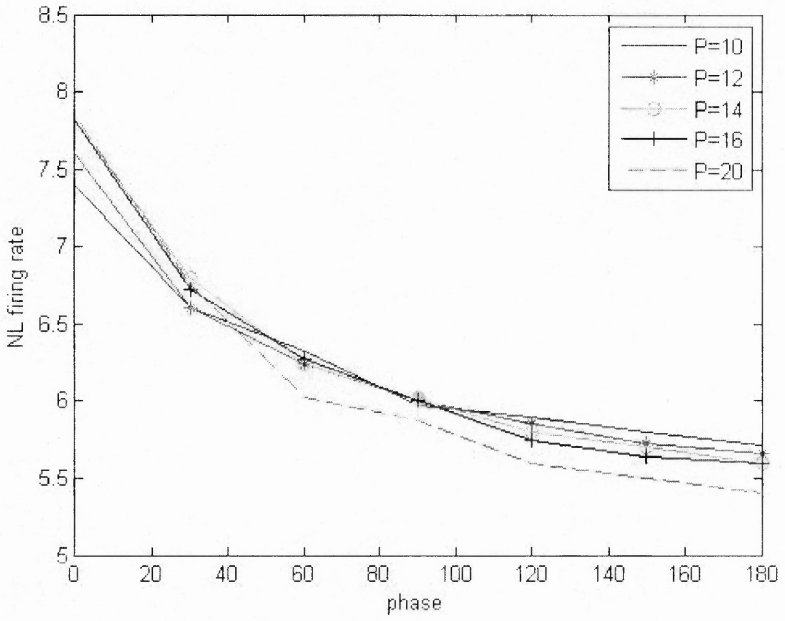

Figure 2.21 NL firing rate with depression: clustering of firing rate curves. MATLAB simulation for $r = .83$, $\tau_k = 4$ and $\tau_d = 15$.

between r and τ_d plays an important role in formation of the clustering of firing rate curves. If we let r be close to one then we require a large value of τ_d for the lower frequency NM synapses to experience the effect of depression. In contrast, if value of r is chosen to be smaller, then a smaller value of τ_d is needed so that depression can affect the higher frequency NM inputs.

Finally, we fix r and τ_d and investigate the effect of τ_k on the clustering of the firing rate curves. For extreme cases, when $\tau_k \to 0$ then both $s_1(t)$ and $s_2(t)$ approaches 0 which nullifies their strengths. Similarly if $\tau_k \to \infty$ then $s_1(t)$ and $s_2(t)$ are proportional to D^*. So it is obvious that in these cases we cannot get the NL firing rates to be independent of input periods, P. Therefore, this implies that for large values of P we cannot let τ_k to be small, since this makes the synapse to decay quickly. As a result of this, the synapse remains in the silent state for a longer time thus not being able to experience the effect of depression. Similarly for small P values, large τ_k values are not preferred since the synapse hardly decays and always

remains close to D^*. So from this analysis it is evident that intermediate values of τ_k are required so that the synaptic input variables $s_i(t)$, $i = 1, 2$ feel the effect of depression.

2.1.2 Conclusions

From both these models, the firing rate and integrate and fire, it is obvious that in the absence of plasticity from the NM synapse to NL, the firing rate is more input frequency dependent and less dependent on phase delay. The inclusion of depression from the NM input to NL presents a gain control mechanism by which clustering of these firing rate curves are obtained. This makes them more dependent on the phase delays thereby enhancing the coincidence detecting ability of the NL neurons.

CHAPTER 3

INHIBITION FROM SON TO NM

In this chapter, we will explore the inhibitory effects of SON onto the NM cells. Rubel et al. [35] have studied the role of GABAergic terminals in the NM and NL neurons and showed that they originate from the superior olivary nucleus (SON). The SON is located in the ventrolateral region of the avian brainstem and receives excitatory inputs from NA and NL. SON sends inhibitory synapse onto NA, NL and NM. The SON cells exhibit a high degree of functional homogeneity. SON cells are excited by stimulation of the fiber tracts from the NL and NA neurons.

The SON morphology shows extensive dendritic arborization within its nucleus when compared to the NM and NL neurons. In the SON, the excitatory synaptic potentials are slow in comparison with the EPSPs of NM and NL cells [69]. Findings in [35] suggest that the NM, NL and NA neurons may be affected by two type of inhibitory neurons- the local interneurons and the SON. They observed that the existence of a unilateral connectivity between SON with NM, NA and NL cells influenced the NM and NL neuronal physiology. Particularly when there is increase in the activity of the NA cell, it could augment the GABAergic SON's effect on both the NM and NL cells. This leads to a relatively new belief that binaural information processing could be more dependent on intensity cues as well.

The NM neurons relay phase-locked inputs to the NL cells for binaural coincidence detection. There have been many studies to reveal the physiological and anatomical properties of the NM neurons which makes them suited for this purpose. It has been shown in [62] that NM receives depolarizing GABAergic input from SON by performing experiments in chick brainstem slices that were taken between the embryonic day and few days, post hatching. But Trussell et. al [62] suggests that even if

GABAergic inhibition is depolarizing, IPSPs may still be inhibitory if their net effect is to suppress the excitatory signals without themselves generating excitation. The NM-NL-SON-NA network is modeled by Dasike et al. [14] using leaky integrate-and-fire neuron for all the individual cells. They suggest that SON is suited to perform gain control. In [14], the depolarizing effect of SON has been specified in an indirect way by decreasing membrane time constant and increasing voltage threshold in their model cells without directly changing the membrane voltage. In spite of including the depolarizing effects of SON, results in [14] demonstrate that the net effect of SON on NM is inhibitory and moves the NM cells away from threshold.

Despite all this work on understanding the effects of SON, the role of SON inhibition in enhancing coincidence detection has not been fully explored. To support this theory of inhibition improving coincidence detecting ability of NL cells, studies in [40], [69] demonstrate that the strength of SON input to NM is proportional to the amount of NM excitation. These discoveries are consistent with the fact that SON plays the role of a gain control mechanism suggested in [44], [35], [61].

One theory is that during cases of input bias, multiple axons could deliver afferent impulses, to each coincidence detector neuron [44]. These signals could arrive at the NL cell simultaneously and could pose problems for the coincidence detecting system. This is because when there is high afferent impulse rate, it increases the chance of same-side coincidence which the NL cell may fail to distinguish in comparison to binaural coincident inputs [44]. The other theory is that in the absence of inhibition when there are biased high sound levels each NM neuron on one side of the brain is strongly excited. This causes an increase of each NM firing rate, on the side with biased input and this leads to stronger drive among the NL neurons on that side, causing "false alarms" among the NL neurons [61]. Rubel et. al [61], suggest that coincident firing of NMs from one side alone is enough to evoke action potentials in the NL neurons, which deteriorates the ability of NL cell in discriminating between

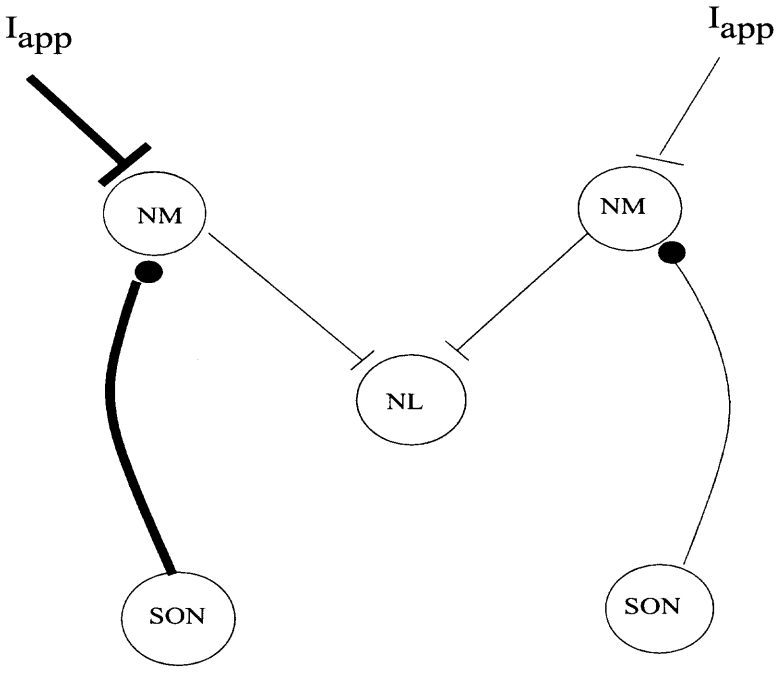

Figure 3.1 SON-NM-NL network with inhibition. The input to left NM is stronger than the right side. Thick lines (connections) on the left indicate NM is driven strongly compared to the right NM.

strong unilateral excitation vs binaural coincidence. It has been suggested that SON inhibition can serve as a mechanism in preventing strong monaural excitation. This is also due to the fact that, the amount of SON input is proportional to the excitatory drive that the NM neurons receive. Thus SON plays a role in suppressing too much excitation on one side due to input bias and thereby balances the NM firing rate on both sides [69]. This implies the potential for an alternate mechanism to make the NL firing rate mainly phase dependent, namely that SON inhibition may narrow the frequency range of NM cells, even when there is input bias without the presence of synaptic depression from NM to NL.

The existence of reciprocal SON innervations shown in [35], [24] implies that inhibition on each side is not entirely independent. But for our purposes we consider a simplified model as shown in Figure 3.1 where we investigate the role of SON inhibition in suppressing excessive NM activity by modulating NM frequency on one

side during input bias and how that affects coincidence detecting ability of the NL neurons. This will be explored in two different ways: 1) With equal NM frequency, 2) With unequal NM frequency.

3.1 Model

To study this problem, we introduce SON on both the sides of the brainstem. The SONs send inhibition onto the NM cells corresponding to the left and right NM neurons which synapse onto the NL neurons, as shown in Figure 3.1.

Although much is known regarding the NM-SON-NL circuitry, much remains open. For example, the firing frequency relationship between the NM and SON neurons and the timing of these SON inputs to the NM cells has yet to be empirically categorized. We make an assumption regarding the timing of the SON and NM inputs. Our goal is to show that this assumption aids in making NL a better coincidence detector.

Assumption:

SON fires n times every time a NM neuron spikes. We arbitrarily choose $n = 3$.

This assumption indicates the strength of the SON synapse onto the NM cell. The choice of the ratio of number of SON spikes to NM spike is random. Therefore, the SON synaptic strength based on n number of spikes can be adjusted by our choice of parameters namely $\tau_s and g_{son}$ which will be discussed in the latter part of this section. We let the variable s denote the synaptic input from the SON. When SON spikes, $s = 1$ and between spikes s is described by

$$\frac{ds}{dt} = \frac{-s}{\tau_s} \tag{3.1}$$

We use the following integrate and fire equation to describe the activity of the NM cell,

$$\frac{dv_{nm}}{dt} = I - v_{nm} - g_{son} s[v_{nm} - E_{inh}] \tag{3.2}$$

where I denotes the input applied current, g_{son} denotes the maximum synaptic conductance variable and s denotes the inhibitory synaptic input to the NM cell. E_{inh} is the reversal potential of the synaptic current. An increase in the SON inhibitory input decreases the firing rate of NM cell. The strength of SON inhibition in the network of the auditory brainstem is proportional to the amount of excitatory drive that the NM receives [61], this implies that the frequency of SON also increases. The way we incorporate this in our model is by letting the timing of SON inputs to NM be an inverse function of I. In other words, if I increases, then there is tighter discharge of SON inputs since the times relative to NM firing time at which the SON inputs synapse onto NM are a decreasing function of I.

In our model since we have arbitrarily chosen three SON inputs per NM input, the synaptic variable satisfies the following equation.

$$s(t) = \begin{cases} 0 & [0,t_1] \\ e^{-(t-t_1)/\tau_s} & [t_1,\, t_2] \\ e^{-(t-t_2)/\tau_s} & [t_2,\, t_3] \\ e^{-(t-t_3)/\tau_s} & \text{else} \end{cases}$$

Here t_1, t_2 and t_3 are discharge times of the SON spikes. We arbitrarily choose $t_1 = .1$, t_2 and t_3 to be inverse functions of I in the following way: $t_1 = \frac{1}{e^{I^2}}$ and $t_2 = \frac{2}{e^{I^2}}$. Figure 3.2 shows a plot of s. As we can see, from Figure 3.2 that to begin with, $s = 0$. At $t = t_1$, $s(t^+) = 1$. After t_1^+, s decays towards 0. This is followed by another reset of s to 1 at $t = t_2$. Again after t_2^+, s decays towards 0 until $t = t_3$. At $t = t_3$, s has similar reset to 1 following which it decays.

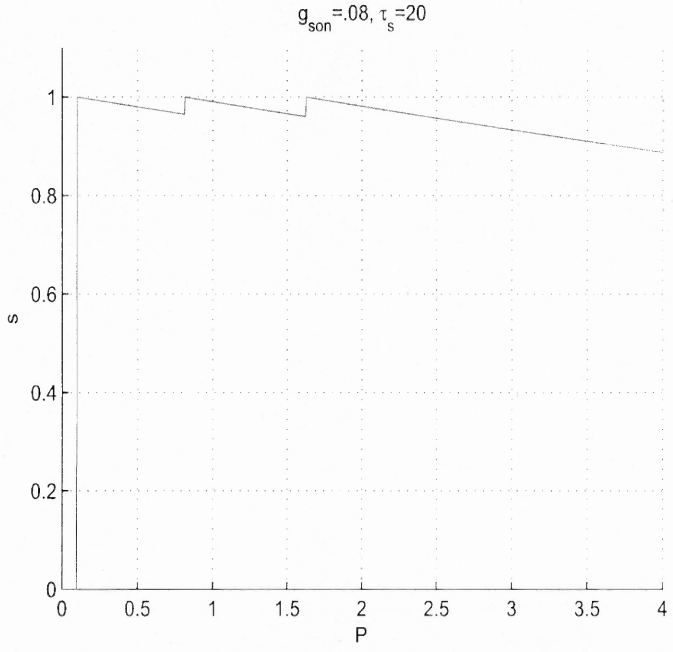

Figure 3.2 Plot of SON inhibition; there are 3 SON spikes. For every SON spike, s is reset to 1 following which, s decays.

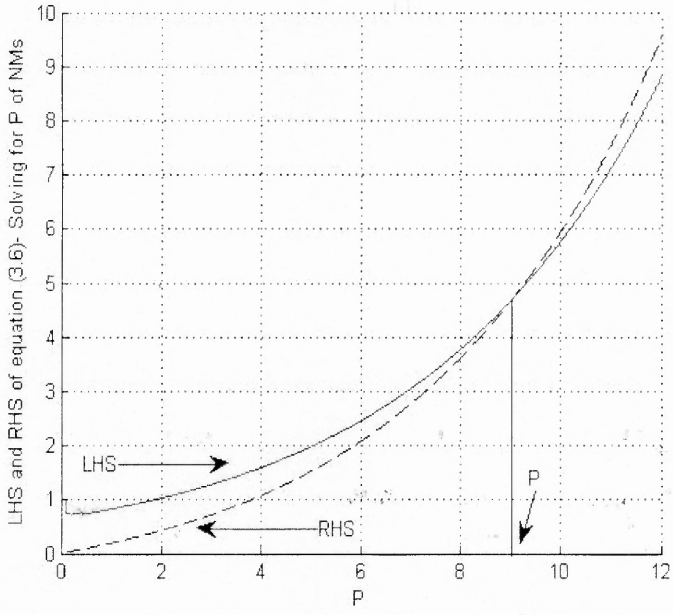

Figure 3.3 Solving for P; intersection of left hand side and right hand side of equation (3.4).

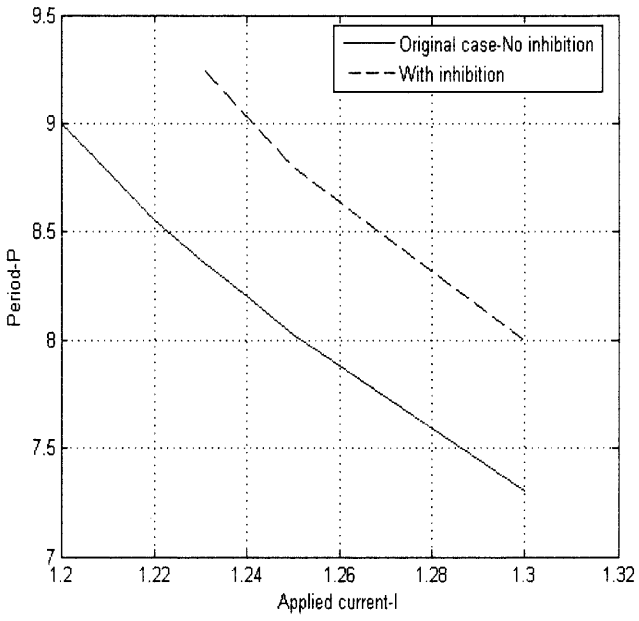

Figure 3.4 Period 'P' as a function of applied current with and without inhibition. In the case with inhibition, as current I increases, inhibition delays NM period for currents ranging from (1.2 to 1.3) to lie within $[8, 9.26]$ compared to the no inhibition case where $P \in [7.3, 9]$.

3.1.1 Role of Inhibition from SON to NM

From equation (3.2), we solve for v_{nm} using the integrating factor method, imposing the fact that $v_{nm}(P) = 1$ and $v_{nm}(0) = 0$ we obtain the following expression,

$$v_{nm} e^{\int_0^P (1+g_{son}s(\hat{P}))d\hat{P}} = I \int_0^P e^{\hat{P}-g_{son}\tau_s e^{-\hat{P}/\tau_s}} d\hat{P} \tag{3.3}$$

After simplifying, we can reduce equation (3.3) to the following.

$$e^{P-g_{son}\tau_s e^{-P/\tau_s}} = I \int_0^P e^{\hat{P}-g_{son}\tau_s e^{-\hat{P}/\tau_s}} d\hat{P} \tag{3.4}$$

In (3.4), the only unknown is P the period of a NM spike. We would like to know how it depends on I. We numerically solve (3.4) using MATLAB. Figure 3.4 shows a graph of the LHS vs the RHS of the equation. Clearly in the no inhibition case, as the applied current increases the frequency of NM firing increases, in other words P decreases.

This can actually be seen from equation (3.4) from the following calculation. If there is no SON inhibition then $g_{son} = 0$, in equation (3.4). Therefore, equation (3.4) reduces to

$$e^P = I \int_0^P e^{\hat{P}} d\hat{P} \tag{3.5}$$

Solving equation (3.5) we obtain

$$P = ln \frac{I}{I-1} \tag{3.6}$$

As we can see from equation (3.6) that as I increases, P decreases. But when SON inhibition to NM is introduced, the NM activity is suppressed, which delays the period of NM cells for a range of applied currents, for a given set of parameters. In other words when there is inhibition in the network, it succeeds in preventing the NM cells from responding with increased excitability to a range of high intensity inputs as illustrated in Figure 3.4. Without inhibition when applied current is increased, we see a decrease in the period P of NM or in other words, increase in NM firing frequency. P value here ranges from [7.3,9]. We are interested in investigating if we can minimize this range of P for increases in applied current, by introducing inhibition. For our purpose, we fix the reference period to be $P = 9$. We are interested in determining the appropriate parameter regimes which will provide us with a range of P (with SON inhibition) that is very close to $P = 9$.

When SON inhibition with $g_{son} = .08$, is included for applied currents in the interval $[1.23, 1.3]$, from Figure 3.4 we can see that it has succeeded in reducing the firing frequency range of NM and therefore, the period P lies between $[8, 9.3]$. It should be noted that, when $g_{son} = .04$, $P \in [7.6, 8.75]$ for the same range of applied currents as the previous case. The cases of two different g_{son} are presented here to illustrate that parameters play an important part in determining the range of NM firing frequencies in the presence of inhibition. The role of other key parameters will

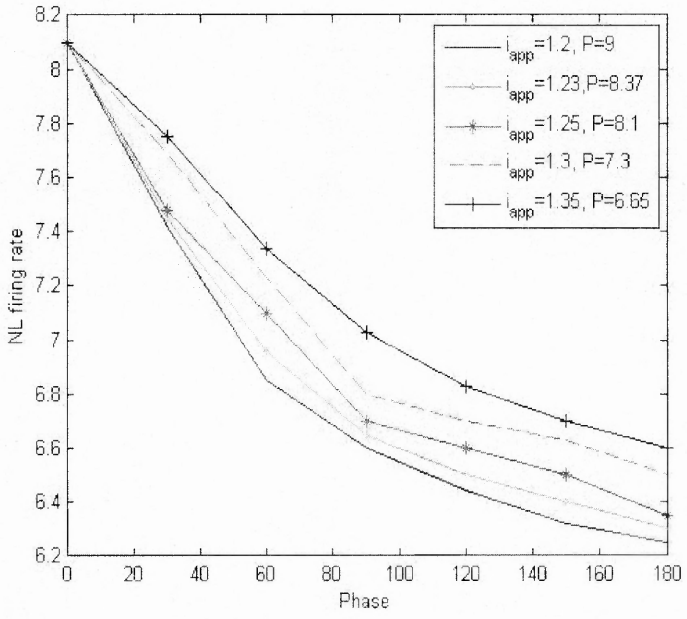

Figure 3.5 NL firing rate for various applied currents to both NM cells-no SON inhibition. XPP simulation with $g_{son} = 0$.

be discussed at the end of this section.

We modeled the network shown in Figure 3.1 in XPP, using integrate and fire neurons for the NM and NL cells. The SON inhibitory input is described as in equation (??). First, we calculated the firing rate of the NL cell by applying equal applied currents to both NMs in the absence of SON inhibition. We then studied how P changes with I as shown in Figure 3.5. Then we introduced inhibition from SON to NM cells and calculated the firing rate of the NL cell, as shown in Figure 3.6. It can be seen from Figure 3.5 that in the absence of inhibition when increased current is applied to both the NM cells, their excitability increases. This leads to an increase in the NL firing rate and the curves are spread apart. In contrast, from Figure 3.6 it is evident that in the presence of inhibition, the NM cells' activity is suppressed and as applied current is increased the overall range of their firing frequencies is reduced, for the given set of parameters. This leads to clustering of NL firing rate curves. When there is no inhibition, for increasing applied current values lying in $[1.2, 1.35]$,

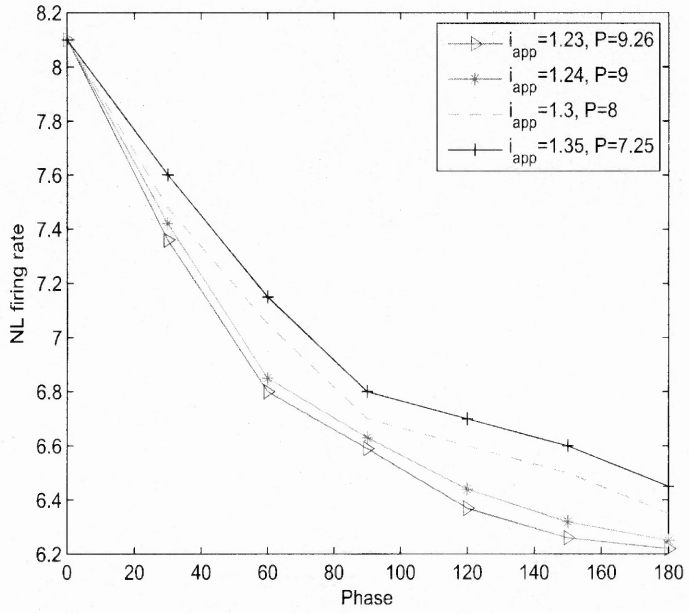

Figure 3.6 NL firing rate for various applied currents to both NM cells-with inhibition. XPP simulation for $g_{son} = .08$ and $\tau_s = 20$.

$P \in [6.65, 9]$. But when we introduce inhibition we obtain a narrower NM period range of $[7.25, 9.26]$. Particularly at $I = 1.24$, the period is larger, $P = 9$ (as opposed to $P = 8$ in the original case from Figure 3.4) which matches, with the period of original applied current value of $I = 1.2$. Therefore, the two NL firing rate curves are exactly the same and overlap with one another.

The coefficient of variation calculations that we performed give us the values 4.98 for the case with no inhibition, referring to Figure 3.5 and 4.4 for the inhibition case which is Figure 3.6. We can see that the firing rate curves are more clustered when inhibition is included.

We solved equation (2.21) with MATLAB for changes in NM frequency due to increasing applied current with no inhibition and obtained the Figure 3.7. We then used both equations (2.21) and (3.4) to calculate the NL firing rate in the presence of SON inhibition to the NM cells and obtained the Figure 3.8. Again we can see that in the no inhibition case, the NL firing rate curves are more spread apart than the

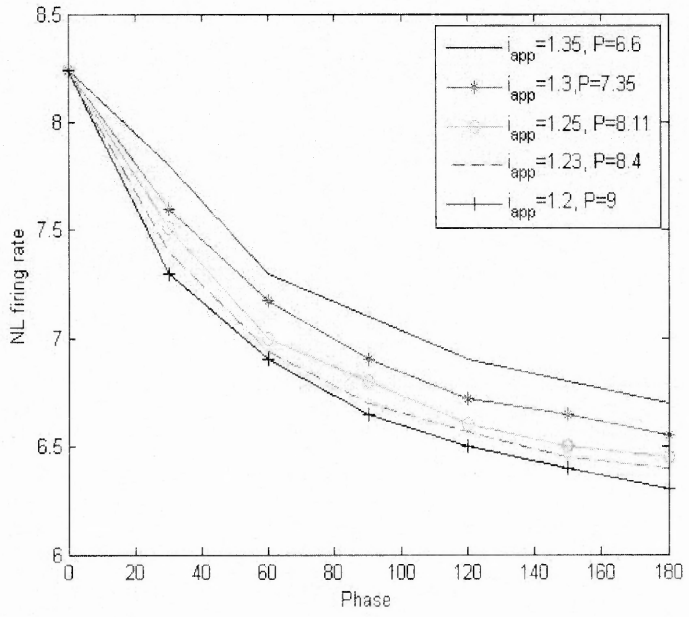

Figure 3.7 NL firing rate for various applied currents to both NM cells-without SON inhibition. MATLAB simulation with $g_{son} = 0$.

case with inhibition. Without inhibition, when applied current is increased from 1.2 through 1.35 the NM period $P \in [6.6, 9]$. Upon inclusion of SON inhibition we obtain a narrower range of P that lies between $[7.3, 9.3]$. In particular, we obtain a NM period value of $P = 9$ when $I = 1.24$ with inhibition, in the MATLAB case as well, as opposed to the original case of $P = 8$ for $I = 1.24$ from 3.7. Therefore, the NL firing rate curves for these two values of applied currents exactly overlap with each other. The coefficient of variation values for Figures 3.7 and 3.8 are 5 and 4.5 repectively, again showing that inhibition helps in clustering of the firing rate curves by narrowing the range of NM periods to lie closer to our frame of reference, $P = 9$. As we can see from the figures and statistical calculations that our results from MATLAB agree qualitatively with our results obtained using XPP. When there is increased input on both sides of the NM neurons it leads to their higher excitability. This causes an increase in the NL activity and without SON inhibition their firing rate curves are spread apart. But in the presence of inhibition, there is reduction of NM activity even

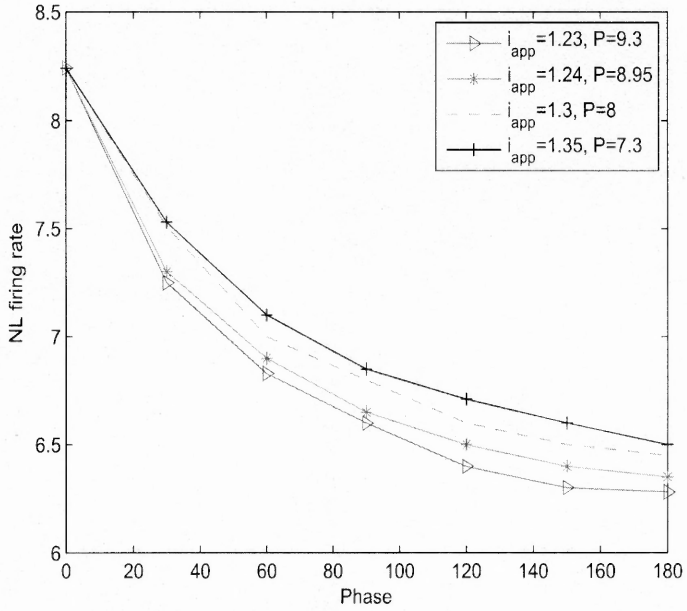

Figure 3.8 NL firing rate for various applied currents to both NM cells-with SON inhibition. MATLAB simulation with $g_{son} = .08$ and $\tau_s = 20$.

when they receive stronger inputs and this leads to clustering of NL firing rate curves. It should be noted however, that in all these simulations, our model does not include NM depression to NL. But in spite of that due to the presence of SON inhibition we obtain clustering of NL firing rate curves making them more independent to changes in NM frequency compared to the non facilitating case. This shows that inhibition from SON inhibition to the NM plays a role of an indirect gain control mechanism and enables the NL neuron to serve as better coincidence detectors even in the absence of NM synaptic depression.

We know from [61] that, during monaural excitation there is an increase in the firing rate of each NM on one side of the brain. This suggests that there is an increase in the firing frequency of the NM neuron on that side. Therefore, now we study the problem of monaural excitation by increasing the applied current on one side of the NM neuron. We investigate how it affects the firing rate of the NL neurons by performing simulations in XPP. Figure 3.9 illustrates the firing rate of the

NL neurons when we increase applied current on one side of the NM cell.

Our original case is when both the NMs receive the same applied currents, which we arbitrarily choose to be $i = 1, 2$ and therefore, their periods are the same i.e. $P = 9$. In this case, we can see the corresponding firing rate of the NL cell from Figure 3.9. Now we model monaural excitation by increasing the applied current to one NM cell, which results in the increase of NM firing frequency on that side. For example, suppose an applied current value of $I = 1.24$ is input to the NM cell on the left side while the right side still has the same applied current value of $I = 1.2$. This leads to an increase in the left NM firing frequency or lowers the NM period. Thus, the left NM period is, $P = 8.1$ and the right NM period remains $P = 9$. In such a situation of different NM firing frequencies on both sides, the way we measure phase difference is as follows. We calculate the phase delay with respect to the left NM period. We let P_1 be the left NM period and P_2 be the right NM period where $P_1 < P_2$. Let the time lag between inputs be $\bar{t}$. Now $\bar{t}$ obeys the following equation.

$$\bar{t} = \frac{\phi P_1}{360^o} \tag{3.7}$$

Since $P_1 < P_2$, we also have that $\bar{t} < t_0$, where $t_0 = \frac{\phi P_2}{360^o}$. Therefore, we obtain an increase in the NL firing rate in this case of input bias, since the time lag $\bar{t}$ between both the inputs is less compared to the original case (equal P on both sides) which has a time lag of t_0. As applied current I is increased from 1.2 to 1.24, 1.3 etc. on one side, there is an increase of NM firing frequency on that side. Therefore, we can see that the increased frequency NM firing leads to a higher NL firing rate. This is evident from Figure 3.9. Thus, from these higher firing rate curves, it seems that the NL neuron responds falsely to increased NM firing rate on one side as though the inputs arrive coincidentally from both sides. This is because, NL is faced with ambiguity between ideally timed inputs and strong unilateral input. Consequently, this could lead to false location of the sound source.

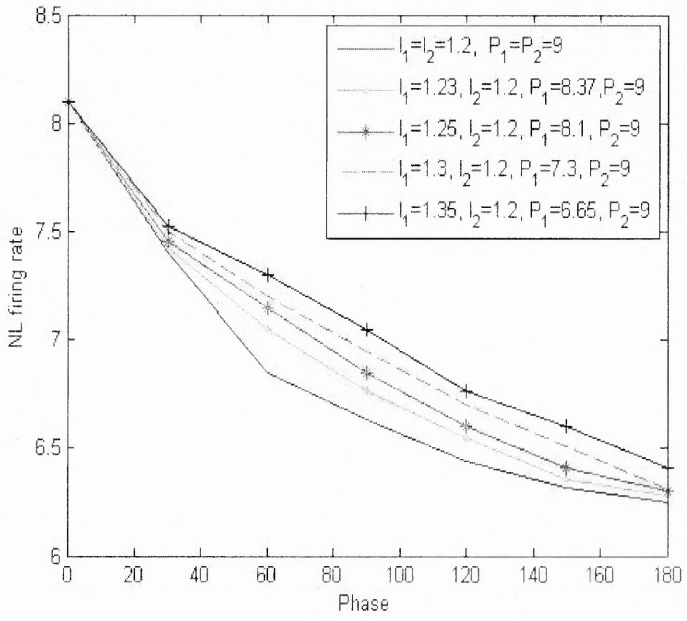

Figure 3.9 NL firing rate for different applied currents on one side of NM-without SON inhibition. In all the input biased cases, the firing rate curves are deviated from the case when $I = 1.2$ on both sides. The value of $g_{son} = 0$.

In order to counter the over excitability of NM on one side, SON inhibition is introduced in our model, as seen in Figure 3.1. Figure 3.10 illustrates the NL firing rate curves when SON inhibition to the NM is introduced, in the monaural excitation case. Since SON inhibition strength is proportional to the amount of excitatory drive that NM receives, the inhibition is more on the side of the NM that receives higher applied current input. This serves to equalize NM activity on both sides over a range of applied currents (which is dependent on our choice of parameters) which is evident from Figure 3.10. We can see from Figure 3.9 that without SON inhibition, during increase in applied current, P_1 ranges from 6.65 to 9, whereas we have been able to restrict the period P_1 to lie between $[7.25, 9.26]$ with the inclusion of inhibition. Again, when $I = 1.24$ on the left side with inhibition, we obtain the left NM period P_1 to equal the right NM period of P_2 at the period value of 9. This results in overlapping of NL firing rate curve when $I = 1.24$ on the left side and $I = 1.2$ on the right side,

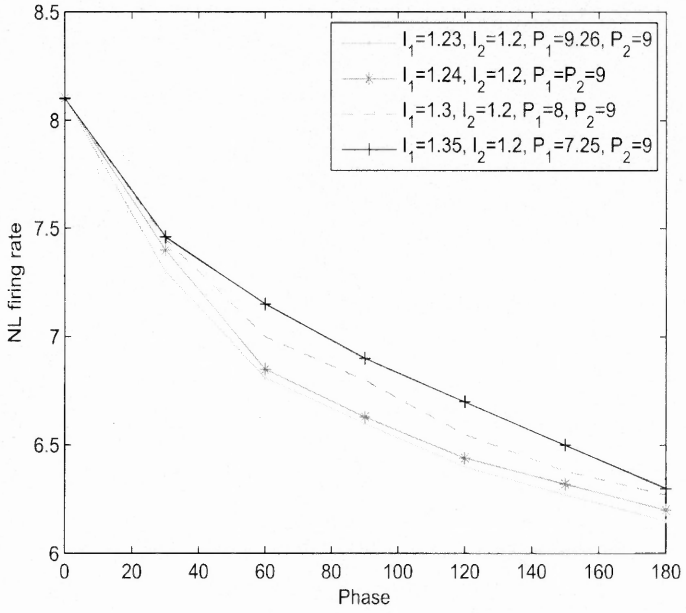

Figure 3.10 NL firing rate for various applied currents on one side of NM cell-with SON inhibition. There is less deviation of the firing rate curves in the input biased cases when compared to $I = 1.2$ on both sides. The value of $g_{son} = .08$ and $\tau_s = 20$.

with the original curve for equal applied current of $I = 1.2$ on both sides. This is evident from Figure 3.10. This shows that even in the presence of input bias with the presence of SON inhibition, the NM activity can be balanced on both sides for a range of applied currents i and that we can obtain a reduced range of NM periods which lie closer to our reference value of $P = 9$.

We performed coefficient of variation calculations for Figures 3.9 and 3.10. The main difference in this calculation compared to our coefficient of variation analysis in Chapter 2 is that, here we do not consider an averaged curve. Instead, we are interested in finding out the amount of deviation of all the curves in comparison to our reference curve where $P_1 = 9$. Therefore, our calculations are with respect to the coefficient of variation of all the curves from the curve with $P_1 = 9$. We obtain the coefficient of variation values of 3 and 1.6 for Figures 3.9 and 3.10, respectively. This shows that in the case of inhibition to NM, the NL firing rate curves are more

clustered and closer to the curve $P = 9$, which is our frame of reference.

As we discussed earlier, this range of P is dependent on our choice of parameters like g_{son} and τ_s. In order to better understand the role played by inhibition in controlling the periodic ranges of the NM cell, we will perform some analysis on the parameters of this problem.

At first, we analyze the role played played by the parameter g_{son}. Originally for $g_{son} = .08$, P lies between $[7.25, 9.26]$. But when we decrease g_{son} its effect on suppressing the NM period reduces. For example if we fix $g_{son} = .02$, then P lies between $[6.8, 8.5]$. On the other hand increasing g_{son} leads to too much inhibition on the NM firing activity. As a result for example, if we let $g_{son} = .2$, then $P \in [8.23, 11.35]$.

Having analyzed g_{son}, we study the effect of the inhibition decay time constant τ_s, next. In the extreme case, for $\tau_s \to 0$, $s \to 0$ very quickly. Therefore, when the value of τ_s is close to 0, there is little effect of SON inhibition on the NM cell. On the other hand if τ_s is large, then the strength of inhibition is more and this leads to too much suppression of NM firing rate. As an example, originally if we let $\tau_s = 20$ then for $I = 1.24$, we obtain $P = 9$, for other parameters fixed. But if we let $\tau_s = 1$, for instance, then it suppresses the NM firing rate less and therefore, its period is $P = 8.25$ for the same value of applied current. This analysis shows that intermediate values of τ_s are preferred so that the SON synapse feels appropriate strength of inhibition.

3.1.2 Conclusions

Our results in this section show that there could be an alternate mechanism to make the NL firing rate behave more as a function of phase difference in NM inputs, namely inhibition from SON to NM. As we mentioned earlier, our model network in this section does not include depression from NM to NL. First, despite the absence of depression, we see clustering of NL firing rate curves in the presence of varying NM frequency inputs. This shows that inhibition aids in making the NL firing rate rela-

tively insensitive to changes in NM frequencies and depend more on phase relationship between inputs. In the monaural excitation we have demonstrated through simulations that, without SON inhibition, the NL neuron faces ambiguity in distinguishing between ideally timed binaural inputs vs strong unilateral inputs. With the inclusion of SON inhibition to NM, the excessive activity of NM neurons due to strong unilateral input, is eliminated and thereby coincidence detecting ability of the NL neuron is enhanced. We, therefore, propose an indirect role of gain control mechanism played by SON through its inhibition to the NM, in eliminating the confounding effects of monaural excitation and preserving the spatial coding property of the NL cell.

CHAPTER 4

GLOBALLY INHIBITORY NETWORK

The ability of a network of neurons to be able to convey multiple pieces of information (temporal codes) is of paramount importance given that the brain is of finite size. For reasons of efficiency it is advantageous for a single network to be able to create, store and transmit multiple codes rather than just one. This leads to the question of how these codes are constructed within the neuronal network and how does a network decide which code to transmit. Mathematically, it is equivalent to asking a very straightforward and general question: What are the circumstances under which a neuronal network exhibits multistability of solutions?

In this chapter, we model a globally inhibitory network that is loosely based on the CA1 hippocampal structure. The network consists of m uncoupled pyramidal cells which send excitatory synapses onto a common interneuron. The interneuron sends inhibitory synapse exhibiting, short-term synaptic depression (STSD) to each of the pyramidal cells.

At first, we describe the mathematical model that we use for cells and as well as the model for synaptic depression. We also exploit time-scale separations to reduce the analysis to a particular slow manifold of the system. Then, we show a few simulations of clustering, and then follow up with mathematical analysis proving the existence and stability of n-cluster solutions. Using methods of geometric singular perturbation theory, we show that any n-cluster solution must satisfy a set of consistency conditions that can be geometrically derived.The basin of attraction of these solutions is analyzed, as is a one-dimensional map based approach for finding solutions. We will use a combination of analysis, simulations and numerical solutions of derived equations. The key aspect underlying our results is that the inhibitory

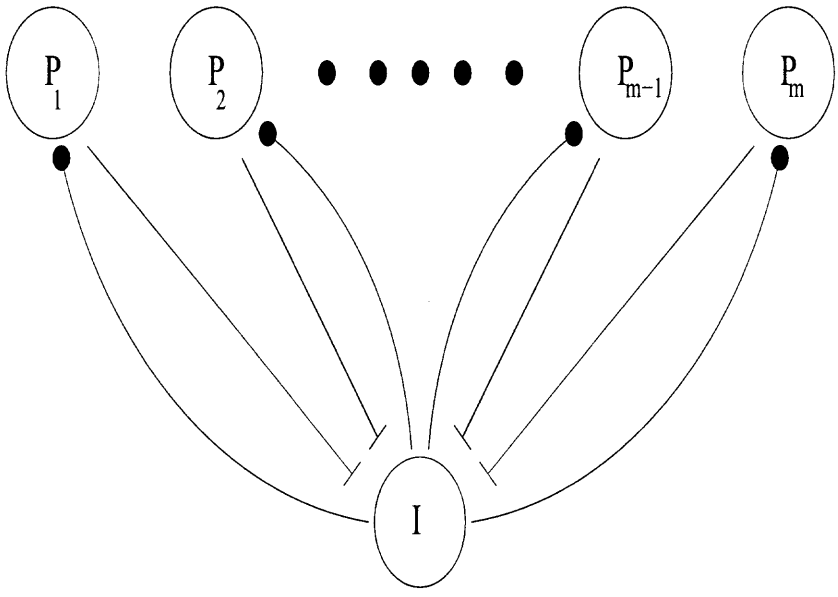

Figure 4.1 An m-cell globally inhibitory network. Each synapse from P to I is excitatory, and each from I to P is inhibitory and displays short-term synaptic depression.

synapses in the network exhibit frequency dependent short-term synaptic depression. We show how there is a functional relationship between the level of synaptic depression, the number of clusters and the interspike interval between neurons. Implications for temporal coding are discussed.

4.1 Model

We describe the mathematical model that we use for cells and as well as the model for synaptic depression. We also exploit time-scale separations to reduce the analysis to a particular slow manifold of the system.

We consider uncoupled pyramidal cells which make excitatory synapses onto a common interneuron; Figure 4.1. The interneuron sends a depressing synapse onto each of the pyramidal cells. The general set of equations that governs the activity of

each pyramidal cell and the interneuron are given by

$$\begin{aligned} \epsilon\frac{dv}{dt} &= f(v,w) \\ \frac{dw}{dt} &= \left[\frac{w_\infty(v)-w}{\tau_w(v)}\right] \end{aligned} \tag{4.1}$$

where $\epsilon \ll 1$. f is the term which contains various ionic currents. The term $w_\infty(v)-w$ is associated with the opening and closing of a potassium channel with the cell. The term $\tau_w(v)$ is the w decay time constant.

The nullclines of the above equations (1) are obtained by setting the right hand side equal to zero. The v nullcline is a cubic shaped curve denoted by C as shown in Figure 4.2. The local max and min values are denoted (v_{rk}, w_{rk}) and (v_{lk}, w_{lk}), respectively. The w nullcline is an increasing sigmoid denoted by S.

We assume the following: Above and below the curve C, $f < 0$ and $f > 0$, respectively. Below and above S, $(w_\infty - w) > 0 (< 0)$. Near the left branch of the cubic where $f = 0$ we require $\frac{\partial f}{\partial w} < 0$ and $\frac{\partial f}{\partial v}$ to be nonzero everywhere except at the minimum and maximum of the cubic. If S intersects C at only one point and this intersection takes place in the middle branch then it is an unstable fixed point causing the cell to undergo oscillations. We will choose parameters such that an isolated P cell has nullclines with this geometry; Figure 4.2. If S intersects C on either the left or the right branch the fixed point is stable. We choose parameters so that I has a fixed point on its left branch.

Equation (4.1) possesses a stable periodic solution if its fixed point lies on the middle branch. By taking ϵ to be small it is easy to construct this solution using geometric singular perturbation theory. Let $\epsilon \to 0$ in equation (1) to obtain the slow subsystem :

$$\begin{aligned} 0 &= f(v,w) \\ \frac{dw}{dt} &= \left[\frac{w_\infty(v)-w}{\tau_w(v)}\right] \end{aligned} \tag{4.2}$$

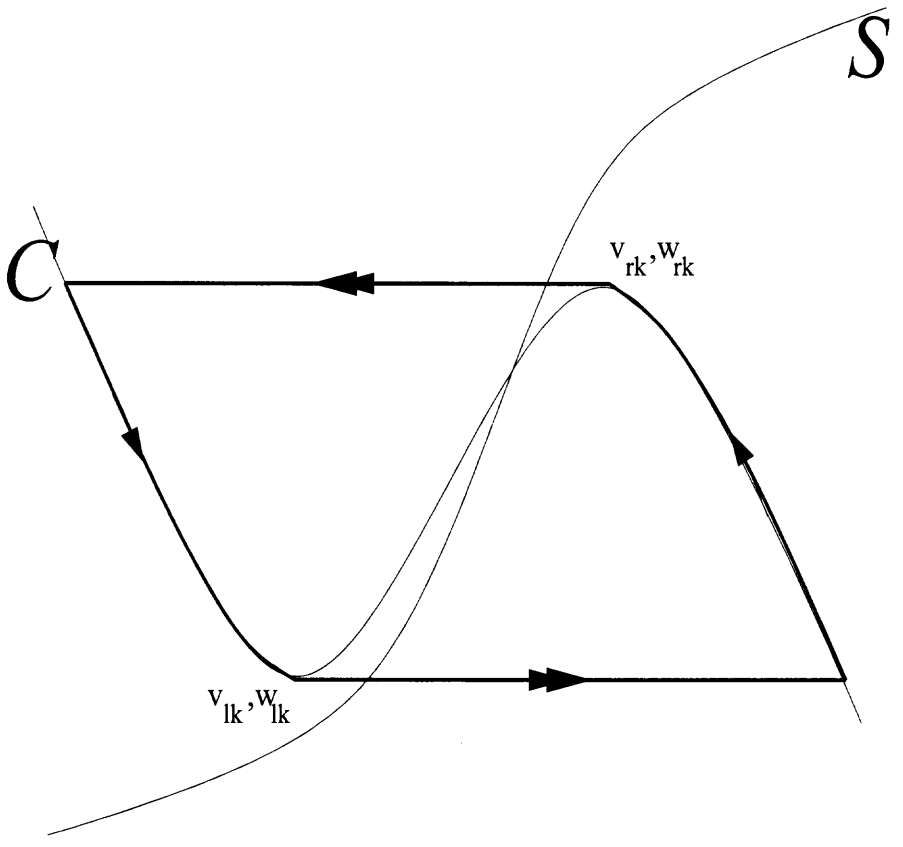

Figure 4.2 Pyramidal cell v-w phase plane and singular orbit. The double arrows denote a fast transition between silent and active stated. A single arrow denotes the slower transition in each of those states. The horizontal axis is v and the vertical axis is w.

Now if time is rescaled to $t = \epsilon\tau$ and then if $\epsilon \to 0$, we obtain

$$\begin{aligned} \frac{dv}{d\tau} &= f(v,w) \\ \frac{dw}{d\tau} &= 0 \end{aligned} \tag{4.3}$$

The singular periodic orbit consists of 4 parts. There are two slow (solutions of (4.2)) and two fast (solutions of (4.3)) parts. These fast transitions are initiated from the right and left knees of the cubic nullcline; Figure 4.2. If ϵ is sufficiently small in the original equation (4.1) then we obtain a relaxation oscillation. In this case, the periodic orbit lies $O(\epsilon)$ close to the singular solution.

Before describing the coupled equations, we make an assumption to make our P cells display spiking behavior. As in [34], we take $\tau_w(v)$ to be small whenever $v > v_{rk}$. This will cause each P cell to spend a small amount of time in the active state and thus make the width of an action potential be small.

4.1.1 Coupled Equations

Each pyramidal cell receives inhibitory input from the interneuron whenever the latter fires. The interneuron, in turn, receives excitatory input whenever a pyramidal cell fires. We will assume that the I cell fires if and only if a P cell fires. Each P cell obeys

$$\begin{aligned} \epsilon \frac{dv_p}{dt} &= f(v_p, w_p) - \bar{g}_{inh} s(t - \Delta t)[v_p - E_{inh}] \\ \frac{dw_p}{dt} &= \left[\frac{w_\infty(v_p) - w}{\tau_w(v_p)} \right], \end{aligned} \tag{4.4}$$

while the interneuron obeys

$$\begin{aligned} \epsilon \frac{dv_I}{dt} &= f(v_I, w_I) - \bar{g}_{exc} s_\infty(v_p)[v_I - E_{exc}] \\ \frac{dw_I}{dt} &= \left[\frac{w_\infty(w_I) - w}{\tau_w(v_I)} \right]. \end{aligned} \tag{4.5}$$

The parameters $\bar{g}_{inh}$, $\bar{g}_{exc}$, E_{inh} and E_{exc} denote maximum synaptic conductances and the reversal potentials of the relevant synapses. In our model, the excitatory synapse from any P to I is non-depressing. For simplicity, we assume that each is instantaneous and thereby model it using s_∞ given by

$$s_\infty(v_p) = \begin{cases} 0, & v_p \leq v_\theta \\ \\ 1, & v_p \leq v_\theta, \end{cases} \tag{4.6}$$

where v_θ is a synaptic threshold lying between v_{lk} and v_{rk}.

The inhibitory synapse from I to any P is modeled as a depressing synapse. This means that the effective maximum strength of the synapse is a function of the

frequency of the interneuron. Whenever I fires, the synapse depresses or weakens. Between spikes of I the synapse recovers. Thus if I fires with high frequency, then its synapse is weak. While if it fires at low frequency, then its synapse will be strong. To model this, for our analysis, we use a standard phenomenological model due to Abbott et. al. [1]. We use a variable D to measure the extent of depression of the synapse and another variable s to incorporate the effect of the synapse onto the P cells. Both depend on the activity of I. In between spikes of I, D recovers toward the value one with time constant τ_a.

$$\frac{dD}{dt} = \frac{1-D}{\tau_a} \tag{4.7}$$

When I spikes at say $t = \hat{t}$, we reset D to rD, where $0 < r < 1$. Specifically, $D(\hat{t}^+) = rD(\hat{t}^-)$. The synaptic variable s decays toward zero with time constant τ_k between I spikes.

$$\frac{ds}{dt} = \frac{-s}{\tau_k} \tag{4.8}$$

At an I spike, s is reset to D by $s(\hat{t}^+) = D(\hat{t}^-)$. Note in (4.4), the variable s appears with a delay of Δt, $s(t-\Delta t)$. Delay of the inhibitory synapse is a necessary condition to obtain stable synchrony for fast rising synapses [58] and will play an important role in the stability of the clustered solutions obtained here.

The Abbott model for D and s assumes that each action potential has zero spike width. However, the simulations in this paper utilize a biophysical model of a CA1 pyramidal cell due to Ermentrout and Kopell [18] that have a non-zero spike width. In the appendix we show the equations that are used for simulations and discuss what modifications on the variables D and s are necessary to incorporate non-zero spike width.

4.1.2 Reduction to Slow Manifold

We make three main assumptions to conduct the analysis

A1) I fires if and only if any P cell fires.

A2) Spikes of both P or I have zero time width.

A3) Inhibition affects each pyramidal cell only when the cell is in its silent state.

It should be noted that assumptions A2 and A3 are just for ease of the analysis. Relaxing either or both of them does not qualitatively change the results. The practical effect of A3 is that when a P cell returns to the silent state, it does so with $w = w_{rk}$, the value of the local maximum of the cubic C. Assumption A1, while not necessary to obtain clustering, drastically simplifies the analysis allowing us to focus only on the spike times of the P cells. Specifically, we can ignore the I dynamics all together and simply track how its synapses onto each P affect the network behavior.

Due to these assumptions, we can understand the dynamics of the entire system by focusing on the behavior of the P cells in their silent state. To do that, we define a two-dimensional $w - g$ slow manifold on which we study the evolution of the P cells. Define $g = \bar{g}_{inh}s$, where g denotes the conductance of the inhibitory synapse. The pyramidal cell P obeys a specific set of slow equations when it is in its silent state. These equations govern the behavior between spikes of I.

$$\begin{aligned} 0 &= f(v,w) - g[v - E_{syn}] \\ w' &= \tfrac{-w}{\tau_w} \\ g' &= -\tfrac{g}{\tau_k} \\ D' &= \tfrac{1-D}{\tau_a} \end{aligned} \tag{4.9}$$

Since $\frac{\partial f}{\partial v} - g$ is nonzero for all points except at the left knees of the null surface, the first equation of (4.9) can be solved for v in terms of w and g, $v = F(w,g)$. This

equation is valid for P in the silent state. The second and third equations of (4.9) are used to find the evolution of w and g which can then be used to calculate v.

The two-dimensional $w-g$ slow manifold (Figure 4.3) has five boundaries: 1) The line $g=0$ which is the case when the P cell receives no inhibition; 2) The line $g=\bar{g}_{inh}$, this is the value of maximum inhibition that a P cell can receive; 3) the curve of critical points which represents the points of intersection of the w nullcline with the left branch of the cubics for different values of g. This curve of critical points exists only for particular interval of $g \in [\hat{g}, \bar{g}_{inh}]$ where the value $\hat{g}$ is the minimum value of g which produces a cubic that intersects the w nullcline in the silent phase; 4) the jump curve that represents the w position of the minimum value of the cubic corresponding to different values of g. The slope of the jump curve is negative as is shown in [58]; 5) the return curve $w=w_{rk}$ that represents where a P cell returns to from the active state. The return curve is vertical, by assumption A3 as inhibition affects only the left branch of the cubic nullcline C and not the right branch.

In Figure 4.3, we show an example of representative trajectories from two P cells on the slow manifold. At any moment in time, both cells receive the same amount of inhibition and thus lie on the same horizontal g-level line. Assume for a moment that the synaptic delay from I to P is given by $\Delta t=0$. If the cells start as shown at $t=0$ and P_1 reaches the jump curve at $t=t^-$, then at t^+, both P_1 and P_2 are reset to $g(t^+)=\bar{g}D(t^-)$ (because I fires whenever any P fires). P_2 is reset vertically, so its w value is unchanged, while P_1 is reset to $w=w_{rk}$ representing that it has spiked.

We will be interested in the steady state behavior of the network. It turns out that the clustered solutions are periodic solutions of the governing equations. This means that I fires periodically with a determinable interspike interval. As we will show below, the length of the interspike interval will depend on the number of clusters as well as various network parameters. We can calculate the maximum and minimum

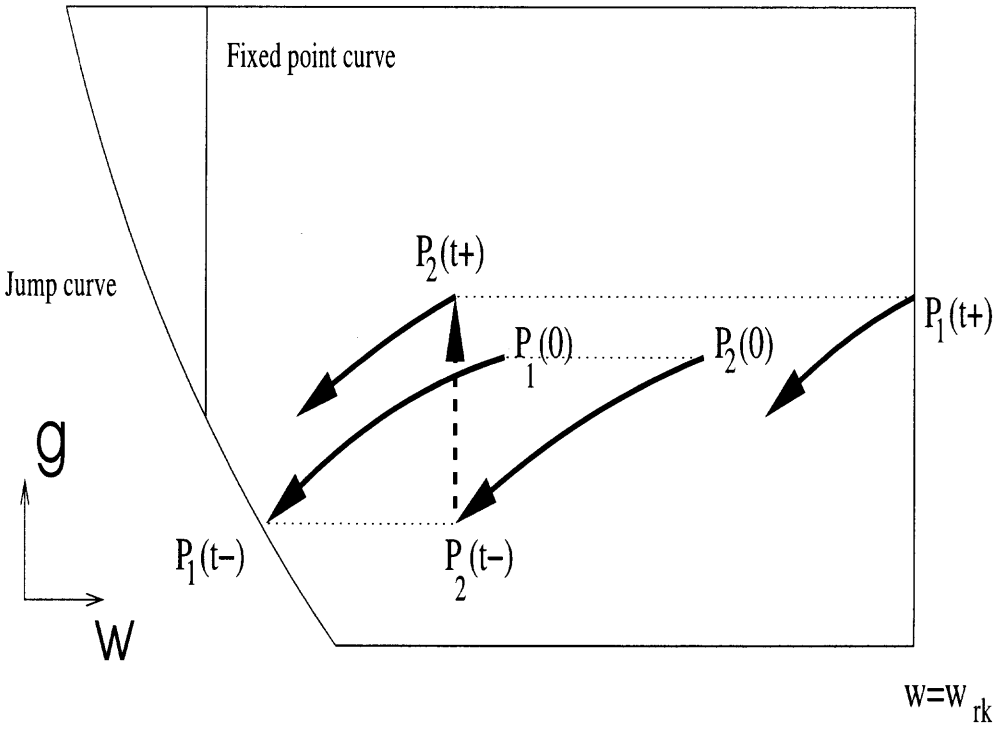

Figure 4.3 Representative trajectories on the $w - g$ slow manifold. Two cells begin at $t = 0$ and evolve toward the jump curve. When P_1 hits the curve at $t = t^-$, it is reset to $w = w_{rk}$ at $t = t^+$, while P_2 is reset vertically to the position shown. The cells then continue to evolve toward the jump curve. The dotted horizontal lines show that at any moment in time, the cells lie on the same g-level.

values that the depression and synaptic variables take over one cycle of a periodic solution. The minimum D value occurs just after an I spike, while the maximum occurs just prior to an I spike. Denote the interspike interval of I by t_{in}. Suppose at $t = 0$ a spike has just occurred and $D(0) = D_{min}$. On the interval $t \in (0, t_{in})$, D follows (4.9), so $D(t_{in}^-) = 1 - (1 - D_{min})exp(-t_{in}/\tau_a)$. After the next I spike, $D(t_{in}^+) = rD(t_{in}^-)$. Thus by periodicity, we require $D_{min} = rD(t_{in}^-)$. Solving for D_{min} yields

$$D_{min} = \frac{r(1 - e^{-t_{in}/\tau_a})}{1 - re^{-t_{in}/\tau_a}}, \tag{4.10}$$

from which it easily follows that D_{max} obeys

$$D_{max} = \frac{1 - e^{-t_{in}/\tau_a}}{1 - re^{-t_{in}/\tau_a}}. \tag{4.11}$$

It should be noted that in both equations above, the value t_{in} is not *a priori* known. In fact, in the analysis below we will determine t_{in} and show that it depends on the cluster size.

If we denote the right-hand side of (4.11) by $h(t_{in})$, it is easy to check that $dh/dt_{in} > 0$. Therefore, D_{max} increases with t_{in} and $h(t_{in})$ can be inverted to solve for t_{in} as a function of D_{max}.

4.2 Results

In Figure 4.4, we show two sets of voltage traces from a 4-cell network. The bottom trace shows a stable 4-cluster solution. Notice that the distance between successive spikes is small. The interspike interval in this case is about 27 ms. The top trace shows a stable 2-cluster solution in the 4-cell network with interspike interval of 34 ms. In this simulation, three cells have synchronized, but remain out of phase with the other cell. The cluster sizes and the specifics of why a particular cell is within a particular cluster has to do with our choice of initial conditions. By changing initial conditions, we could, for example, obtain a 2-cluster solution with each cluster containing two cells. Note that the distance between spikes is larger in the 2-cluster case, as can be seen by viewing the activity of I given by the v_I trace. Both simulations are obtained for the same set of parameters (see Appendix). Moreover, in simulations not shown we can obtain 1- and 3-cluster solutions as well, with corresponding interspike intervals of 70 and 30 ms. The distance between spikes decreases with the number of clusters in the network. Further, the size of an individual cluster does not affect this distance. Below, we will mathematically explain why this network is capable of producing multistability of solutions.

4.2.1 Existence of a n-cluster Solution

We first prove the existence of a 2-cluster solution. For this argument we need only consider two P cells. We shall also assume that the synaptic delay from I to P is $\Delta t = 0$, a condition we will later relax when discussing stability of solutions. To prove the existence of the 2-cluster solution, we will derive two different necessary conditions and show that when both are satisfied, the solution exists. Assume that at $t = 0$, the leading cell starts on the $w - g$ slow manifold at (w_0, g_0), while the trailing cell starts at (w_{rk}, g_0). There exists a time $t_{g_0}(w_0)$ for the leading cell to reach the jump curve. We would like to determine if the trailing cell can reach the original w location, w_0, of the leading cell after this time. That is we want to determine if there exists a w_0 such that

$$w_{rk} e^{(-t_{g_0}(w_0)/\tau_w)} = w_0. \tag{4.12}$$

Clearly if we fix g_0 and let the initial position of the leading cell approach the jump curve, $t_{g_0}(w_0) \to 0$. However, the trailing cell starting at w_{rk} would need a large amount of time to reach w_0. Alternatively, if we let the initial position of the leading cell approach the return curve, then $t_{g_0}(w_{rk}) > t_0(w_{rk})$, in this limit, where the latter time satisfies $w_{lk} = w_{rk} \exp(-t_0(w_{rk})/\tau_w)$. Now the trailing cell would need very little time to reach the initial position w_0.

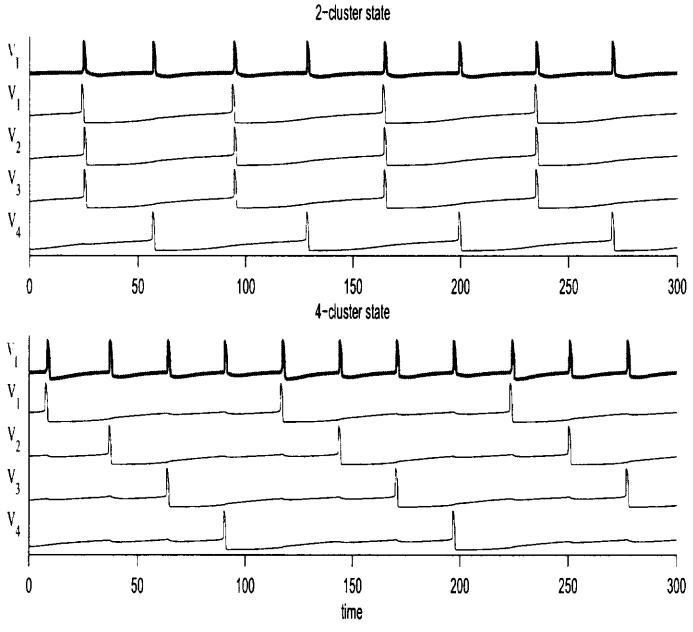

Figure 4.4 Clustered solutions in a 4-cell network.

Moreover as w_0 is smoothly increased from the jump curve to w_{rk}, the time $t_{g_0}(w_0)$ is a strictly increasing function. Thus by the intermediate value theorem and monotonicity, there exists a unique value $w^\star$ such that $t_{g_0}(w^\star)$ satisfies (4.12).

The above argument holds for any initial value of g_0. Thus we can extend it to any $g \in [0, \bar{g}]$. Doing so allows us to establish the existence of a curve $\mathcal{C}_w = \{(w, g) : w = w^\star(g_0)\}$ for which the time for the leading cell from this curve is exactly the time for the trailing cell to reach $w^\star$ satisfying (4.12); Figure 4.5. Thus if one cell starts on $\mathcal{C}_w$ and the other at w_{rk}, both with the same g_0 value, then in the time $t_{g_0}(w^\star)$ the leading cell reaches the jump curve, and the trailing cell reaches the initial $w^\star$ value of the leading cell. It is easy to establish that $\mathcal{C}_w$ is negatively sloped in the $w - g$ plane.

What we next want to know is whether the time $t_{g_0}(w^\star)$ allows the synapse from I to recover sufficiently to be reset to g_0. Note that the value of g is "slaved" to the value of D, since g is reset at spike time to $g(t^+) = \bar{g}D(t^-) = \bar{g}D_{max}$, and

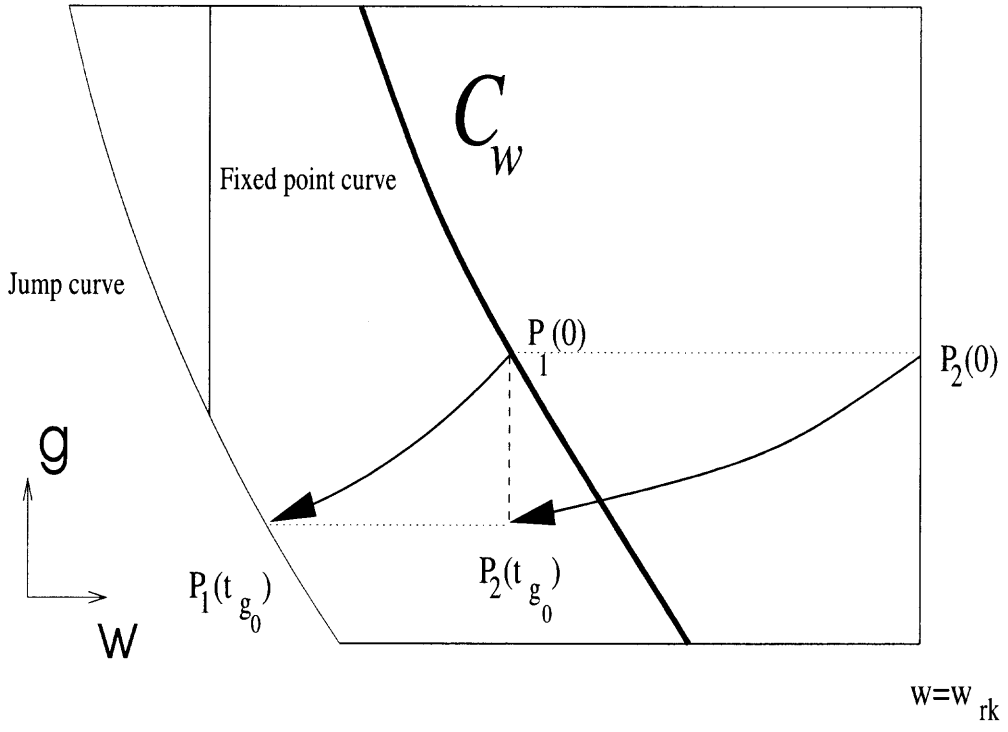

Figure 4.5 The curve $\mathcal{C}_w$ on the $w - g$ slow manifold. If the leading cell begins on $\mathcal{C}_w$ at $w = w_0$, $g = g_0$ and hits the jump curve at $t = t_{g_0}$, then the trailing cell starting at $w = w_{rk}$, $g = g_0$ will reach $w = w_0$ at this time. The dotted horizontal lines show that at any moment the two cells lie on the same g-level.

therefore, periodicity in g is ensured if $D(t)$ is periodic. Thus $g_0(t_{in}^+) = \bar{g}D_{max}$, where D_{max} satisfies the periodicity condition (4.11), and we obtain

$$g_0(t_{in}) = \frac{\bar{g}(1 - e^{-t_{in}/\tau_a})}{1 - re^{-t_{in}/\tau_a}}. \tag{4.13}$$

This relation can be inverted to find t_{in} as a function of g_0 given by

$$t_{in} = \tau_a \ln \frac{(rg_0 - \bar{g})}{g_0 - \bar{g}}. \tag{4.14}$$

Thus given an initial g_0 value, equation (4.14) determines the length of the interspike interval needed for the synapse to recover to be able to be reset to g_0.

To briefly summarize, we have now determined two different times, $t_{g_0}(w^\star)$ from $\mathcal{C}_w$ to the jump curve and $t_{in}(g_0)$ for the necessary reset time length. We want to know if there exists a g_0 value (say g^*) that satisfies these two times simultaneously,

$t_{g^*}(w^*) = t_{in}$. If one cell begins at (w^*, g^*) and the other at (w_{rk}, g^*), then in the time $t_{g^*}(w^*) = t_{in}(g^*)$, the leading cell will reach the jump curve and be reset to (w_{rk}, g^*), while in the same time, the trailing cell will evolve toward the jump curve and be reset to (w^*, g^*). Thus we will have established the existence of the 2-cluster solution.

Since we already have an analytic expression for t_{in}, let us focus now on obtaining one for $t_{g_0}(w^*)$. As noted earlier, the jump curve is negatively sloped. As in [34], we assume the jump curve is linear, and can be written as $g + Mw = c$ where M and c are the negative slope and intercept in the $w - g$ plane. These constants can be calculated since the jump curve passes through the points $(0, \hat{g})$ and $(w_{lk}, 0)$. Assuming that a cell starts on $\mathcal{C}_w$ at (w_0, g_0), we find that t_{g_0} satisfies

$$g_0 e^{-t_{g_0}/\tau_k} + \frac{\hat{g} w_0}{w_{lk}} e^{-t_{g_0}/\tau_w} = \hat{g}. \tag{4.15}$$

In the above equation, there are three unknowns, t_{g_0}, w_0 and g_0. But two are related in that equation (4.12) must be satisfied. Substituting into (4.15), we obtain

$$g_0 e^{-t_{g_0}/\tau_k} + \frac{\hat{g} w_{rk}}{w_{lk}} e^{-2t_{g_0}/\tau_w} = \hat{g}, \tag{4.16}$$

Note that in (4.16), we now have a relationship for t_{g_0} solely as the function of the unknown g_0. This forms one of the two necessary conditions for the 2-cluster solution. The other is contained in equation (4.14). Figure 4.6 shows a plot of t_{g_0} and t_{in} versus the initial conductance g_0 for two different values of τ_w. The intersection of the t_{in} curve with a t_{g_0} curve represents a 2-cluster solution where the value $t_{g_0} = t_{in}$ provides the interspike interval of the I cell or correspondingly, the time distance between the different P cells. Interestingly, in the case τ_w small, there can be three intersection points as shown in Figure 4.6, yielding three potential interspike intervals for a 2-cluster solution. The stability of these solutions will be addressed below. Note that the curve t_{in} is affected only by parameters associated with the synapses from I and thus there is a single curve for both values of τ_w. The curve t_{g_0} on the other hand is

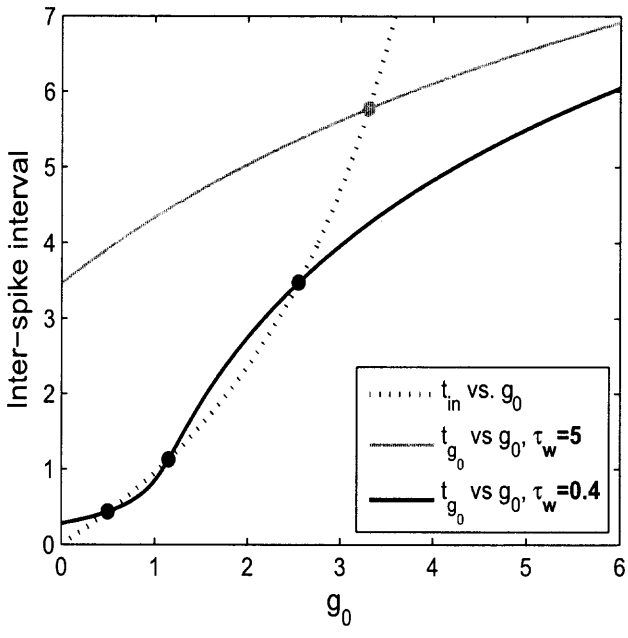

Figure 4.6 The curves t_{in} and t_{g_0} for two different cases. The concave up grey curve is t_{in}, the concave down curve is t_{g_0} for the case $\tau_w = 5$ and the sigmoidal curve is t_{g_0} for the case $\tau_w = 0.4$. Points of intersection of either of the t_{g_0} curves with the t_{in} curve represent 2-cluster solutions. Note that in the case of small τ_w there are multiple intersections.

affected by the synapse from I (first term on the left-hand side of (4.16)), the intrinsic properties of each P cell (second term on the left-hand side) and the interplay of the two ($\hat{g}$ on the right-hand side).

To get a better understanding of this, consider (4.16). If we take $g_0 = 0$, then the equation simplifies to one in which an explicit solution for t_{g_0} can be obtained as

$$t_{g_0} = \frac{\tau_w}{2} \ln \frac{w_{rk}}{w_{lk}}. \tag{4.17}$$

Thus in this case, the time t_{g_0} is solely dependent on the intrinsic properties of each P cell. In general if τ_w is very small, then t_{g_0} can be made small whenever $g_0 < \hat{g}$, not just for $g_0 = 0$. From (4.16), the second term on the left hand side will still dominate the determination of t_{g_0} since the first term will always be less than $\hat{g}$. Thus for small τ_w, (4.17) applies and one expects the curve to have near zero slope and a small value

for all $g_0 < \hat{g}$. Alternatively, if τ_w is larger, then the curve t_{g_0} can be made to intersect the vertical axis $g_0 = 0$ as at large a value as one wants, consistent with what is shown in Figure 4.6. Next let us consider what happens to t_{g_0} if $g_0 \geq \hat{g}$. If τ_w is small, the synapse plays no role in determining t_{g_0} until $g_0 \geq \hat{g}$. Then the synapse is the sole determinant of t_{g_0}. In fact in this case, one can easily estimate t_{g_0} from (4.16) as

$$t_{g_0} = \tau_k \ln \frac{g_0}{\hat{g}}. \tag{4.18}$$

Here the value of τ_k becomes important. Small (large) τ_k implies a small (large) t_{g_0}. However, for any value of τ_k, t_{g_0} is bounded from above as g_0 is bounded by $\bar{g}$. If τ_w is not small, then (4.16), in general, cannot be simplified. Nonetheless, it is easy to see that t_{g_0} is bounded as $g_0 \to \bar{g}$ since the first term in (4.16) is bounded in this limit.

Next let us consider the curve $t_{in}(g_0)$. As can be seen from (4.14), this curve is only affected by the parameters associated with the synapse, depression and the synapse's recovery from depression. Consider two different limits, $g_0 \to 0$ and $g_0 \to \bar{g}$. In the former, $t_{in} \to 0$, while in the latter, $t_{in} \to \infty$. Moreover its easy to show that $dt_{in}/dg_0 > 0$ implying that the curve is unbounded and monotone increasing. Since $t_{in}(0) = 0$, $t_{g_0}(0) > 0$, $t_{g_0}(\bar{g})$ is bounded, $t_{in}(g_0)$ is unbounded as $g_0 \to \bar{g}$ and both curves are continuous, the curves must intersect at least once. This intersection corresponds to a 2-cluster solution

We have derived a consistency condition that must be satisfied for the 2-cluster solution. The above procedure, however, does not define a map whose fixed points correspond to a solution. Indeed, the curve t_{g_0} only yields information when the leading cell starts on $\mathcal{C}_w$ and the trailing cell starts at w_{rk}. Thus, the stability of the solution cannot be obtained simply by checking the derivatives of t_{g_0} and t_{in} at a point of intersection. In Section 4.2.3 below, we will derive an actual one-dimensional map involving the interspike interval to determine the existence of cluster solutions.

Prior to assessing stability, let us show how the above argument can be extended to prove the existence of clusters of size $n < m$ in a network of m pyramidal cells. The curve t_{in} is not affected by the number of cells, nor the number of clusters in the network. The curve t_{g_0} however will be. Suppose we seek an n-cluster solution. Now instead of having a single curve $\mathcal{C}_w$, we can find $n-1$ curves $\mathcal{C}_{w_i}$. Each curve is defined so that if a cell starts on $\mathcal{C}_{w_1}$ at $t = 0$ and reaches the jump curve at $t_{g_0}(w_0)$, then a cell starting on $\mathcal{C}_{w_j}$ would reach the initial w position of the immediately preceding cell starting on $\mathcal{C}_{w_{j-1}}$ at time $t_{g_0}(w_0)$. This allows us to generalize equation (4.12) for $1 \leq j \leq n$ to

$$w_{j-1} = w_j e^{-t_{g_0}/\tau_w}, \tag{4.19}$$

where $w_n = w_{rk}$. By successive substitutions into (4.19), we obtain

$$w_0 = w_{rk} e^{-(n-1)t_{g_0}/\tau_w}. \tag{4.20}$$

Thus the time t_{g_0} for the n-cluster case must satisfy the generalization of (4.16) given by

$$g_0 e^{-t_{g_0}/\tau_k} + \frac{\hat{g} w_{rk}}{w_{lk}} e^{-n t_{g_0}/\tau_w} = \hat{g}. \tag{4.21}$$

Equation (4.21) is valid for any $n \leq m$. For any value n, the curve of solutions satisfying (4.21) is qualitatively similar to the curve obtained for the 2-cluster case; see Figure 4.7. The main difference is that if $n_1 < n_2$, then the curve for the n_1 case lies strictly above that for the n_2 case. All of these curves will still have at least one intersection with the curve $t_{in}(g_0)$, thus guaranteeing the existence of an n-cluster solution for any $n \leq m$. Note that this argument does not depend on, nor does it determine, the size of each cluster. For example if $m = 4$, there can exist two distinct 2-cluster solutions displaying the same interspike interval. One has clusters of size 1 and 3 and the other has clusters of size 2 and 2.

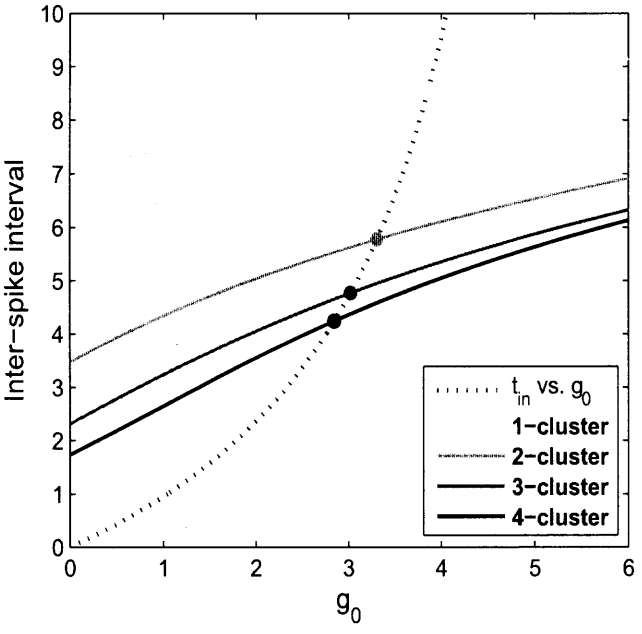

Figure 4.7 Existence of multiple cluster solutions. The concave up t_{in} curve intersects the various t_{g_0} curves corresponding to different sized cluster solutions; equation (4.21) solved for $n = 1, 2, 3$ and 4. As the number of clusters decreases, the inter-spike interval associated with the solution increases.

4.2.2 Stability and Basin of Attraction of Solutions

We have shown the existence of multiple cluster solutions all for the same set of parameter values. The major question to now answer is whether any of these solutions are stable. If so, then what are their basins of attraction?

Let us first address the question of stability. Until now, we have set the synaptic delay from I to P to be $\Delta t = 0$. If we continue with this restriction, then in an m cell network, all solutions are unstable except the m cluster solution. The reason for this is straightforward. Suppose two cells are very close to one another at the moment that one of them is at the jump curve. With zero synaptic delay, an arbitrarily small difference between these cells will be expanded since the trailing cell will be reset vertically in the $w - g$ phase plane, while the leading cell will be reset to w_{rk}. Thus a non-zero synaptic delay is a necessary condition for stability of an

n-cluster solution for $n < m$. This is consistent with several other modeling studies [34, 51, 58]. Therefore, let us assume that $\Delta t > 0$. In [34], it is shown that the stability of the synchronous solution is guaranteed by the fact that the jump curve is negatively sloped in the $w-g$ slow manifold. That same analysis establishes here that any of the n-cluster solutions are also stable. Consider a perturbation to 2-cluster solution in a m-cell network in which one cluster of cells lies at $w_1 = w^\star(g_0)$ on $\mathcal{C}_w$, a second cluster lies at $w_2 = w_{rk}$ with $g = g_0$ and a single cell lies along the line g_0 at $w_3 = \tilde{w} = w_1 \exp(\Delta t/\tau_w)$. Note that the "$w$"-time distance between w_1 and w_3 is exactly Δt. Now evolve these cells so that the leading cell hits the jump curve at time $t = t_1$. The w-time distance between $w_1(t_1)$ and $w_3(t_1)$ is still Δt since both cells follow the same linear equation. However, time distance for the perturbed cell starting at $\tilde{w}$ to the jump curve is less than Δt. This is because as time evolves, the cell at $\tilde{w}$ will not stay on the line $g = g_0$ but will instead have $g(t) < g_0$ for $t_1 < t < t_1 + \Delta t$. Because the jump curve is negatively sloped, this cell will have to travel less in the w distance to reach the jump curve and will be able to reach it in time less than Δt. When the cells are eventually synaptically reset at $t = \Delta t$, they will be near the return curve $w = w_{rk}$ and the new w-time distance between the cells will be less than Δt. This argument can be extended to arbitrary perturbations of the 2-cluster solution and, in general, to n-cluster solutions, thus implying their stability.

The above stability argument says nothing about the basin of attraction of specific n-cluster solutions. However, the analysis in [34] begins to address the issue. To understand whether two initial conditions will merge into the same cluster, let us consider again the dynamics along the $w - g$ slow manifold. Consider two cells with initial conditions given by (w_1, g_0), (w_2, g_0), $w_1 < w_2$ and $\Delta w_0 = w_2 - w_1$; Figure 4.8. Suppose the leading cell (the one starting at (w_1, g_0)) reaches the jump curve after time $t = t_f$ with $g = g_f$. The difference in the w values of the two cells at this time is $\Delta w(t_f) = \Delta w_0 \exp(-t_f/\tau_w)$. Since the cells always have the same g level, the

trailing cell will lie on the horizontal line $g = g_f$. If the trailing cell can reach the jump curve in less than Δt, it will be able to fire prior to being inhibited, resulting in the two cells being more synchronized than when they began. Let $(w_2(t_f), g_s)$ denote the point on the jump curve where the vertical line $w = w_2(t_f)$ intersects it, assuming that the perturbation of $w_2(0)$ from $w_1(0)$ is small. Let $\tilde{t}$ satisfy $g_s = g_f \exp(-\tilde{t}/\tau_k)$. The time $\tilde{t}$ is an upper bound for how long the trailing cell needs to reach the jump curve. It is an upper bound because this time is computed by assuming that the trailing cell travels vertically on the slow manifold and that its w variable does not change. Since the trajectory is not vertical, the trailing cell will actually reach the jump curve with $g > g_s$, and the time of evolution from g_f to that point will be less than $\tilde{t}$. Let $\Delta g = g_s - g_f$. Then using the linear approximation for the jump curve, $\Delta g = -M\Delta w$, we obtain

$$g_f(e^{-\tilde{t}/\tau_k} - 1) = -M\Delta w_0 e^{-t_f/\tau_w}. \tag{4.22}$$

Solving for $\tilde{t}$, we obtain

$$\tilde{t} = \tau_k \ln \frac{g_f}{g_f - M\Delta w_0 e^{-t_f/\tau_w}}. \tag{4.23}$$

Thus if $\tilde{t} < \Delta t$, the trailing cell will reach the jump curve before the inhibition from the leading cell affects it. Therefore,

$$\tau_k \ln \frac{g_f}{g_f - M\Delta w_0 e^{-t_f/\tau_w}} < \Delta t, \tag{4.24}$$

or alternatively

$$\Delta w_0 < \frac{g_f e^{t_f/\tau_w}}{M}(1 - e^{-\Delta t/\tau_k}) \tag{4.25}$$

provides a condition which when satisfied allows the two P cells to be in the same cluster.

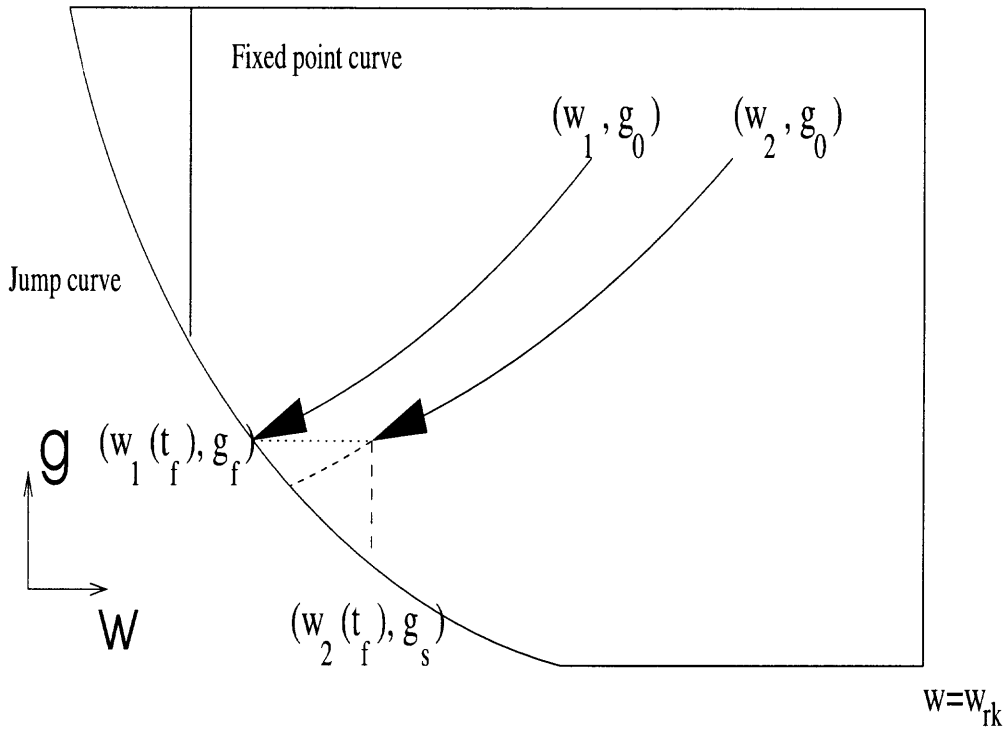

Figure 4.8 Clustering of two initial conditions. At $t = 0$ the two cells start at (w_i, g_0). When the first cell reaches the jump curve at $t = t_f$, we calculate an upper bound for the second cell to reach the jump curve given by the time to vertically travel to the jump curve. If this time is less than the synaptic delay time, then the two cells will merge together into the same cluster.

Although (4.25) only provides an estimate for whether two cells will synchronize, it can be used to infer several things about the basin of attraction of a n-cluster solution in a m-cell network. First note that if $\Delta t = 0$ then (4.25) can never be satisfied. This implies that a synaptic delay is a necessary condition to obtain clusters of size $n < m$. Moreover as the delay $\Delta t \to 0$, (4.25) becomes harder to satisfy, and as a result, the basin of attraction of the m cluster solution grows as that solution becomes globally attracting. Second, observe that the right-hand side of (4.25) grows exponentially with t_f and linearly with g_f, both of which can be estimated for a particular n-cluster solution. For example, suppose τ_k is very large, implying that the synaptic decay rate is very slow. In (4.25), the term $1 - \exp(-\Delta t/\tau_k)$ would be small but bounded away from zero. For this case, the synchronous, 1- and 2- cluster

solutions will be the ones with the largest basin of attractions, while the solutions with more clusters will have very small basins. For the solutions with large number of clusters, the synapse from I would be very weak and thus g_f would be small. Moreover, t_f would be determined solely by τ_w and could be small if τ_w is. Thus Δw_0 satisfying (4.25) would be small. Alternatively, for the synchronous or few cluster solutions, t_f would be much larger due to the fact that τ_k is now setting this time. The value g_f would also be larger since the I synapses would have more time to recover between spikes. As a result, Δw_0 would be larger than in the large cluster solution case. Therefore, cells with larger differences in w can be brought together into the same cluster due to the slow decay of inhibition. In the opposite scenario where τ_k is too small, the term $1 - \exp(-\Delta t/\tau_k)$ would not be so small. Thus even when t_f and g_f are small, the right hand side of (4.25) isn't necessarily. Thus the many cluster solutions have larger basin of attractions in this limit.

Equation (4.25) can also be used to assess the basin of attractions of the different types of 2-cluster solutions that exist for τ_w small. In this case, based on the argument above, the 2-cluster solution with the largest interspike interval will have the largest basin of attraction. The same analysis shows that for the case τ_w small, there can exist 2 or 3 n-cluster solutions as well. Again, the one with the largest interspike interval will have the largest basin of attraction relative to the others.

4.2.3 A Complementary Discrete Map Approach

The above analysis relies on the satisfaction of consistency conditions embedded in computing the times t_{in} and t_{g_0}. We now present a complementary method to study existence and stability of cluster solutions. Suppose we consider a network of m cells, where each cell lies on the slow manifold of the system at some initial conditions $(w_i(0), g(0))$. As time evolves, we record the time interval T at which the P cell closest to the jump curve reaches the threshold. All cells that reach the jump curve

within the Δt synaptic delay interval of T are assumed to spike, and their w_i values are reset, as is the $I \to P$ synaptic conductance variable, g. This iterative process is then repeated, leading to a sequence of inter-spike intervals $\{T_j\}$. If this sequence converges to say T^*, then we will have obtained a stable solution in which the time T^* denotes the time between I spikes.

We numerically calculated such an inter-spike interval sequence by evolving four cells on the slow manifold with the linear equations (4.9), solving the equation

$$g_0 e^{-T/\tau_k} + \frac{g w_0}{w_{lk}} e^{-T/\tau_w} = \hat{g}, \tag{4.26}$$

for the time T needed for each cell to reach threshold. The minimal among these T values represents the next inter-spike interval, T_j. We continue to evolve the slow manifold equations during the synaptic delay interval Δt, resetting the w value of each cell that reaches the jump curve to w_{rk}. As described above, the common synaptic conductance value g is reset to $g_j = \bar{g} D(t^-)$ at time $t = T_j + \Delta t$, where $D(t)$ is evolved according to Eq. 4.7. One instance of this iterative process is shown in Figure 4.9 where the solution converges to a 2-cluster solution with $T^* = 35.5$. In panel A, the filled circles indicate different pairs (g_j, T_j) which are shown to converge to the intersection of the curves t_{in} and t_{g_0}, representing a periodic solution. These curves are computed from equations (4.14) and (4.21) using MATLAB with $n = 2$ (because we seek a 2-cluster solution). Panel B shows the dynamics of the w_i values of the four cells and documents how the interspike interval changes from cycle to cycle. Parameter values for the map and for the MATLAB solution were matched to those used for the XPP simulations shown in Figure 4.4 (values given in Appendix). By varying parameters and initial conditions, we can obtain convergence to other cluster solutions. The values for the interspike intervals that are obtained by this method fairly well approximate what we obtained by numerically solving the full set of equations in XPP. In particular, from (4.14) and (4.21), we obtain interspike intervals

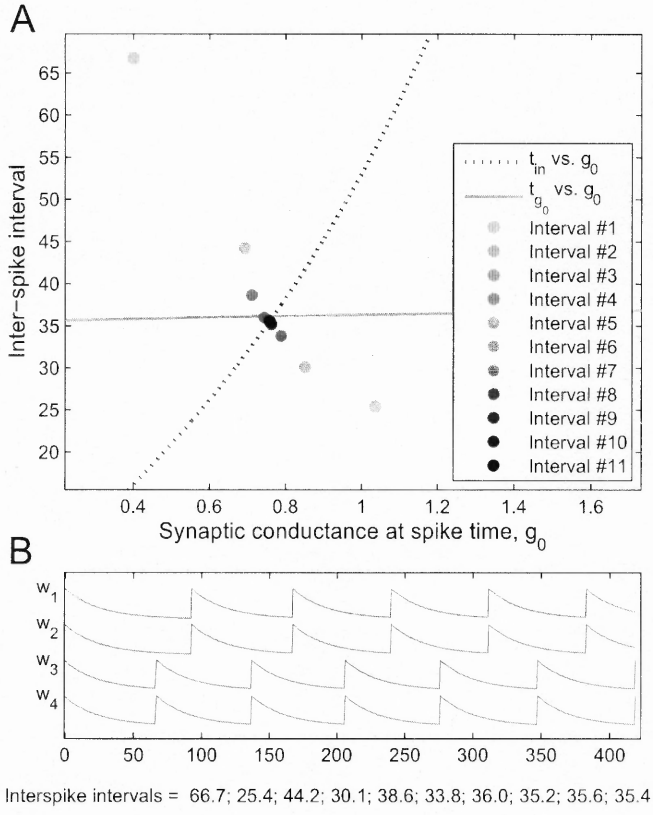

Figure 4.9 Convergence to a 2-cluster solution. **A.** The intersection of the two curves represents a 2-cluster solution found by solving (4.14) and (4.21). The filled circles are different iterates of the one-dimensional map of interspike intervals as they converge to the intersection point. **B.** The corresponding time traces of the recovery variable w of the four cells shows how the interspike interval approaches the value 35.5.

of 71, 35.5, 26.5 and 22 ms for the 1- through 4-cluster solutions, respectively. These compare with the values 70, 34, 30 and 27 obtained from XPP. The method presented is conceptually simple, but yields less information about properties of the n-cluster solution. In particular, even if we find a T^* implying the existence of a clustered solution, we have no way of *a priori* knowing how many clusters this solution will have. Thus we consider the map-based method to be complementary, rather than an alternate, to the above analytic method.

4.2.4 Conclusions

Short-term synaptic plasticity and global inhibition are ubiquitous features in a variety of neural systems, in particular the mammalian cortex and hippocampus, and our results of the globally inhibitory network problem, elucidate the possible functional roles of the interplay between these two properties of neural circuits. We show that such interplay can lead to a highly non-trivial network activity profile, and suggest that global inhibition characterized by short-term synaptic depression can endow a neural network with a multitude of stable activity states representing different neural codes or memory states. Oscillatory networks often have components that interact through inhibition. This is a common feature leading to anti-phase oscillations in central pattern generating networks [37]. These type of networks often involve reciprocally connected pairs of neurons. But in other networks, inhibition from a single neuron or groups of neurons can reach a large number of targets. For example, a variety of interneurons in the hippocampus provide feedback inhibition to a large number of pyramidal cells from whom they receive excitation [19]. In Drosophila, it is postulated that a globally inhibitory network exists to help in odor discrimination [52]. Weakly electric fish use a global feedback mechanism to discriminate between communication and prey stimuli [16]. Mathematical modeling has shed light on the role of the global inhibition in the hippocampus [34], in the thalamus [51] and in scene segmentation [68], to name only a few. The present study builds on these works to propose novel ways in which global inhibition can be utilized by a network.

CHAPTER 5

CONCLUSION

5.1 Summary of Results and Discussion

Short-term synaptic plasticity is widely observed in neuronal networks [71]. It has been shown to play a role in a variety of computational tasks as reviewed by Grande and Spain [20]. In particular, it has been suggested to be important for sound localization and coincidence detection in the avian auditory brainstem [13], in novelty detection in the rat barrel cortex [45] and in phase maintenance in the crab pyloric network [36]. These results all provide examples of neurons involved in temporal coding. Namely, they describe situations in which the relative timing of neuronal firing is critical for the correct functioning of that network and for downstream circuits. A great example of temporal coding of neuronal networks is coincidence detection. Short-term synaptic plasticity commonly occurring in the central nervous system has been shown to contribute towards coincidence detection to a large extent [13], [20]. In this work, we have neglected all the intrinsic properties of the NL cell for coincidence detection. We have also not considered a very extensive model for the neuron involving soma, dendrites as the model in [13] did. Nor have we considered inputs from many NM neurons on either side. Instead we have used a very straightforward non-biophysical firing rate model and integrate and fire neuron model for our SON-NM-NL network. Using these simple models through simulations and simple mathematical analysis, we have shown that with the inclusion of synaptic depression, the NL firing rate can be made to behave more as a function of phase delays of inputs as opposed to the change in input frequencies. In other words depression plays a role of gain control mechanism in the NM-NL network. This is because high frequency NM input strength is reduced due to weak recovery and low frequency NM inputs

exhibit stronger recovery in the presence of depression. Therefore, depression aids the NL firing rate in behaving more as a function of phase delays in NM inputs and being less sensitive to changes in input frequencies. As a result there is improvement in the ability of the NL cell to locate the sound source. Thereby we have shown that NL preserves spatial coding. Our simulation results have a good qualitative agreement with the experimental results in [13] and [20].

One of the many other interesting problems in the auditory brainstem is that of monaural excitation. When the NM cell on one side of the brainstem receives stronger drive than the other side, it has been observed from the literature [24] and [61], that the NM activity on that side of the brain is stronger than the other. As a result there is ambiguity among the NL neurons in being able to distinguish between strong monaural excitation versus binaural coincidence detection. Through the literature, we know that the GABAergic SON plays a role in affecting coincidence detection [44], [24], [61] during cases of input bias to the NM cell. Studies in [14] suggest that the other main mechanism which maintains interaural time difference sensitivity among NL cells apart from depression from NM to NL, is that of SON feedback inhibition. It has been observed that the strength of SON activity is proportional to the NM activity on that side [61]. Therefore, when the NM firing rate is greater on one side than the other during input bias, there is stronger recruitment of SON activity on that side. Thus SON plays a role in suppressing too much excitation on one side due to input bias and thereby balances the NM firing rate on both sides [61] and [69]. Thus SON plays the role of an indirect gain control mechanism by controlling the activity of the NM cells and eliminating the ambiguities among the NL cell caused by input bias.

Even though there is much evidence from past literature showing the existence of GABAergic inhibition from SON to NM, there still are a few unknowns about the relative timing of SON and NM spike times. We studied this problem by making use

of some assumptions regarding the timing of SON inputs to the NM and also the existence of plasticity from SON-NM synapse. We have modeled monaural excitation by increasing the applied current on one side of the NM neuron. In the monaural excitation case, as suggested by [44] [61] and [24] we have shown through our simulations, that when there is input bias it leads to ambiguity of the NL neurons in discriminating between binaural coincidence detection and strong unilateral inputs. As a consequence of this, there could be false location of sound source by the NL cell. We have shown the inclusion of facilitating inhibitory synapse from SON to NM helps to eliminate this ambiguity by suppressing the excess discharges in the target NM neuron, for a range of increasing applied currents which are dependent on our choice of parameters. In other words, without any inhibition it is obvious that when the applied current to a cell is increased, that causes an increase in the firing frequency of the cell. When we increase the applied current input to NM on side, it leads to increase in the NM firing frequency on that side or decrease in the period of the firing of NM cell. We do not change the applied current to the other NM and fix the NM firing frequency in this side as our frame of reference. We compute the NL firing rate curves for the various unequal NM firing frequency cases. We have shown that without inhibition there is larger deviation of these NL firing rate curves from our original NL firing rate curve with equal NM firing rates on both sides. But when we include facilitating SON inhibition to the NM cell which receives input bias, there is suppression of the NM firing rate to a certain extent, depending on the choice of our parameters. This leads to clustering of the NL firing rate curves to the original curve of frame of reference. The clustering of NL firing rate curves in the case of inhibition has also been shown through our coefficient of variation calculations. This shows that the SON inhibition to NM could serve as a mechanism to offset inaccuracies in the NL firing rate caused by ambiguities during input imbalances to the NM cells. Therefore, we have proposed a theory of gain control mechanism through the SON

facilitating synapse to the NM neurons which indirectly enhances the coincidence detecting ability of the NL neurons, in the presence of input bias and even in the absence of depression from NM to NL.

Our work on the second project involving globally inhibitory network, attempts to provide further insight on how synaptic depression affects temporal coding properties of neurons. We find that synaptic depression allows a globally inhibitory network to create and transmit at least m different temporal patterns, all for the same set of parameter values. These patterns can be construed as codes because each pattern can transmit a different interspike interval (ISI) that a downstream target could interpret. For example, if there is a long ISI, the downstream target could infer that the globally inhibitory network is in the synchronized state. As smaller ISIs are transmitted, the downstream neuron would be able to infer that the network has broken up into progressively more clusters. Thus, the timing of spikes of the interneuron, encoded in the ISI, codes for the overall state of the network.

We derived mathematical criteria and techniques to prove the existence and stability of cluster solutions. To prove existence, we showed that when two different sets of timing constraints are met, then a cluster solution will exist. Interestingly, one of the constraints, equation (4.14) is completely controlled by the inhibitory synapses from the global inhibitor. The other constraint, equation (4.21) is determined by parameters associated with both the globally inhibitory synapse, but also by parameters associated with the P cells. We showed how adjusting either sets of parameters can lead to different ways in which the two constraints could simultaneously be met. Stability of the solutions followed from the geometry of the slow manifold, namely that the jump curve is negatively sloped in the $w-g$ phase plane. This is a common feature for many Hodgkin-Huxley type neurons.

An important aspect of our modeling was a reduction to the $w-g$ slow manifold of the system. This allowed us to solve a linear set of differential equations on

that manifold to derive equations (4.14) and (4.21). We then used a combination of analysis and numerics on these equations to show the existence and stability of cluster solutions. We also used the slow manifold to define a one-dimensional map involving ISIs. This map is easy to numerically compute and provides an example of the stability of solutions together with their basin of attraction. Despite the apparent severity of the reduction procedure, the resulting simplified model was still capable of making qualitatively and quantitatively accurate predictions for the full model. Indeed simulation results using the full set of model equations compared quite well.

5.2 Future Work

There are several open questions in this problem of coincidence detection which are very interesting and useful to consider. In this work of monaural excitation we have considered only the change in NM firing rates when there is input bias. An immediate extension of this problem could be in investigating if there are multiple NM neurons firing at the same time as suggested in [44] on the side receiving intense input, how does this affect the coincidence detecting ability of the NL cell? This translates to increasing the synaptic conductance of the NM on the side which receives stronger input, as opposed to increasing their firing rate. In this case, the ambiguity lies in the NL cell responding with higher firing rates when there is synchrony of inputs from one side, as opposed to looking for coincident inputs from both sides. The most challenging case for the NL neuron in this problem would be if there is increase in both the NM firing rate, as well as the synaptic conductance on the side which receives intense input compared to the other side. During this asymmetry in bilateral inputs it would be interesting to study what mechanism does the NL cell have to distinguish between strong unilateral excitation versus binaural coincidence detection of inputs and preserve its property of spatial coding.

We know from the literature that there is reciprocal inhibition among the

SONs to both the right and left sides of the brainstem [7]. This implies that SON inhibition to NM on each side is not independent. For instance, if the SON activity depends on the left side sound level it also has to depend on the amount of opposite SON inhibition (from the right side). Burger et al. [7] conjecture that disparities in input periods among the NM neurons can be reduced by reciprocal SON inhibition even if sounds located off the midline generate differences in interaural sound intensities [7]. Therefore, another issue to explore would be to include reciprocal connections among the left and right ear SONs to observe their effect on the NM neurons and the NL firing rate.

We would also like to include NL excitatory feedback onto the SON and study if it affects the firing rate of the SON neurons thereby having an impact on the NM cell dynamics.

In the present work we have not explored the effect of IID in the processing of sound. Like the NM neurons, there is another group of major neurons, nucleus angularis (NA), in the auditory brainstem which have a specialized function of encoding sound intensity information. NA also receives inhibition from SON and sends excitation back to SON. It has been shown experimentally that short term synaptic facilitation and depression at the NA synapse are instrumental in affecting the encoding of sound intensity information [10]. To gain a better understanding of the phenomenon of coincidence detection, we would like to model the NA cells using a spiking neuron model and add both facilitation and depression to the NA synapse.

So far we have only been looking at sound processing in the auditory brainstem. We want to extend our model by including cells from the higher regions of the brain, namely the auditory midbrain known as inferior colliculus (IC). The IC is sensitive to ITD and receives excitatory inputs from NL cells. The external nucleus of IC has space specific neurons which receive inputs from a wide range of frequency channels that are selective to a unique ITD [67]. It would be interesting to model

how sound information is processed among these cells in IC.

Another interesting aspect of future work could be to include NL dendrites in our model as it has been observed from the literature that dendrites play a significant role in enhancing the coincidence detecting ability of the NL cell [2], [21]. The extensive cell morphology and the spatial distribution of the NM inputs has been shown to strengthen the computational power of the NL cells with a capability far superior than the point neurons [66]. The way that dendrites enhance coincidence detection among NL neurons is the following. A NL neuron which linear summates inputs would not be able to distinguish between inputs arriving coincidentally from the same neural source versus that of inputs arriving simultaneously from two independent neural sources. The presence of dendrites helps to distinguish between the two different scenarios as observed by modeling studies in [21] and [53]. This is because when inputs arrive at the same dendritic compartment they sum in a non-linear fashion due to the decrease of the driving force with depolarization [2]. Therefore, the total synaptic current obtained by various inputs that arrive coincidentally at nearby sites on the same dendrite is smaller than the total current that is obtained from all these inputs if they were to arrive at different dendrites [66]. As a result the NL firing rate is higher in the case, when inputs arrive simultaneously at two different sources on the dendrites compared to coincident arrival of inputs from the same source on the dendrites [66].

Furthermore, it has been illustrated in the literature that ion channels for example, low-threshold potassium channels reduce response to less in-phase inputs [14]. The present model of integrate and fire neuron in my study of coincidence detection does not include any ion channels. It would be interesting therefore, to study this phenomenon of coincidence detection with a more realistic bio-physical model for the NM-NL cells with the inclusion of ion channels.

CHAPTER 6

APPENDIX

The model used to represent a single neuron (which could be excitatory and inhibitory) is based on the Hodgkin-Huxley model for the spiking neurons. This was developed by Traub and Miles [60] and then reduced to a single compartment model by Ermentrout and Kopell [18]. $C\frac{dv}{dt} = I_0 - g_l(v-V_l) - g_k w^4(v-V_k) - g_{Na}m_\infty^3(v)h(w)(v-V_{Na}) - I_{syn}$ and $\frac{dw}{dt} = (w_\infty(v) - w))/\tau_w(v)$. The gating variable for potassium activation w is defined by $w_\infty(v) = a_w(v)/(a_w(v) + b_w(v))$ and $\tau_w(v) = \tau_w$ when the cell is in its silent phase. When the cell is in its active phase $\tau_w(v) = \tau_r$, where $\tau_w = 25$ ms and $\tau_r = 1$ ms, $a_w(v) = .032(v+52)/(1-e^{-\frac{v+52}{5}})$ and $b_w(v) = .5e^{-\frac{57+v}{40}}$. The sodium activation curve at steady state is given by $m_\infty(v) = a_m(v)/(a_m(v) + b_m(v))$ where $a_m(v) = .32(v+54)/(1-e^{-(v+54)/4})$ and $b_m(v) = .28(v+27)/(e^{\frac{v+27}{5}} - 1)$. The inactivation curve is given by $h = \max(1\text{-}1.25w,0)$. The parameter values used in the simulation are: $C = 1\ \mu F\ cm^{-2}$, $g_{Na} = 100$ ms cm^{-2}, $V_{Na} = 50\ mV$, $g_K = 80$ ms cm^{-2} ,$V_K = -100\ mV$, $g_L = .1$ ms cm^{-2}, $V_L = -65.625\ mV$ for the pyramidal cells and $V_L = -64.6\ mV$ for the interneuron. The injected current $I_0 = 0.5$ for the pyramidal cells and $I_0 = -0.5$ for the interneuron. The synaptic delay $\Delta t = 0.5$. The synaptic parameters are $\bar{g}_{inh} = 2$ ms cm^{-2}, $V_{isyn} = -80$ mV, $g_{esyn} = 5$ ms cm^{-2} and $V_{esyn} = 0$ mV, $\tau_b = 1$ ms,$\tau_a = 100$ ms and $\tau_k = 5$ ms. We use XPP for all our simulations [17]. To solve (4.14) and (4.21)using MATLAB, we use the Abbott model for depression. For Figs. 4.6 and 4.7. We set $r = .6$, $\tau_w = 5$, $\tau_k = 3$, $\tau_a = 10$, $\bar{g}_{inh} = 5$, $\hat{g} = .8$, $w_{lk} = .2$ and $w_{rk} = .8$ For Fig. 4.9 where we compare to the XPP simulations, we take $r = .236$. This value is calculated by noting that in the simulations, each action potential has length of about 1.2 ms. We let $r = exp(-1.2/\tau_b)$, where $\tau_b = 1$.

We also chose the values of $\hat{g} = .01$, $w_{lk} = .05$ and $w_{rk} = .85$ by estimating these values from our simulations.

REFERENCES

[1] L. F. Abbott, J. A. Varela, K. Sen, and S. Nelson, "Synaptic depression and cortical gain control," *Science*, vol. 275, pp. 220-224, 1999.

[2] H. Agmon-Snir, C. Carr, and J. Rinzel, "The role of dendrites in auditory coincidence detection," *Nature*, vol. 393, pp. 268-272, 1998.

[3] W. Bialk, F. Rieke, R. de Ruyter van Steveninck, and D. Warland, "Reading a neural code," *Science*, vol. 252, pp. 1854-1857, 1991.

[4] R. Boord, "The anatomy of the avian auditory system," *Ann NY Acad Sci*, vol. 167, pp. 147-155, 1969.

[5] A. Brand, O. Behrend, T. Marquardt, D. McAlpine, and B. Grothe, "Precise inhibition is essential for microsecond interaural time difference coding," *Nature*, vol. 417, pp. 543-547, 2002.

[6] D. Buonomano, "Decoding temporal information: a model based on short-term synaptic plasticity," *J Neurosci*, vol. 20, pp. 1129-1141, 2000.

[7] R. Burger, C. KS., J. Pfeiffer, and E. Rubel, "Avian superior olivary nucleus provides divergent inhibitory input to parallel auditory pathways," *Journal of Comparative Neurology*, vol. 481, pp. 6-18, 2005.

[8] R. Cajal, "The acoutic nerve: its cochlear branch or cochlear nerve(translated from histologie du systeme nerveux de l'homme et des vertebres, tome i)," *National Technical Information Service*, pp. 205-473, 1971.

[9] C. Carr and R. Boudreau, "Central projections of auditory nerve fibers in the barn owl," *J Comp Neurol*, vol. 314, pp. 306-318, 1991.

[10] C. Carr and R. Boudreau, "A role for short-term synaptic facilitation and depression in the processing of intensity information in the auditory brainstem," *J Neurophysiol*, vol. 97, pp. 2863-2874, 2007.

[11] C. Carr and M. Konishi, "A circuit for detection of interaural time differences in the brainstem of the barn owl," *J Neurosci*, vol. 10, pp. 3227-3246, 1990.

[12] F. Chance, S. Nelson, and L. Abbott, "Synaptic depression and the temporal response charecteristics of v 1 cells," *J Neurosci*, vol. 18, pp. 4785-4799, 1998.

[13] D. L. Cook, P. C. Schwindt, L. A. Grande, and W. J. Spain, "Synaptic depression in the localization of sound," *Nature*, vol. 421, pp. 66-70, 2003.

[14] V. Dasika, J. White, L. Carney, and H. Colburn, "Effects of inhibitory feedback in a network model of avian brain stem," *J Neurophysiol*, vol. 94, pp. 400-414, 2003.

[15] J. Dittman, A. Krietzer, and W. Regehr, "Interplay between facilitation, depression and residual calcium at three presynaptic terminals," *J Neurosci*, vol. 20, pp. 1374-1385, 2000.

[16] B. Doiron, M. Chacron, L. Maler, A. Longtin, and J. Bastian, "Inhibitory feedback required for network oscillatory responses to communication but not prey stimuli," *Nature*, vol. 421, pp. 539-543, 2003.

[17] B. Ermentrout, *Simulating, Analyzing and Animating Dynamical Systems: A Guide to XPPAUT for Researchers and Students.* Philadelphia: SIAM, 2002.

[18] B. Ermentrout and N. Kopell, "Fine structure of neural spiking and synchronization in the presence of conduction delays," *Proc. Natl Acad. Sci USA*, vol. 95, pp. 1259-64, 1998.

[19] T. Fruend and G. Buzsaki, "Interneurons of the hippocampus," *Hippocampus*, vol. 6, pp. 437-70, 1996.

[20] L. Grande and W. Spain, "Synaptic depression as a timing device," vol. 20, pp. 201-210, 2005.

[21] V. Grau-Serrat, C. Carr, and J. Simon, "Modeling coincidence detection in nucleus laminaris," *Biol Cybern*, vol. 89, pp. 388-396, 2003.

[22] B. Grothe, "New roles for synaptic inhibition in sound localization," *Nature reviews-Neuroscience*, vol. 4, pp. 1-11, 2003.

[23] J. Hopfield, "Pattern-recognition computation using action-potential timing for stimulus representation," *Nature*, vol. 376, pp. 33-36, 1995.

[24] R. Hyson, E. Overholt, and W. Lippe, "Cochlear microphonic measurements of interaural time differences in chick," *Hear Res*, vol. 81, pp. 109-118, 1994.

[25] E. Izikevich and F. Hoppensteadt, *Weakly Connected Neural Networks*, 3rd ed. New York: Springer-Verlag, 1997.

[26] L. Jeffress, "A place theory of sound localization," *J Comp Physiol Psychol*, vol. 41, pp. 35-39, 1948.

[27] S. Jhaveri and D. Morest, "Neuronal architecture in nucleus magnocellularis of the chicken auditory system with observations on nucleus laminaris: a light and electron microscope study," *Neuroscience*, vol. 7, pp. 809-836, 1982a.

[28] S. Jhaveri and D. Morest, "Sequential alterations of neuronal architecture in nucleus magnocellularis of the developing chicken: a golgi study," *Neuroscience*, vol. 7, pp. 837-853, 1982b.

[29] P. Joris, P. Smith, and T. Yin, "Coincidence detection in the auditory system: 50 years after jeffress," *Neuron*, vol. 7, pp. 1235-1238, 1988.

[30] E. Kandel, J. Schwartz, and T. Jessell, *Principles of Neural Science*, 4th ed. New York: McGraw Hill, 2000.

[31] E. Knudsen and M. Konishi, "Mechanisms of sound localization in the barn owl," *J Comp Physiol*, vol. 133, pp. 13-21, 1979.

[32] E. Koyano, L. Yang, and P. Monsivais, "Gabaergic inhibition in nucleus magnocellularis: Implications for phase locking in the avian auditory brainstem," *J Neurosci*, vol. 20, pp. 2954-2963, 2000.

[33] H. Kuba, K. Koyano, and H. Ohmori, "Synaptic depression improves coincidence detection in the nucleus laminaris in brainstem slices of the chick embryo," *Eur J Neurosci*, vol. 15, pp. 984-990, 2002.

[34] S. Kunec and A. Bose, "High-frequency, depressing inhibition facilitates synchronization in globally inhibitory networks," *Network : Comput. Neural Syst.*, vol. 14, pp. 647-672, 2003.

[35] E. Lachica, R. Rubasamen, and E. Rubel, "Gabaergic terminals in the nucleus magnocellularis and nucleus laminaris originate from the superior olivary nucleus," *J Comp Neurol*, vol. 348, pp. 403-418, 1994.

[36] Y. Manor, A. Bose, V. Booth, and F. Nadim, "The contribution of synaptic depression to phase maintenance in a model rhythmic network," *J. Neurophysiol.*, vol. 90, pp. 3513-3528, 2003.

[37] E. Marder and R. Calabrese, "Principles of rhythmic motor pattern generation," *Physiol Rev*, vol. 76, pp. 687-717, 1996.

[38] D. McAlpine and B. Grothe, "Sound localization and delay lines- do mammals fit the model?" *TRENDS in Neurosci*, vol. 26, pp. 347-350, 2003.

[39] M. Mishchenko and N. Rozov, *Differential equations with a Small Parameter and Relaxed Oscillations.* New York: Plenum, 1980.

[40] A. Moiseff and M. Konishi, "Binaural characteristics of units in the owl's brainstem auditory pathway: precursors of restricted spatial receptive fields," *J Neurosci*, vol. 3, pp. 2553-2562, 1983.

[41] F. Nadim, Y. Manor, N. Kopell, and E. Marder, "Synaptic depression creates a switch that controls the frequency of an oscillatory circuit," *Proc Natl Acad Sci*, vol. 96, pp. 8206-8211, 1999.

[42] J. Nicholls, A. Martin, B. Wallace, and P. Fuchs, *From Neuron to Brain*, 3rd ed. Massachussetts: Sinauer Associates Inc, 2000.

[43] J. O'Keefe, "Place units in the hippocampus of the freely moving rat," *Exp. Neurol.*, vol. 51, pp. 78-109, 1976.

[44] J. Pena, S. Viete, Y. Albech, and M. Konishi, "Tolerance to intense sound of binaural coincidence detection in the owl's nucleus laminaris," *J Neurosci*, vol. 16, pp. 7046-7054, 1996.

[45] C. Petersen, "Short-term dynamics of synaptic transmission within the excitatory neuronal network of rat layer 4 barrel cortex," *J. Neurophysiol.*, vol. 87, pp. 2904-2914, 2002.

[46] W. Reichardt, *Autocorrelation, a principle for the evaluation of sensory information by the central nervous system. In: Sensory Communication*, rosenblith, w.a. ed. Cambridge: MIT, 1961.

[47] A. Reyes, E. Rubel, and W. Spain, "Membrane properties underlying the firing of neurons in the avian cochlear nucleus," *J Neurosci*, vol. 14, pp. 5352-5364, 1999.

[48] E. Rubel and T. Parks, "Organization and development of brainstem auditory nuclei of the chicken:tonotopic organization of n.magnocellularis and n.laminaris," *J Comp Neurol*, vol. 164, pp. 411-434, 1975.

[49] E. Rubel, L. Yang, and P. Monsivais, "The superior olivary nucleus and its influence on nucleus laminaris: A source of inhibitory feedback for coincidence detection in the avian auditory brainstem," *J Neurosci*, vol. 19, pp. 2313-2325, 1999.

[50] J. Rubin and A. Bose, "The geometry of neuronal recruitment," *Physica D*, vol. 221, pp. 37-57, 2006.

[51] J. Rubin and D. Terman, "Analysis of clustered firing patterns in synaptically coupled networks of oscillators," *J. Math Biology*, vol. 41, pp. 513-45, 2000.

[52] A. Silbering and C. Galizia, "Processing of odor mixtures in the drosophila antennal lobe reveals both global inhibition and glomerulus-specific interactions," *J. Neurosci*, vol. 27, pp. 11 966-77, 2007.

[53] J. Simon, C. Carr, and S. Shamma, "A dendritic model of coincidence detection in the avian brainstem," *Neurocomputing*, vol. 26-27, pp. 263-269, 1999.

[54] N. Suga, J. Olsen, and J. Butman, "Specialized subsystems for processing biologically important complex sounds: cross-correlation analysis for ranging in the bat's brain," *Cold Spring Harbor Symp Quant Biol*, vol. 55, pp. 8400-8404, 1990.

[55] W. Sullivan and M. Konishi, "Segregation of stimulus phase and intensity coding in the cochlear nucleus of the barn owl," *J Neurosci*, vol. 4, pp. 1787-1799, 1984.

[56] J. Tabak, W. Senn, M. O'Donovan, and J. Rinzel, "Modeling of spontaneous activity in developing spinal cord using activity dependent depression in an excitatory network," *J Neurosci*, vol. 274, pp. 3041-3056, 2000.

[57] T. Takahashi, A. Moisell, and M. Konishi, "Time and intensity cues are processed independently in the auditory system of the owl," *J Neurosci*, vol. 4, pp. 1781-1786, 1984.

[58] D. Terman, N. Kopell, and A. Bose, "Dynamics of two mutually coupled slow inhibitory neurons," *Physica D*, vol. 68, pp. 241-75, 1998.

[59] E. Thomas, H. Sjovall, and J. Bornstein, "Computational model of the migrating motor complex of the small intestine," *Am J Physiol Gastrointest Liver Physiol*, vol. 286, pp. G564-G572, 2004.

[60] R. Traub and R. Miles, *Neuronal Networks of the Hippocampus*. Cambridge University Press, 1991.

[61] E. Trussell, L. Yang, and P. Monsivais, "Gabaergic inhibition in nucleus magnocellularis: Implications for phase locking in the avian auditory brainstem," *J Neurosci*, vol. 20, pp. 2954-2963, 2000.

[62] L. Trussell and T. Lu, "Mixed excitatory and inhibitory gaba-mediated transmission in chick cochlear nucleus," *J Physiol*, vol. 535, pp. 125-131, 2001.

[63] L. Trussell and M. Rathouz, "Characterization of outward currents in neurons of the avian nucleus magnocellularis," *J Neurophysiol*, vol. 80, pp. 2824-2835, 1998.

[64] M. Tsodyks and H. Markram, "The neural code between neocortical pyramidal neurons depends on neurotransmitter release probability," *Proc Natl Acad Sci USA*, vol. 94, pp. 719-723, 1997.

[65] M. Tsodyks, K. Pawelzik, and H. Markram, "Neural networks with dynamic synapses," *Neural Computation*, vol. 10, pp. 821-835, 1998.

[66] J. van Hemmen and T. Sejnowski, *23 problems in systems neuroscience*. New York: Oxford University Press, 2005.

[67] H. Wagner, T. Takahashi, and M. Konishi, "Representation of interaural time difference in the central nucleus of the barn owl's inferior colliculus," *J Neurosci*, vol. 7, pp. 3105-16, 1987.

[68] D. Wang and D. Terman, "Locally excitatory globally inhibitory oscillatory networks," *IEEE Trans. Neur. Net.*, vol. 6, pp. 283-86, 1995.

[69] L. Yang, P. Monsivais, and E. Rubel, "The superior olivary nucleus and its influence on nucleus laminaris: a source of inhibitory feedback for coincidence detection in the avian auditory brainstem," *J Neurosci*, vol. 19, pp. 2313-2325, 1999.

[70] S. Zhang and L. Trussell, "Voltage clamp analysis of excitatory synaptic transmission in the avian nucleus magnocellularis," *J Physiol*, vol. 480, pp. 123–126, 1994b.

[71] R. Zucker and W. Regehr, "Short-term synaptic plasticity," *Annu. Rev. Physiol.*, vol. 64, pp. 355-405, 2002.